AD-A051 242 PRINCETON UNIV N J DEPT OF AEROSPACE AND MECHANICAL--ETC F/G 1/3
A HELICOPTER SIMULATOR STUDY OF CONTROL DISPLAY TRADEOFFS IN A --ETC(U)
MAY 77 J C ADAMSON

UNCLASSIFIED NL

1 OF 2
AD
A051242

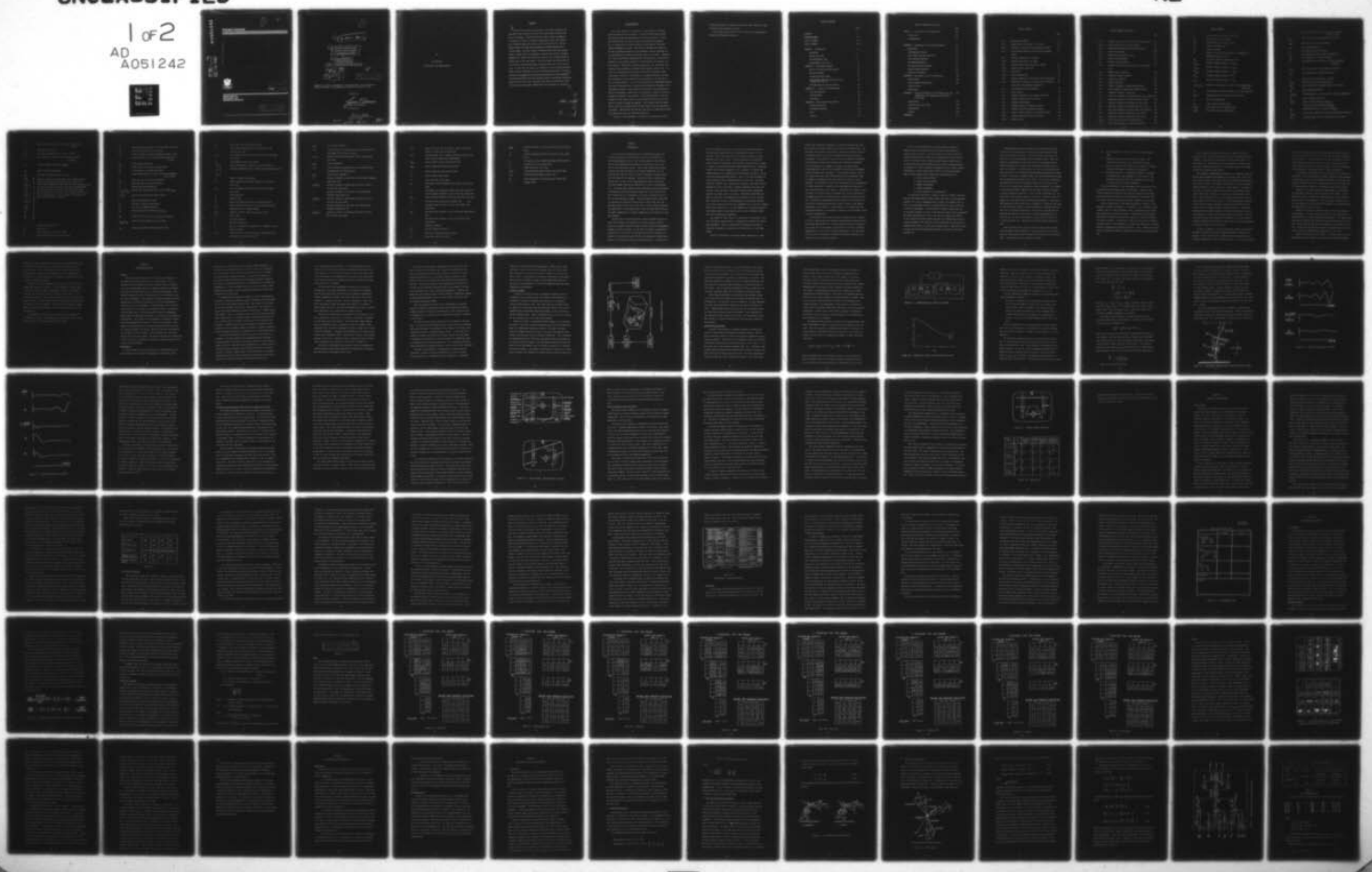

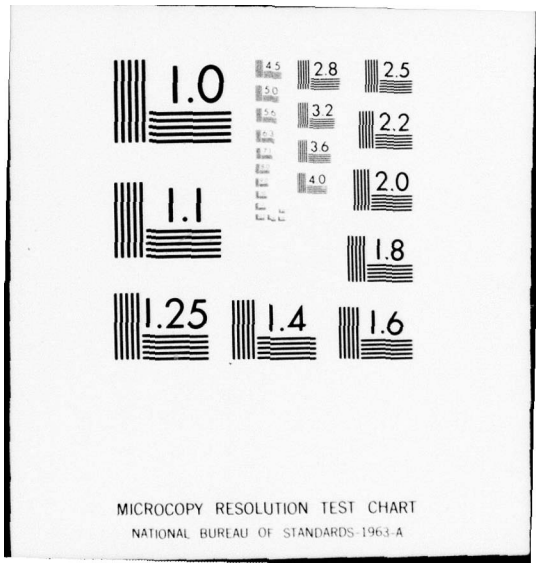
1.0
1.1
1.25
1.4
1.6
1.8
2.0
2.2
2.5
2.8
3.2
3.6
4.0
4.5
5.0
MICROCOPY RESOLUTION TEST CHART
NATIONAL BUREAU OF STANDARDS-1963-A

(1)

Princeton University

Department of Aerospace and Mechanical Sciences

(1)

(9) Master's thesis

(6) A HELICOPTER SIMULATOR STUDY OF CONTROL DISPLAY TRADEOFFS IN A DECELERATING APPROACH.

By

(10) James Craig Adamson
Princeton University
School of Engineering and Applied Science
Aerospace and Mechanical Sciences Department

(11) May 77

(12) 177p.

Submitted in partial fulfillment of the requirements for the degree of Master of Science in Engineering from Princeton University, 1977.

Prepared by:

James C. Adamson

James Craig Adamson

Approved by:

Theodor Dukes

Theodor A. Dukes

May, 1977

TO

Sue and Erik

For Patience and Understanding

ABSTRACT

A total force nonlinear analog model of the UH-1 helicopter was developed which simulates the entire low speed flight envelope from hover to 60 knots. Classical multiloop control theory was applied to design five levels of automatic stabilization which were used as test variables along the control axis of the test matrix. An integrated display was used which superimposes analog symbology over a terrain image. The basic display format,which had been used successfully in flight tests, was modified to provide four levels of display augmentation. These four levels were used as test variables along the display axis of the test matrix. Four helicopter test pilots acted as test subjects and furnished pilot ratings in each cell of the test matrix. In each cell the subject was required to fly the same prescribed flight profile involving a low level decelerating approach to a hover. Data was taken during each run which was indicative of pilot workload and performance. The data was evaluated based on significant differences among the test cells, and conclusions were drawn concerning the nature of the control and display augmentation most beneficial to the pilot.

ACKNOWLEDGEMENT

The author wishes to acknowledge the contributions of the many people who made this work possible. The United States Army granted the permission and the sponsorship for the project, and it is hoped that these efforts will help to make that sponsorship worthwhile. Mr. T.A. Dukes acted as faculty advisor and provided an invaluable counsel throughout the study. His creative thinking led to many of the more interesting aspects of the experiment, and his experience as an experimentalist afforded the bonding effect in the study. Professors H.C. Curtiss and Dunstan Graham offered countless hours of instructive guidance in the technical aspects of the helicopter and automatic control systems. Their help is greatly appreciated. Mr. Gerard Born provided practical solutions to problems which appeared almost daily. He acted as a sounding board for ideas and offered the methods to make those ideas a reality. His aptitude as an applied engineer, and unselfish assistance in this study will not be forgotten. Mr. Don Carter was the master builder. It is to his credit that the experimental apparatus, much of which he built, survived the tinkering and changing of the preliminary research. His patience with the author and willingness to share his knowledge, together with the incredible reliability of the experimental equipment, are testimony to his professionalism. Heartfelt thanks go to Mrs. Betty Brost for her unswerving devotion even in the midst of personal tragedy and hardship. Her constant smile and sympathetic ear were a constant source of moral support and encouragement to the author. Appreciation for the many long hours of typing and retyping this manuscript cannot be adequately expressed.

Finally, to the Department of Aerospace and Mechanical Sciences,

Princeton University, colleagues and friends, many thanks for a most stimulating and rewarding two years.

This thesis carries 1329-T in the records of the Department of Aerospace and Mechanical Sciences.

TABLE OF CONTENTS

TABLE OF CONTENTS (continued)

LIST OF FIGURES

LIST OF FIGURES (continued)

LIST OF SYMBOLS

A	area swept out by the main rotor (ft^2)
A_{ls}	lateral cyclic control (rad)
B_{ls}	longitudinal cyclic control (rad)
C_T	thrust coefficient (nd)
C_G	center of gravity
D	general term for total drag force, or halfwidth of landing pad (lbs) or (ft)
D_{fp}	flat plate equivalent drag force (lbs)
$G_{\delta_{Als}\phi}$	feedback transfer function $\phi \rightarrow \delta_{Als}$
$G_{\delta_{Bls}u}$	feedback transfer function $u \rightarrow \delta_{Bls}$
$G_{\delta_{Bls}\theta}$	feedback transfer function $\theta \rightarrow \delta_{Bls}$
$G_{\delta_c h}$	feedback transfer function $h \rightarrow \delta_c$
$G_{\delta_r r}$	feedback transfer function $r \rightarrow \delta_r$
I_{xx}, I_{yy}, I_{zz}	moments of inertia about x,y, and z axes, respectively (slug ft^2)
I_{xz}	cross product of inertia between x and z axes (slug ft^2)
$K_h, K_{\dot{h}}$	feedback gains for altitude and rate of climb
K_r	yaw rate feedback gain
K_u	x axis velocity feedback gain
$K_\theta, K_{\dot{\theta}}$	pitch angle and rate feedback gains
$K_\phi, K_{\dot{\phi}}$	roll angle and rate feedback gains

L	moment about the roll axis or landing pad length (ft-lbs) or (ft)
$L_{A_{lp}}$	pilots input to rolling moment minus Bell Bar
L_{BAR}	Bell Bar's input to rolling moment
L_p	roll damping derivative
L_r	roll due to yaw rate derivative
L_{sp}	roll damping from rate feedback augmentation
$L_{s\phi}$	roll moment due to attitude feedback
L_v	roll moment due to side slip or dehedral derivative ($L_v=L_{\beta/V_o}$)
$L_{\delta_{Als}}$	pilots total control effectiveness derivative
L_{δ_r}	roll moment due to rudder control input
M	moment about the pitch axis (ft CBS)
M_{BAR}	Bell Bar's input to pitching moment
$M_{B_{lp}}$	pilots control effectiveness minus Bell Bar input
M_q	pitch damping derivative
$M_{sq}, M_{s\theta}$	pitching moment to rate and attitude feedback augmentation
M_u	speed stability derivative
$M_\alpha, M_{\dot{\alpha}}$	angle of attack stability ($M_w=M_{\alpha/V_o}$) and angle of attack damping ($M_{\dot{w}}=M_{\dot{\alpha}/V_o}$)
M_β	pitching moment due to sideslip ($M_v=M_{\beta/V_o}$)
$M_{\delta_{Bls}}$	pilots total longitudinal control effectiveness derivative
M_{δ_c}	pitching moment caused by collective control input

N	moment about the yaw axis or numerator term (ft lbs) or (nd)
N_r	yaw damping derivative
N_{sr}	yaw damping augmentation due to rate feedback
N_v	yaw moment due to sideslip, weathercock derivative ($N_v = N_{\beta/V_o}$)
$N_{\dot{v}}$	sideslip damping derivative ($N_{\dot{v}} = N_{\dot{\beta}/V_o}$)
N_{δ_r}	rudder control effectiveness
N_{θ_c}	yaw moment caused by main rotor torque
$N_{\delta_{Als}}^{\phi}$	numerator terms used in multiloop control system analysis. They are determined by substituting the column of the control matrix indicated by the subscript into the column of the system matrix indicated by the superscript and multiplying out the cofactors of the matrix, eg. $N_{i\ j}^{k\ n}$ is the system matrix multiplyed out with the k and n columns of the system matrix replaced by the i and j columns of the control matrix (for more details, see Ref.21).
$N_{\delta_{Als}\ \delta r}^{\phi\ r}$	
$N_{\delta_{Bls}}^{n}$	
$N_{\delta_{Bls}\ \delta_c}^{u\ h}$	
$N_{\delta_{Bls}\ \delta_c}^{\theta\ h}$	
$N_{\delta_{Bls}}^{\theta}$	
$N_{\delta_c}^{h}$	
$N_{\delta_r}^{r}$	
R	radius of main rotor (ft)
SF	scale factor
T	thrust produced by main rotor (lbs)
V	Flight path velocity (instantaneous)(fps)

V'	resultant velocity vector at the main rotor disc (fps)
V_o	trim point flight path velocity (fps)
W	aircraft weight or waveform designation (lbs) or (nd)
X	force along the x axis or waveform designation (lbs) or (nd)
X_q	X force due to pitch rate
X_u	X force due to x velocity, drag derivative
X_w	X force due to z velocity derivative
Y	force acting along the y axis or waveform designation (lbs) or (nd)
Y_p	side force due to roll rate derivative
Y_r	side force due to yaw rate derivative
Y_v	lateral drag force derivative
$Y_{\delta_{Als}}, Y^*_{\delta_{Als}}$	lateral force produced by cyclic control ($Y^*_\delta \equiv Y_{\delta/V_o}$)
$Y_{\delta_r}, Y^*_{\delta_r}$	lateral force produced by rudder control
Z	force acting along the z axis
Z_q	lift due to pitch rate derivative
Z_u	lift due to airspeed derivative
Z_w	vertical drag force derivative ($Z_w = Z_{\alpha/V_o}$)
$Z_{\dot{\beta}}$	vertical force due to rate of change in sideslip
$Z_{\delta_{Bls}, \delta_{Als}}$	vertical force produced by cyclic inputs
Z_{δ_c}	collective control effectiveness derivative

a	lift curve slope of main rotor blades
a_1	longitudinal flapping coefficient measure wrt the control axis (rad)
a_{1s}	longitudinal flapping coefficient measure wrt the shaft axis (rad)
a_o	coning angle of main rotor blades
a_{xs}, a_{ys}, a_{zs}	total accelerations in the x,y, and z directions including accelerations due to flight path curvature (ft/sec^2)
b	number of blades in main rotor
b_1	lateral flapping coefficient measured wrt the control axis (rad)
b_{1s}	lateral flapping coefficient measured wrt the shaft axis (rad)
c	chord width (ft)
g	gravity force
h	height or altitude above the reference plane (ft)
h_{cg}	height from the aircraft CG to the main rotor hub (ft)
j	imaginary part of a complex number
ℓ_{TR}	length to the tail rotor hub from the CG (ft)
m	mass (slugs)
p	roll rate (rad/sec)
q	pitch rate (rad/sec)
r	yaw rate or distance to approach point (rad/sec) or (ft)
s	Laplace operator
$u, \dot{u}$	x axis velocity, acceleration due to gravitational and aerodynamic forces (fps), (ft/sec^2)

$u_{w/g}$	x_g axis gust component
$v, \dot{v}$	y axis velocity, acceleration due to gravitational and aerodynamic forces (fps), (ft/sec^2)
v_i, v_h	induced velocity (instantaneous), hover induced velocity (fps)
$v_{w/g}$	y_g gust component
w, $\dot{w}$	z axis velocity, acceleration due to gravitational and aerodynamic forces (fps)(ft/sec^2)
$w_{w/g}$	vertical gust component
x	position coordinate in shaft axis system unless otherwise subscripted (ft)
$x_g, \dot{x}_g, \ddot{x}_g$	position, velocity, acceleration along the x axis of the inertial axes system
y	position coordinate in the shaft axis system unless otherwise subscripted (ft)
$y_g, \dot{y}_g, \ddot{y}_g$	position, velocity, acceleration along the y axis of the inertial axes system
z	position coordinate in the shaft axis system unless otherwise subscripted (ft)
$z_g, \dot{z}_g, \ddot{z}_g$	position, velocity, acceleration along the z axis of the inertial axes system

$\alpha, \dot{\alpha}$	angle of attack, rate of change in angle of attack of shaft wrt flight path (rad)(rad/sec)
$\beta, \dot{\beta}$	sideslip angle, rate of change in sideslip angle of the shaft axis wrt flight path (rad)(rad/sec)
δ_{Als}	pilots lateral cyclic control stick input
δ_{Bls}	pilots longitudinal control stick input
δ_c	pilots collective pitch control input
δ_r	pilots rudder control input
ϕ	angle about the x axis (rad)
ϕ_f	bank angle of the fuselage wrt the inertial axis system (rad)
γ	lock number or longitudinal flight path angle (nd)(rad)
λ	inflow parameter measured in the control axis system (nd)
λ_{TP}	inflow parameter measured in the tip path plane axis (nd)
λ_1	blow back effect predicted by Coleman, ref. (nd)
μ	tip speed ratio along the x axis of the control axis system (nd)
μ_{TP}	tip speed ratio along the x axis the tip path axis system (nd)
ν	tip speed ratio along the y axis of the control axis system (nd)
ω	frequency (rad/sec)
ω_n	natural frequency (rad/sec)
Ω	main rotor rotational speed (rad/sec)
ψ	angle about the z axis (rad)

ψ_{REF}	aircraft heading at the time of marker star activation (rad)
ψ_f	aircraft heading measured in the inertial axis system (rad)
ρ	air density in the standard atmosphere (MSL)(slug/ft)
σ	solidity ratio of the main rotor
θ	angle about the y axis (rad)
θ_c, θ_o	collective pitch angle of main rotor blades (rad)
θ_{ch}	collective pitch angle in hover (rad)
θ_f	pitch attitude wrt the inertial axis system (rad)
ζ	damping ratio

CHAPTER I

Introduction

One of the most demanding control coordination maneuvers routinely encountered by the helicopter pilot is the low-level decelerating approach to hover. The primary reason for the difficulties is that simultaneous excursions are required in cyclic, collective and anti-torque control. These rather large control deflections are not only functions of the desired flight path, but are also strongly coupled. One of the most troublesome of these occurs near the bottom of the approach. While the pilot is arresting the descent rate, as well as the longitudinal and lateral velocities, the power changes required are amplified by a loss of translational lift. The large power changes require simultaneous pedal coordination. In helicopters with reciprocating engines this control task is further complicated by a requirement for throttle coordination with angle of attack and power changes. Control problems such as these tend to complicate the piloting of helicopters in their VTOL role, and generally restrict their use in this role to visual flight conditions. The possibility of alleviating some of these problems through the use of control augmentation or display augmentation is the subject of this investigation.

A great deal of research has been conducted within the past ten years which reflects the interest in low level approach problems and in the possible solution of some of these problems using augmented display and control systems. In the field of display instrumentation research, Ref. 11 and Ref. 1 illustrate the efforts of numerous researchers to provide the pilot with the most appropriate flight information, in a form which could be quickly assimilated. In the field of

automatic stabilization prior to 1971, most of the work directed at VTOL approaches emphasized the handling qualities aspects of the problems. One of the first efforts to combine the areas of instrumentation and control is Ref. 13 which documents the deceleration rates, effects of crosswinds, and performance resulting from a series of flight tests performed at NASA Langley Research Center. Continuing research such as that presented in Ref. 2 and Ref. 17 indicate the strong potential for a combination control display solution to the low level decelerating approach problem. Ref. 17, in fact, documents the first successful fully automated approach of this kind. The report indicates, however, that a satisfactory solution to the manual control problem is still in the future. Research conducted since that time indicates that solutions to the proper control-display combination question are rather elusive in nature. Essentially researchers have begun to reevaluate the fundamental characteristics of the problem. Ref. 22 and Ref. 32 look at the mathematical relationships involved in the visual approach and two more candidates for an electronic display. These later works point to a renewed emphasis on the manual aspects of the problem; those of assisting the pilot in his performance rather than fully automating the approach.

The purpose of this study is to investigate the potential of control and display augmentations in reducing pilot workload and increasing performance. This is a preliminary investigation directed at eventually promoting the usefulness of the helicopter in instrument flight.

Before the helicopter can achieve maximum usefulness as a VTOL

vehicle under instrument conditions, it must be configured such that the task may be performed safely by the pilot on a routine basis. Fundamentally this involves reducing pilot workload so that the task may be performed easier, and with a consistently satisfactory level of performance. The problems of the past have been primarily associated with providing the pilot with necessary and sufficient information. It is not feasible, for example, to attempt a low level decelerating approach to hover in an unprepared area solely on instruments, with no outside visual references. It is apparent, however, that if one could provide the right instrumentation and an appropriate level of automatic stabilzation, this task would be as easy as a visual approach. The hypothesis is that pilot performance in the instrumented low level approach is a function of his instrumentation cues and of the control difficulty of the vehicle. Using these two factors as test variables, the study proposes to determine the relative usefulness of incrementing automatic stabilization and incrementing display information. The absolute quantitative results obtained in the various test cells must be interpreted with great caution because of the inherent limitations of the simulator. Nevertheless, it is assumed that the relative information to be obtained is indicative of the relative values of various augmentations.

The experiment itself was a fixed base simulator study, sponsored by the U.S. Army Air Mobility Research and Development Laboratory (Contract Number NGR 31-001-277). The test subjects were four helicopter test pilots and the test matrix consisted of five levels of stability augmentation vs. four levels of display augmentation. The data taken was in the form of objective performance and workload measures, and subjective pilot ratings and comments.

The low level approach task was chosen primarily because it embodies most of the difficult control problems, and normally requires visual references. An overall look at the nature of the low approach reveals several factors which determine the relative difficulty of the control task. Generally these factors either tend to decrease the time interval within which the control applications must be executed, or tend to increase the magnitude of the required control deflections. In many cases, they do both or are directly coupled. Some of these factors which increase the task difficulty are:

- lower initial altitude
- higher initial airspeed
- higher gross weight
- steeper glideslope
- wind condition in the landing area

In many cases, the pilot is unable to predict in advance precisely how the interrelationship of these factors will affect a given approach. Usually it is only by experience that he learns, for example, that on slow steep approaches he will lose translational lift much sooner than on low fast approaches. If the aircraft is lightly loaded, this may not present a problem, in fact, it may ease the control task by separating the power applications for loss of lift and for stopping the descent. If the aircraft is heavily loaded, however, this maneuver may result in serious problems, since there may not be enough power or anti-torque to compensate for the loss of lift out of ground effect. Many sets of landing gear have been unintentionally modified in testimony to this miscalculation!

Notwithstanding the control difficulties described above, this task can be, and is performed routinely by helicopter pilots flying under visual flight conditions. This implies other reasons why the maneuver is not safely performed using instruments alone. These problems are wide-ranging, but basically they are associated with providing the pilot with accurate rate and position information with respect to the earth. In visual flight the pilot can see obstacles and avoid them, and he can perceive his ground speed decreasing as he comes to hover. He is able to combine visual rate cues with aircraft attitude and to respond with accurate control inputs. Not only do conventional instruments fall short of providing accurate rate and position cues, they do not, in many cases, provide the right information. For example, a conventional altimeter displays mean sea level altitude not ground proximity information, and does so with a notable instrument lag. The pitot-static type airspeed indicator not only is inaccurate at low airspeeds, but also cannot provide ground speed information. While these instrumentation problems may seem too elementary to enumerate, they must be the basis of any attempt to provide appropriate instrumentation for this sort of helicopter utilization. The low level approach task establishes the need for a new concept in flight instrumentation. In this respect, the low level approach is a most difficult task, and is therefore useful for a tradeoff study requiring high subject workload.

When translated into a control task for research, the low level approach demands careful definition. The objectives of the study dictated that the approach task be realistically presented to the test subjects. The approach task was defined as follows:

- initial condition of cruise at 120 ft., 60 kts, heading 360^{o}
- landing pad appears at ½ mile range and within a 30^{o} viewing angle centered on the nominal 360^{o} heading
- pilot is required to decelerate in level flight, correcting heading as necessary to approach the landing pad
- upon interception of a 9^{o} glideslope, descend, continuing the deceleration, and terminate at a 50 ft hover on the glideslope (the 50 ft hover was selected because of display constraints in terrain simulation)

The above definition of the task implies that the aircraft is far from equilibrium throughout most of the maneuver. Because of the large decelerations involved in the task, and because the helicopter trim calculation is nonlinear, it was decided that a nonlinear total force model would provide the best vehicle simulation for the study.

The helicopter model is described conceptually in Chapter II and developed in detail in Appendix A. Basically, it is a nonlinear analog computer model of a UH-1 helicopter, which is interfaced with a fixed-base cockpit and conventional controls. The design and development of this model was conducted to provide as realistic a vehicle as possible for the test subject. The goal was to give the test pilot a fixed-base simulator which he could identify as a single rotor helicopter, and which had basic response characteristics similar to a UH-1. Within the limitations of fixed-base simulation, this goal was realized quite satisfactorily.

Five different stabilization systems were added to the basic helicopter model. These systems became the control augmentation test variables. Each system was designed to ease the control task in a particular area. Collectively the five systems were arranged to vary the control difficulty from that of a moderately damped rate command system to an attitude command system.

The simulator instrumentation consisted of a cathode ray tube display of analog symbology superimposed on a terrain image. While, for this simulator study, the terrain images were generated electronically, the aircraft version of the display would employ a body fixed Forward Looking Infrared (F.L.I.R.) camera for terrain imagery. Providing the pilot with a television image of terrain offers the immediate advantage of giving him a window to the outside in instrumentation conditions. Many, although not all, of the normally visual flight cues become available via the terrain image. The analog symbology represents various critical flight instruments which, when superimposed on the terrain, form an integrated flight information display. This format integrates the instrument flight cues and the visual flight cues in an area requiring a significantly reduced visual scan distance. This basic display concept made possible the performance of the task under instrument conditions and afforded the opportunity to use analog symbology as display variables in the test matrix.

In order to augment or vary this particular display, and to obtain data which reflected the value of augmenting display information in general, the test variables were chosen such that they essentially represented integrations in the pilot/vehicle loop. Four levels of display

were chosen which took the form of flight path and positioning aids. The first format had no aids. The second level provided a stabilized "terrain marker". The third offered error rate information, and the fourth displayed quickened error rate or quasi-acceleration error. These forms are described in detail in Chapter II, and the background and development of the display itself is given in Appendix B.

The preceding paragraphs provide an introduction to the goals of this study, to the task which was defined to facilitate the attainment of those goals, and to the experimental environment in which the test subjects performed that task. The main body of the report deals with the preparation and conduct of the experiment and with the results.

Chapter II outlines in detail the requirements on the design of the experiment, given the stated objectives of the study. It also elaborates on the concepts of the helicopter model and the display as they are used in the simulation. Then, the chapter describes in detail the design of the test matrix and discusses the reasoning behind the organization of the test cells.

Chapter III involves a detailed account of the actual conduct of the experiment. It starts with the selection of test subjects and a brief description of their background and experience. The chapter then discusses the briefing and training program for both groups of test pilots, and the problems associated with preparing the subjects for the test. Finally the data-taking procedures are described, and an account is given of the recordkeeping and sequencing of test cells.

Chapter IV concerns the data itself. It outlines some of the considerations which were given to the problem of measuring performance.

Further, it briefly attempts an explanation of the potential pitfalls in using only objective data as a measure of "goodness" of a man-machine system. Third, the chapter identifies the variables which were measured, and describes the methods used in the reduction of the raw data. Finally, the data are presented, accompanied by a discussion of significant trends.

Chapter V is a brief summary of conclusions and of some of the significant aspects of the work. It is an attempt to take an objective look at what the study accomplished in terms of the stated objectives, and at some of the areas in which it fell short. It is necessary to point out that at this writing, not all of the data has been analyzed. In this regard, some of the subtleties resulting from the work may not have appeared. At the end of this chapter recommendations are made for improvements in test methodology and for future investigation.

The appendices contain detailed information concerning the development of the model, the background of the display, and the design method used for the automatic stabilization systems.

CHAPTER II

Experimental Design

Purpose

The purpose of this chapter is to detail the requirements of the study and to discuss the design of the experiment. The requirements will be analyzed in terms of explicit tasks, or specific goals for the experiment itself; and, implicit tasks, or preliminary work which had to be done in order to perform the experiment. The simulation scheme will then be described as it was conceived to meet the study requirements. This simulation scheme is presented in block diagram form to illustrate the design of the overall experimental apparatus to fit the requirements. Following this, each of the functional blocks of the simulator is discussed in detail, starting with the helicopter model. These descriptions provide the fundamental theory behind the modeling and include a few illustrative mathematical relationships. The details of the mathematical derivations, scaling, and analog mechanization, however, is left to the appendices. Subsequent to the descriptions of the basic helicopter model and the basic simulator display, the various control and display configurations are introduced as test variables. They constitute the control and display axes of the test matrix. The chapter ends with the introduction of the test matrix, and Chapter III begins the detailed account of the conduct of the experiment.

Requirements

As was indicated in the Introduction, the requirements for this study stemmed from an interest in expanding the usefulness of the

helicopter, in its VTOL role, into instrument flight conditions. It was desired to determine whether or not state of the art instrumentation and automatic stabilization equipment might be used in combination to make this expansion possible. In view of this desire, the U.S. Army Air Mobility Research and Development Laboratory sponsored this study at Princeton University as a preliminary step in making that determination. It was intended that this be a low cost study to help determine the potential, and help guide the direction of future more extensive work in this area.

In keeping with this general guidance, the first requirement was to perform a fixed base simulator study of helicopter pilots performing the low level decelerating approach task. The reasons for the choice of task was discussed earlier in the introduction. The reasons for using a fixed base simulation instead of moving base or flight testing were twofold. First, a preliminary study such as this did not warrant costly modification of a variable stability research aircraft for use as a test bed, when the desired relative data can be obtained from a simulator. Secondly, since the pilot responses of interest are his responses to the incremental changes in display and vehicle stability, seat-of-the-pants cues were not considered to be a significant factor.

The second requirement concerned the nature of the study to be performed. A terrain display with superimposed analog symbology developed by Dukes at Princeton, and proven effective in hover test performed at the U.S. Army Electronics Command (Ref. 4), would be used in conjunction with a variable stability helicopter model to perform a control vs. display tradeoff study. More specifically, the tradeoff determinations were directed at gaining a substantially sound indication of the relative usefulness of incrementing display cues

vs. incrementing vehicle stability. It was hypothesized, in this regard, that if the vehicle stability and displayed information were each augmented in a way which would make the pilots'task easier, and if the increments of this augmentation were chosen to be significant, a test matrix could then be defined which would demonstrate the relative value of the increments.

The third and fourth requirements concern the use of the resulting data. The third requirement of the study was to determine from the data taken which of the control and display configurations defined tradeoffs well enough to warrant further more costly investigation. In essence, this was a two part requirement. First, that some conclusions be drawn concerning the prognosis for success of future study; and second, that some recommendation be given of specific areas identified in the test matrix for closer scrutiny.

Finally, the fourth explicit requirement of the study was to provide a data base in this area, to be used as a reference for comparison with data from future studies. This requirement simply implied that all appropriate data be recorded, and that the methods of data taking and data reduction be documented carefully enough to be of value to future researchers. Although this requirement can be simply stated, a great deal of ambiguity exists concerning the validity of performance measures in this area. Problems of what to measure and how to analyze these measurements are discussed in more detail in Chapter IV.

The implicit requirements were generally those of designing and constructing the experimental apparatus and planning the test format to meet the explicit requirements stated above.

The first of these implicit requirements, of course, was to design and construct a helicopter model capable of performing the low level task with satisfactory handling fidelity and realism. In this regard the model had to be a reasonably accurate facsimile of the actual aircraft over the entire low speed flight region indicated in the task. In addition, since the task demanded that the vehicle be far from its trim condition throughout most of the maneuver, care had to be exercised in the use of linearizing assumptions. Finally, the model had to be flexible enough to allow stability configuration changes to be accomplished quickly; and, it must be readily interfaced with the existing fixed base cockpit.

The second implicit task was that of determining a reasonable ladder of automatic stabilization levels, and designing the various feedback systems to effect that stabilization. Each successive level of augmentation was planned to add a significant increment of stability to the vehicle.

Thirdly, the same sort of analysis had to be applied to the display. For the given basic display format, various cues had to be added which would increment the usefulness of the display to the pilot, with consideration given to avoiding display clutter. To this end as few symbols as possible were added to the basic display, but each change in symbology was calculated to take the display one integration closer to providing control position information. This requirement involved simply modifying the existing display to fit the needs of the experiment.

Finally, the parameters to be measured as raw data had to be determined. Inherent in this determination is a need to estimate which parameters are, independently or in combination, a reasonable

indication of pilot workload and performance. While there is some agreement at least in the area of workload, there is little conclusive information in the area of pilot performance in a task as complex as this. In the absence of definitive information in this area, and to insure fulfillment of explicit requirement number four, the approach to this problem was to record all parameters which may prove indicative of performance.

Simulation Scheme

In order to provide the type of simulator indicated in the requirements, it was essential that each element of the simulator be integrated to provide a continuous real time flow of information around the pilot/vehicle loop. This meant that the helicopter model, in addition to being linked with the fixed base cockpit, must also be compatible with the existing hard-wired display, as well as with the terrain simulation plan. Also, the simulator had to be easily accessed for the necessary data to be taken during testing.

Figure II-1 shows a conceptualized block diagram of the experimental set-up. The pilot provides voltage inputs to the analog helicopter model via conventional helicopter controls. The model continually solves the dynamic equations of motion to produce instantaneous translational and rotational rate and position information. This information is simultaneously used to drive the superimposed display symbology and the simulated terrain imagery. The superimposed symbology provides the pilot with the information, such as attitude, airspeed, etc., required to pilot the vehicle. Each symbol on the display is driven by a vehicle motion variable, and integrated to provide motion information about and

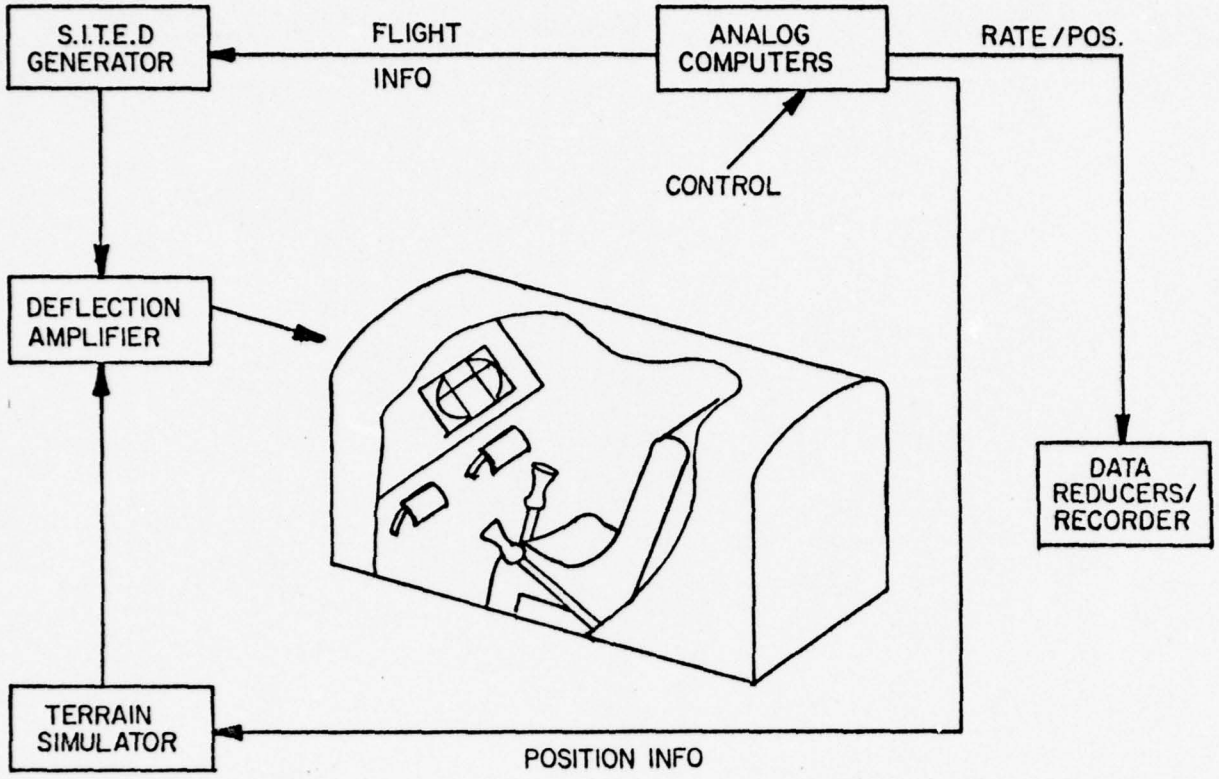

FIGURE II-1. EXPERIMENTAL APPARATUS

along the aircraft's body axes. The terrain imagery is also driven by the aircraft's motion variables, but these variables are rotated into earth fixed coordinates. The terrain motion on the display provides ground proximity and ground rate information to the pilot. The deflection amplifier is simply the interface element between the terrain simulator and display symbol generator, and the CRT display in the cockpit. The data gathering equipment is shown in Figure II-1 to access the helicopter model for the information recorded as data.

This scheme was designed and mechanized using equipment housed in one room which also served as the training, testing and pilot debriefing room. The simulator could be operated by a single individual with three other individuals required to take data and monitor the tests. Communication between the test pilot and the simulator operator was effected using aircraft-type headsets. This description of the simulation scheme provides an overview of the experimental set-up. What follows is a detailed description of the functional elements of the simulator.

Dynamic Helicopter Model

A wealth of information is currently available on modeling vehicles for pilot/vehicle performance and dynamics studies. Most of this information, however, is based on linearizing assumptions and perturbation analysis. The basis for the mathematical model as it finally evolved came from work done at Princeton by Born, et.al. (Ref. 3). In this work, and a later study by Tsoubanos (Ref. 32), a nonlinear longitudinal model was developed which represented the vehicle dynamics near hover and in the low speed regime quite well. The basic principles of this early model were used to develop the model for the present work.

The momentum theory, thrust and flapping relations as outlined in Gessow & Myers (Ref. 14) are used to define the magnitude and incidence of the resultant thrust vector with respect to the shaft. The moment and force imbalances which result from magnitude and inclination changes in the resultant force vector (which is here assumed perpendicular to the plane of tips), perturb the dynamic equations of the vehicle. The resulting accelerations are integrated to produce rate/position information which is then used in the momentum equation, and also in the terrain simulator and flight information display. Figure II-2 shows a generalized block diagram of the information flow through the model. The development of each section of the model involved certain constraints which affect the model's overall performance limitations. A brief look at these blocks in sequence is therefore warranted in order to provide a clearer insight into the capabilities and limitations of the simulator.

The momentum theory provides a prediction of induced velocity which must be determined in order to calculate the trim condition of the aircraft. When this equation is normalized with respect to the hover induced velocity, the resultant velocity is resolved into its shaft components, and the thrust is normalized wrt weight, it takes the quartic form below.

$$\bar{v}_i^2[(\bar{u} + \bar{w}\, a_{1s})^2 + (\bar{w} - \bar{u}\, a_{1s} - \bar{v}_i)^2] - (1 + \frac{\Delta T}{W})^2 = 0$$

This relationship must be continually solved on a real time basis in order to produce values of the inflow and advance parameters λ and μ. It will be noted that these parameters are identifiable in the above

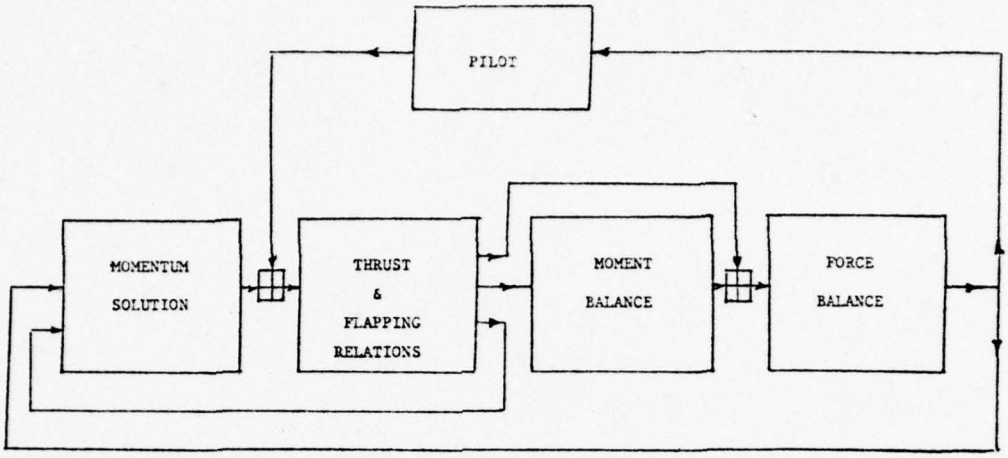

FIGURE II-2. COMPUTATIONAL FLOW SCHEME OF THE MODEL

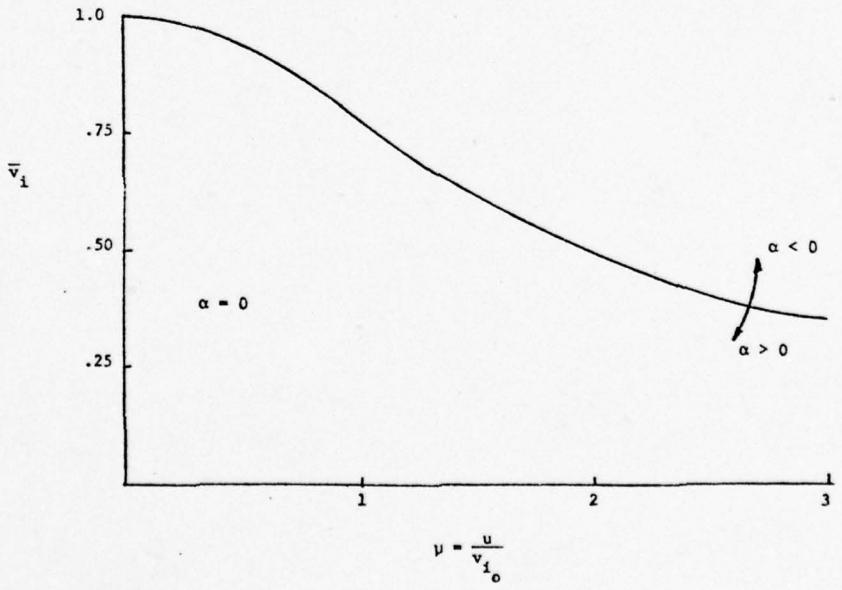

FIGURE II-3. VARIATION OF INFLOW WITH TIP-SPEED RATIO (α=0)

equation as the sum of two squares, and they are relative to the tip path plane. They are converted easily to control axis system for solution of the quasi steady flapping coefficients a_1 and b_1. In this simulation the momentum equation was hard-wired using solid state analog devices. Mechanized in this fashion, the analog produced real time values for λ and μ at various angles of attack. Figure II-3 shows this relationship for the special case $\alpha = 0$.

The most significant assumptions inherent in the momentum theory can be summarized as follows:

> The rotor is assumed to be an infinitely thin actuator disc with an infinite number of blades; this disc propels a uniform air mass, which is assumed to be an inviscid fluid, with no tip losses or energy lost to the slipstream; the resulting induced velocity is assumed to be perpendicular to the disc and to have a magnitude downstream twice that at the disc.

Factors resulting from a non-uniform induced velocity distribution, such as wake blow-back were considered in the model's development, but were not included. Treatment of these factors is a part of Appendix A.

The thrust and flapping relations are basically those found in Ref. 14 with consideration given the modifications found in work by Curtiss and Seckel (Ref. 30). These equations were mechanized on the analog computer to utilize the λ and μ parameters generated by the momentum equation, together with the collective and cyclic control inputs, θ_o, B_{ls}, A_{ls}, to describe the magnitude and inclination of the thrust vector wrt the shaft. Aside from the lack of fully described

blade dynamics, it is assumed that the thrust vector is the resultant vector and is perpendicular to the tip path plane. This is equivalent to the assumption that the H force, as defined in the control axis, equals Ta_1. The thrust and flapping equations are summarized here in the form they were used:

$$\frac{2C_T}{a\sigma} = \frac{\theta_o}{3} + \frac{\lambda}{2}$$

$$a_1 = \left\{ \mu\left(\frac{8}{3}\theta_o + 2\lambda\right) - \frac{16}{\lambda\Omega} q \right\}$$

$$b_1 = \left\{ \frac{4}{3}\mu a_o - \frac{16}{\lambda\Omega} p \right\}$$

Note that $a_{1s} = a_1 - B_{1s}$ and $b_{1s} = b_1 + A_{1s}$, therefore, either a control application (ΔA_{1s}, ΔB_{1s}), or a flapping change (Δa_1, Δb_1), causes a thrust vector inclination (Δa_{1s}, Δb_{1s}). Figure II-4 shows the resulting force/moment imbalance on the vehicle.

The three rotational degrees of freedom were modeled using linearized moment balance relationships. The moment balance around the pitch axis, for example, is:

$$\sum M = I_{yy} \ddot{\theta}_f \approx h_{cg} T \sin a_{1s}$$

The effect of the Bell Bar was modeled by augmenting the pitch and roll damping. When the above equation is expanded and terms added which represent rate and position feedback augmentation, the closed loop helicopter transfer function can be written. This transfer function for the constant speed pitching response is shown below in Laplace operator form, for rate and attitude feedback augmentation.

$$\frac{\theta_f}{B_{1s}} = \frac{K}{s - (m_q + m_{sq})s + m_{s\theta}}$$

where s is the Laplace operator.

The K represents the system gain comprised of pitching moment of inertia, thrust and distance from center of gravity. The parameters m_q, m_{sq}, and $m_{s\theta}$ are damping and frequency terms corresponding to aircraft parameters and/or feedback gains. In the unaugmented helicopter, of course, the m_{sq} and $m_{s\theta}$ terms do not appear. They were included in the above transfer function to show their presence as system feedback gains. Careful attention to feedback gains in the various stability configurations produced very realistic frequency response characteristics. In this regard the model's transient response behavior is quite compatible with actual aircraft data. Figures II-5 and II-6 show sample response characteristics at hover and at u = 100 fps.

The three translational degrees of freedom were modeled using conventional total force balance relationships. These were normalized wrt weight to produce the required acceleration parameters along the three shaft axes. The X axis equation is given here for illustration.

$$\frac{\Delta T}{W} a_{1s} + a_{1s} - \theta_f - \frac{D}{W} \cos(\theta-\gamma) = \frac{\dot{u}}{g}$$

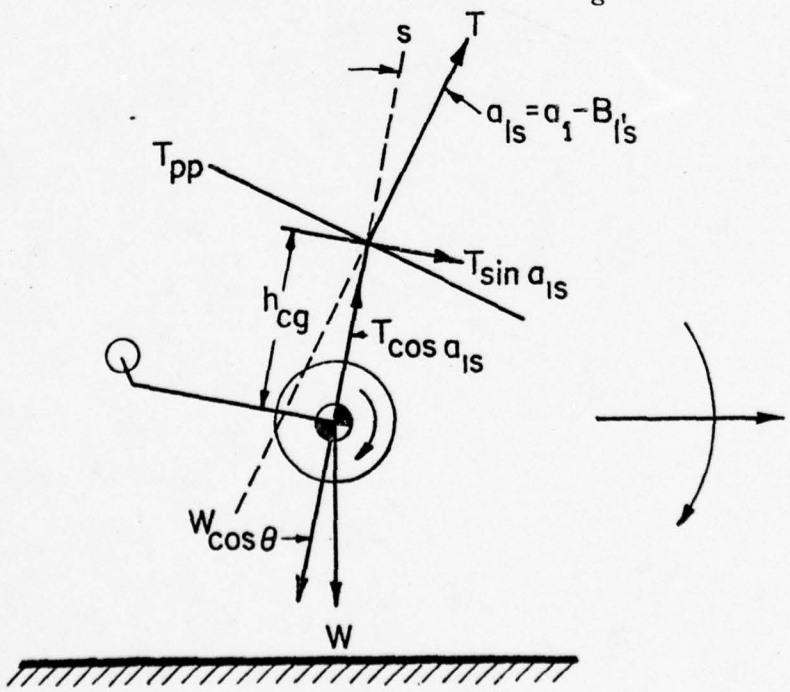

FIGURE II-4. FORCE/MOMENT IMBALANCE FROM CONTROLLER FLAPPING CHANGE

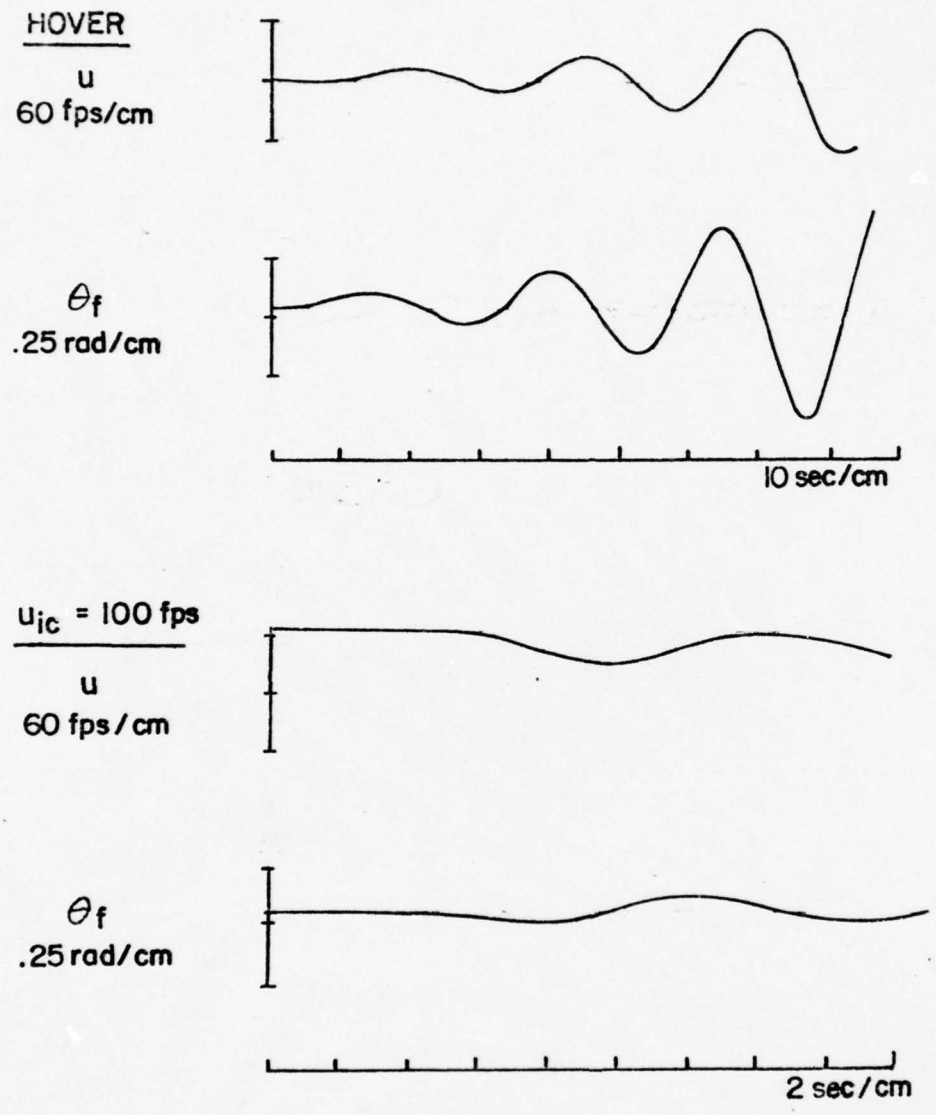

FIGURE II-5. PITCHING TRANSIENTS OF THE MODEL

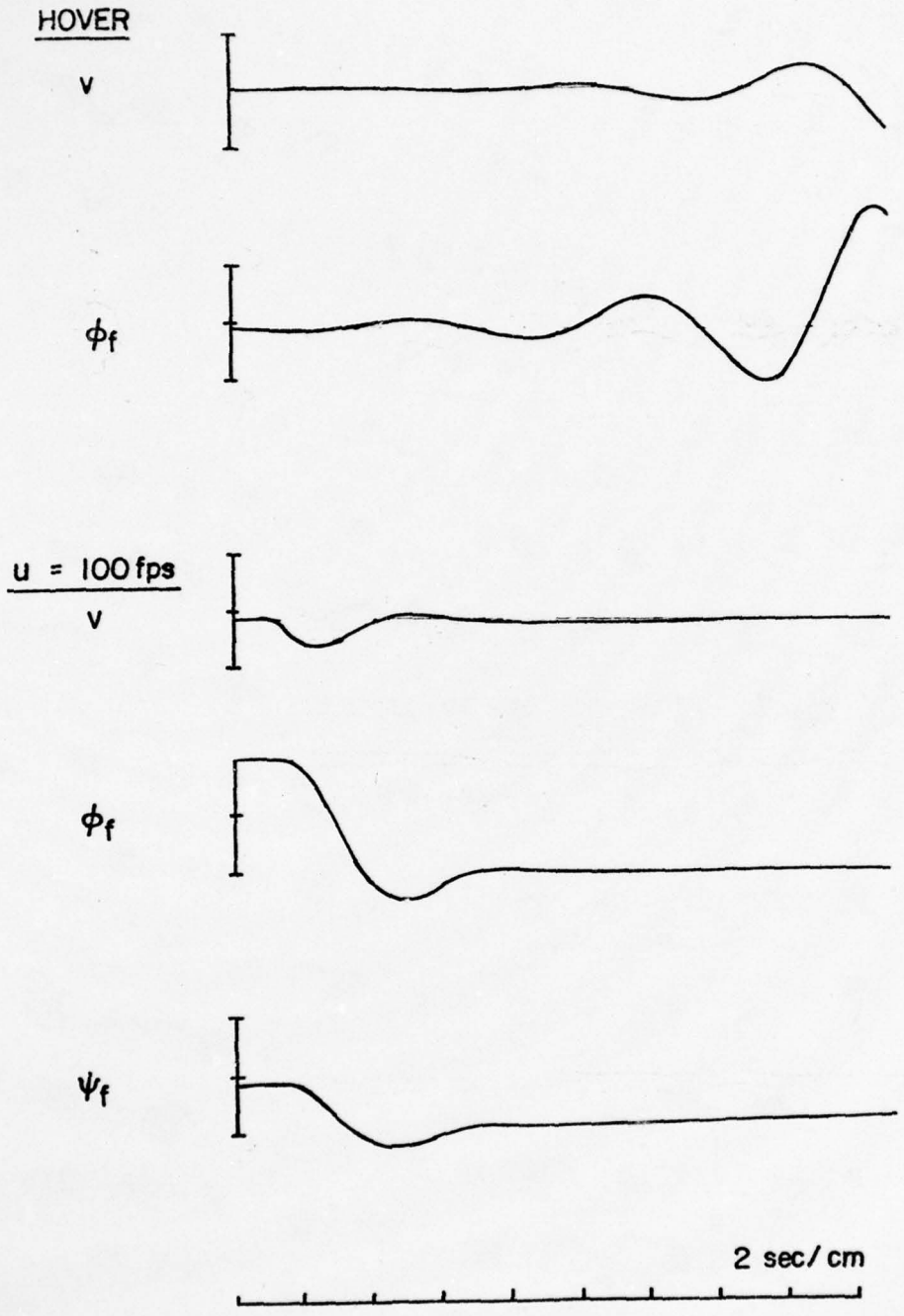

FIGURE II-6. ROLLING TRANSIENTS OF THE MODEL

Second order small angle approximations were used in the longitudinal force balance relationships, i.e. ($\cos\theta \tilde{=} 1 - \frac{\theta^2}{2}$). The quadratic terms have a modifying effect on the vertical acceleration which appeared to be noticeable during the initial simulator testing, probably because of the large pitch attitude changes during deceleration. The shaft axis accelerations are then rotated through the attitude angles to produce inertial acceleration parameters. These are integrated to provide rate and position information to the terrain simulator, and to provide flight path information for error measurements. The sum inertial velocities and gusts are rotated back through the attitude angles to produce shaft air speed components, which are used in the system of equations described above and for the simulator display. The axis conversion, like the momentum equation, was hard-wired using analog devices to allow the rotation to take place continually on a real time basis. All of the other relationships described conceptually above, were patched on two TR48 and one TR20 analog computers. This computational scheme constitutes the essence of the simulation.

This model represents a quite satisfactory nonlinear representation of the single rotor helicopter's flight characteristics. This in part is attributable to the closed loop solution of the momentum equation in real time. Second, the model is modular and extremely flexible. It could be expanded to include blade dynamics, or more detailed modeling of stability parameters. This characteristic makes the model useful in variable stability simulation. The model is also straightforward to mechanize. This alone makes the model a very useful tool in special purpose simulator research.

In the case of this study, the flexibility of the model as a variable stability simulator allowed changing feedback stabilization from one configuration to another by activating a set of relay switches. There were five such stability configurations in the test, which comprised the stability augmentation variables for the test matrix.

The Superimposed Symbology Trajectory Error Display (S.I.T.E.D.)

The display development was the work of Dukes at Princeton, who first introduced it in 1969 (Refs. 10 and 12). The symbology used in this study evolved from that original work. Portions of this background material have been selected for inclusion in Appendix B which is a more detailed description of the basic format of the display used in this work. No attempt was made during this investigation to perform display research. The intent here is merely to document the significant aspects of the display used, as it represents a novel concept in instrument flight. Of critical importance to this study was the necessity to proffer this new concept; without it, performance of the task would have been impossible.

The key feature of the display, which makes possible the performance of a visual flight task using instruments only, is the integration of conventional instrument cues with visual approach cues. This is accomplished via the superposition of symbols on the T.V. image of the terrain. The pilot is able to obtain most of the information he normally gets looking out his windscreen by referring to the CRT display. Some cues are lost, of course, in the two dimensional representation of the terrain. In fact, some very important altitude and descent rate

information comes to the pilot from his peripheral view of the terrain. These cues cannot be duplicated on a small two dimensional display. These losses can be restored in other ways, however, and in some respects the display can supply a greater precision. One very significant example of the display's superiority to visual cues is the reduced scan time required. In the visual approach the pilot must divide his attention between critical aircraft instruments in the cockpit and the surrounding terrain outside. He derives all of the rate, attitude and position information he needs from outside the aircraft. There are certain items of importance, however, which demand that he divert his attention periodically to his instrument panel. Examples of these are torque or applied power, and rotor rpm in the case of the reciprocating engine. Many times experienced pilots are able to rely partially on tactile cues for this information. Collective stick position and vibrations are examples of these. Usually, however, the experienced pilot keeps a good instrument crosscheck going even during visual approaches. Herein lies one of the significant strengths of the display. Visual and aircraft information are integrated into a small enough area so that the instrument scan rate is performed with almost no physical eye movement. In fact, one of the more subtle features of the display is that with some training, the crosscheck can be virtually replaced by mental processing of integrated information.

The analog symbols which comprise the aircraft and flight information take the form of geometric shapes. These shapes are generated electronically, and are driven by dc voltages from the helicopter model which

are applied to horizontal and vertical deflection circuits. The details of this circuitry are developed for the terrain simulation near the end of Appendix B. Figure II-7 shows the display format with all symbols included. The marker star and error rate vector are used as test variables and will be described later. The remainder of the symbology represents flight information and terrain. The flight symbols are discriminated from their reference scales and the terrain through the use of color coding. Using a color CRT allowed provision of green terrain and yellow flight symbols with orange reference lines and scales. Additionally, in order to reduce clutter, some scales are used for more than one symbol. In the vertical information band, the altimeter, rate of climb diamond, and torque meter all use the same reference scale. Each division represents 25 feet of altitude, 500 fpm rate of climb, or approximately 10 PSI of torque pressure. The pitch reference scale moves with respect to the cusp of the pitch reference triangle as a quantitative display of pitch attitude at $2\frac{1}{2}$ degrees per division. The pitch triangle also acts as a bank angle reference. When the roll reference bar or artificial horizon intersects the junction of the pitch triangle and the airspeed scale, 15 degrees of bank is indicated.

The terrain was simulated for this study by a line which represented the real horizon and a lissajous shape which represented a rectangular landing pad measuring 100 ft by 200 ft. The horizon line and the landing pad were driven by pitch roll and yaw information which made them appear rolled and displaced as they would normally to a pilot observing them through his windshield. In addition, the perceptual size and shape changes of the landing pad symbol were accomplished using a special deflection circuit described in Appendix B. This circuit made the pad

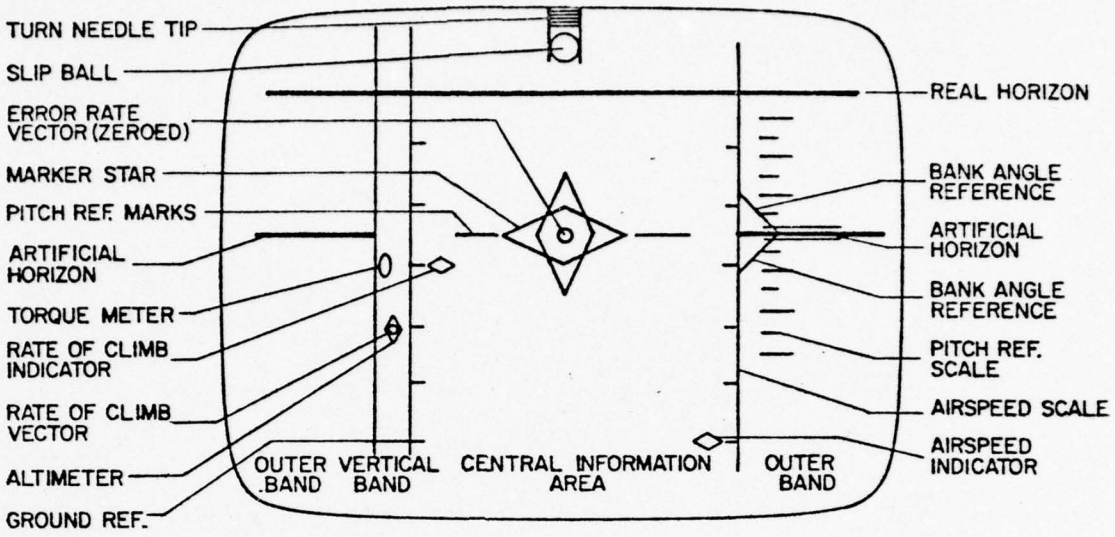

a.

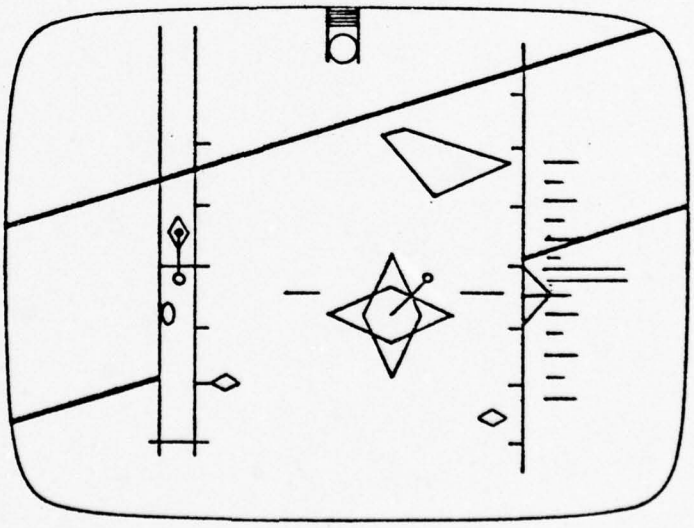

b.

FIGURE II-7. DISPLAY FORMAT, IDENTIFICATION OF SYMBOLS

grow in size as the pilot approached it, and tapered and skewed the sides depending on the pilot's perspective vantage position. This rather elaborate circuitry was essential to provide the same sort of proximity and motion information normally derived from the terrain.

Test Variables and the Test Matrix

The test variables consisted of five different levels of automatic stabilization of the basic helicopter model, and four levels of display augmentation. Each of these configurations is described here as they were used in the test matrix.

The first or basic stability configuration consisted of rate feedback only, or damping augmentation in pitch, roll and yaw. The criteria used to establish damping levels were: one, to stabilize the helicopter in hover; two, to increase damping in all three axes proportionally with the original levels; and three, to end up with a pitch rate response affording good controllability. This response was determined to be about .1 rad/sec per inch of stick at hover. This first configuration is a reasonable lower limit on stability augmentation for this task. Based on exploratory testing, it did not seem feasible to perform this task on instruments with less than damping augmentation.

The second configuration was identical to the first in the pitch and roll axis, but with a heading hold system added to the yaw channel. This represents a sizeable step in easing the task since it relieves the pilot of much of the pedal coordination normally required during large power changes. The hold circuits employed in this simulation were conceptually the same as those used by Calspan in their X-22 simulator (Ref. 2). This consisted of an attitude feedback system in the yaw axis,

with an integrated control input, plus a lead.

The third feedback configuration consisted of pitch and roll attitude hold system (rate control) and yaw damping. Here again the pilot is commanding pitch and roll rates with about the same control sensitivities; but, since the test was conducted using light turbulence the hold system is less gust sensitive. For this reason, it constitutes a significant increase in stability augmentation for this task. The turbulence was simulated using Gaussian white noise with a low-pass filter. The fourth configuration was identical to this third system with the heading hold added to the yaw channel.

The fifth and highest stability configuration was comprised of a complete attitude feedback system in pitch and roll, and the same heading hold system used in configurations two and four. In this system, of course, the pilot commands attitude with cyclic and yaw rate with anti-torque pedals. The time constant of this system is about .3 sec with a damping ratio of .7. The stick sensitivity is about .1 rad/inch. These parameters and those used throughout the stability augmentation were based on an automatic control system design for the helicopter modeled. Appendix C presents the method of calculation of the most complex design considered. This example illustrates the methods used in the multiloop analysis and some of the reasoning behind the design variations. The five configurations resulting from this work and briefly described above represent one axis of the test matrix.

In terms of display augmentation the marker star is the most significant display element in this work, and constitutes a rather unique concept in display technology. Basically, it is a totally self-contained,

onboard, course and glideslope indicator which may be used for approach or hover. As a glideslope, its principle of operation is to illuminate a spot on the terrain image which represents the desired approach point. The downlooking angle of the marker star represents the nominal glideslope angle. The Marker Star is stabilized in the aircraft with respect to the angular motions of the airframe, therefore, it moves with respect to the terrain only when the aircraft's CG translates wrt the earth. Perhaps the easiest way to visualize this is to imagine a spotlight mounted on an inertial table at the aircraft's CG illuminating a spot on the ground ahead of the aircraft. The downlooking angle of the spotlight wrt the horizon represents the glideslope. If the pilot flies down the glideslope, the spotlight beam stays on the same spot. The Marker Star can be pre-set at a desired glideslope, and the aircraft maneuvered to center the marker star over the desired approach point, and the aircraft landed along this pre-set glideslope. This Marker Star represents the first display augmentation.

The second display augmentation mode is a glideslope error rate vector. The origin of this vector is at the center of the Marker Star, and its magnitude and direction indicate the rate and direction of marker star movement with respect to the intended approach point. If the pilot is holding course and glideslope, the vector will show zero rate and appear as a dot in the center of the star. If the pilot flies above glideslope and drifts right, of course the vector will point up and to the right. Its magnitude will be proportional to his error rate. The vector has a second mode of operation for hover. In this mode the vector indicates inertial velocities in the X and Y directions over the terrain

and is decoupled from the altitude rate. This concept allows the pilot to use the vector as a positioning cue over an intended hover point. Figure II-8 shows the Marker Star and vector being used in the hover mode. In this illustration the vector indicates a rate forward and to the right. Unless the pilot zeroes the vector the aircraft will move in the direction indicated by the vector.

The third display augmentation is a "quickened" error rate vector. In this configuration the vector described above is driven by a combination of rate and acceleration information which reduces the requirement for pilot lead compensation. Since CG acceleration information is a difficult parameter to obtain accurately in the aircraft, this quickening is accomplished using modified attitude information. The quickened vector can be used by the pilot as a control positioning indicator which reduces workload by reducing the inherent velocity cue lag in the pilot/vehicle loop.

These three landing/hover aids constitute the display test variables. The basic display with no augmentation is the baseline configuration for the test matrix. The second configuration adds the marker star. The third configuration adds the error vector, and the fourth adds the vector quickening. These display augmentation levels are designed so that each increment essentially reduces by one the number of integrations between the display information and the control movements. In the test cell combining the highest feedback augmentation and highest display augmentation the quickened vector becomes a control positioning indicator. Figure II-9 is the complete test matrix incorporating the stability

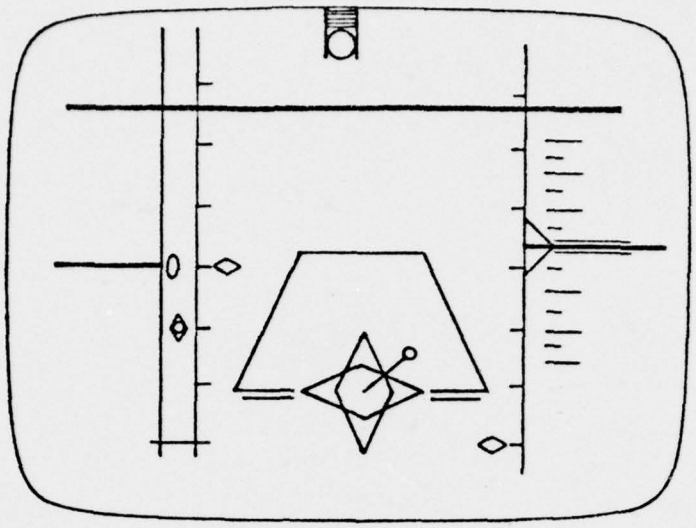

FIGURE II-8. DISPLAY FORMAT, HOVER MODE

Controls / Displays	I RATE AUG. $\dot{\theta}\ \dot{\phi}\ \dot{\psi}$	II PITCH & ROLL RATE AUGMENTATION W/HEADING HOLD $\dot{\theta},\dot{\phi},\psi_H$	III PITCH & ROLL ATTITUDE HOLD $\theta_H,\phi_H,\dot{\psi}$	IV PITCH & ROLL ATTITUDE HOLD W/HEADING HOLD θ_H,ϕ_H,ψ_H	V PITCH & ROLL ATTITUDE FEEDBACK W/HEADING HOLD θ,ϕ,ψ_H
Without Marker Star	No Test	2,1	3,1	4,1	No Test
Marker Star Without Velocity Vector	1,2	2,2	3,2	4,2	5,2
Marker Star, Velocity Vector	1,3	2,3	3,3	4,3	5,3
Marker Star Quickened Velocity Vector	1,4	2,4	3,4	4,4	No Test

FIGURE II-9. TEST MATRIX

and display configurations described above. Each of the four test subjects was required to perform the approach task three times in each cell of the matrix for record.

CHAPTER III

Conduct of the Experiment

Test Subjects

One of the most significant aspects of conducting tests involving human test subjects is the consideration of the type of subject to be used. Generally this consideration results in a decision between the experienced, and inexperienced subject. In this case, the latter category (non-pilots) was almost immediately eliminated because the objective was to view performance of helicopter pilots in an inherently specialized task. This elimination, however, did not significantly simplify the problem. Because of the varied nature of pilot backgrounds, and the desire to keep the subjects' experience level as uniform as possible, consideration was given to three broad categories of pilots. These candidates for a source of subject material were rookie pilots (just out of flight school), experienced operational pilots, and test pilots. These sources had to be weighed against the requirements of the study, the time needed with each subject, and the relative availability of subjects in each group.

The test pilots have a great deal of flight experience and have flown many different systems. Since the Test Pilot is trained to quickly evaluate systems he may do so before the test can begin, and this may introduce an unconscious bias. The distinct advantage of this group, however, is the ability to make sound system evaluations based on a uniformly accepted rating scale. In general, more information can be gained from this group, per unit of test time, than from any other group. Test pilots have one other characteristic which

eventually emerged as the overriding consideration in the choice of subjects. Because of the test pilot's highly specialized training in evaluating research systems, he is normally able to compensate for much of his bias. He is able to do this because of a systematic process of comparison against accepted standards. Based on this comparison, the test pilot can quickly sum up system performance in terms of a rating scheme which, for this study, was the Cooper Harper scale. Because of the rather large test matrix defined for the experiment, and the amount of time required to train a subject and take the data, a large number of subjects could not be processed. It was decided, in view of this, that the use of test pilots afforded the most reliable and consistent information possible for a low sample size and low repetition rate.

Test subject A was a lieutenant commander in the U.S. Navy at the time of the tests. He had nearly 14 years of pilot experience, and was assigned to NASA Langley in an operational flying status. His duties included research and development type test flying as well as research simulator studies. He graduated from the U.S. Navy Test pilot School in 1969 and holds the Navy's special instrument qualification. Subject A had approximately 3000 hours of total flight time; of which about 250 hours were in rotary wing aircraft. In addition to training simulator time, he had about 300 hours in research simulators, with half of that time being in fixed base and the other half in moving base. In addition, approximately 100 hours of his simulator time had been with display research, and the remaining 200 hours with control augmentation systems.

Test subject B was a major in the U.S. Air Force with 13 years of active service and flight experience. Like pilot A, B was assigned to

NASA Langley in an active flying status for research and development. He graduated from the U.S. Navy Test Pilot School in 1971, where he qualified in both helicopter and fixed wing courses. His total flight time was approximately 3700 hours with an additional 800 hours spent in flight research simulators. Of the simulator time, about 600 hours had been in fixed wing simulators and included research in areas such as a Terminal Control Vehicle, Advanced Supersonic Transport, and Space Shuttle Reentry. The remaining 200 hours had been spent in helicopter simulators involved in research in areas such as Real World Cue, Visual Approach and Landing Task, and low altitude, high speed, sling load control. B had considerable knowledge of display work, and was actively interested in research in this area.

Test subject C was a captain in the U.S. Army with 14 years of helicopter experience. Having attended the Army's Rotary Wing Flight School in 1963, pilot C had a total of 3200 hours. He was also an Army fixed wing pilot, and a CH-47 test pilot. In addition, he had about 1000 hours of flight experience in aircraft with augmented control systems, and brief experience with a remotely piloted UH-1. Captain C was, at the time of the test, assigned at Fort Eustis, Vs. in an operational flying status.

Subject D retired from the U.S. Army after 20 years of flying duty. He had been a CW4 pilot qualified both in fixed and in rotary wing aircraft since attending Army Flight School in 1957. He was qualified as an instructor in both fixed wing and rotary wing, and was an instrument examiner. He had accumulated a total of 5000 hours of flying time with considerable experience in a variety of different aircraft. Like pilot C, D had experience with augmented control systems and a remotely piloted UH-1. Pilot D was at the time of the tests, working in a civilian

status with pilot C at Fort Eustis, Va. His duties included instructor pilot, instrument examiner, and test pilot.

Table III-1 provides a summary of the flying experience of the four test subjects. The hours given are approximate since flight records were not solicited.

	A	B	C	D
Total hours	3000	3700	3200	5000
Helicopter hours	250	2000	1700	3000
Instrument qual.	SPECIAL	STANDARD	STANDARD	EXAMINER
Approx. hours in augmented aircraft	2000	2000	1000	110
Research simulator hours	300	800	--	--

TABLE III-1

Test Subject Training

The test subjects were made available in groups of two for five consecutive working days per group. The work time was divided into 2.5 training days and 2.5 testing days, each day consisting of about 8 hours of work time. During the first 2.5 days the pilots were briefed for one half day and trained in the simulator for the remaining two days. Every effort was made to expose the two groups to similar training programs, while accomodating individual learning problems. The objective of the training program was to raise the proficiency level of each subject, as rapidly as possible, to the point where additional practice runs showed little or no beneficial effect.

The purpose of the pilot briefing was to acquaint the subjects with the study, and to instruct them on the task, the display, and the model. The organization and presentation of the briefing was planned to generate interest in the project, and provide a fundamental understanding of the task and the equipment used to perform the task. The details of the modeling and data taking procedures were not presented, nor was information concerning methods of evaluation. The subjects were merely asked to do the best they could, and not to become discouraged with portions of the test matrix known to be difficult. Since the study utilized highly knowledgable subjects, it was felt that better motivation could be achieved by illuminating some of the more technical aspects of the simulator. This approach gained the subjects confidence in the work, and afforded a challenge in task performance. In actuality, the subjects required little motivation. They were all highly dedicated professionals who took the study seriously and worked very hard throughout the test.

The task was presented in the form of a mission briefing. Each portion of the task was defined in terms of the primary flight parameters. In particular, the deceleration portion was discussed in detail. Since the task did not precribe any special deceleration profile, this was left to the individual pilot. Preliminary test runs had shown that a constant attitude deceleration worked very well at least for the initial phases of the task. This was discussed in the briefings and recommended as a starting point for the training. The pilots were encouraged to experiment with their own techniques and employ any method which would help them fly as close to the task profile as possible.

The pilots were briefed on the model in terms of its functional elements.

In general, a conceptualized description was given of the method used to combine the momentum, control, force balance, and moment balance relationships to simulate the real helicopter. In addition, each of the feedback systems was discussed in terms of how it would affect the vehicle's controllability. These systems were presented as variables in the test matrix, but no premonishment was given as to the relative difficulty of the configurations. In this regard, every effort was made not to bias the subjects with respect to any configuration.

The display was discussed at greater length than any other aspect of the simulation. This was principally because it represented a different approach to instrument flying. Each symbol of the display was carefully discussed in terms of the information it presented and was placed into a category of flight information, terrain information or landing aid information. The marker star and error rate vector were dealt with in detail as to their role as test variables and as to the physical theory of their operation.

Following the initial briefing the subjects were introduced to the actual equipment and to the stabilization configurations. At this point some latitude was allowed, in terms of personal preference, and the subjects were allowed to pick the configuration which seemed easiest for them to fly. The task and display configurations were introduced to the individual subject while flying his chosen aircraft configuration. This latitude was permitted for two reasons. First, it was deemed essentail that the pilots learn first the appearance of the task on the display. In order to accomplish this they had to learn the display. It was desirable to let this process evolve with as little distraction from the aircraft as possible. Second, any imbalance in time spent in this initial stability configuration could easily be compensated later

in training. Generally the subjects chose stability configratuions closest to those used in aircraft they had flown in the past rather than the most augmented configuration in the test matrix. As familiarity with the various stability configurations increased, however, this preference changed. The various stability configurations did not seem to present much of a barrier to acceptance, and proficiency in control techniques started increasing from the first day. Considerable time was spent with learning the display and on the second day of simulator training significant progress in this area was evident. The two days of simulator training were very intensive and by the end of this period each subject had considerable practice in each cell of the test matrix. The latter portion of the second day was spent switching from one cell to another in the matrix in order to build subject flexibility among the configurations, and minimize the transition shock in going from cell to cell during the test.

This was a rather ambitious training schedule even for test pilots. The program undertook to teach a new concept in instrumentation to the subject while flying five different aircraft configurations. The success of the program hinged on the subjects' thorough understanding of the elements of the display, and his acceptance of the helicopter simulator as a reasonable vehicle. Given that these teaching goals could be achieved, the subject had to be exposed to enough practice to minimize any learning curve effects on the test data.

The problems related to subject acceptance of the simulator as a representation of the real aircraft were minor and for the most part were overcome quite easily. There was, of course, some difference of opinion among pilots regarding control "feel" and sensitivity. These

problems involved subtleties and there was no common agreement, so the controls were left as they were. There was no magnetic brake type force trim in the simulator as there is in the UH-1, so the subjects were obliged to fly the approach in a force trim off condition. That seemed to be the source of the control "feel" disagreement. This is an option that is normally afforded the pilot but was not available in this test. The subjects agreed, however, that this was a minor point and would not significantly affect performance. The most significant problem with the helicopter model was a characteristic problem with heading hold systems. It is well known that without a washout in the yaw rate feedback, this system will tend to oppose steady turns. This washout circuitry was left out of the heading hold system for this study because it was felt that the task was close enough to a head on maneuver that the turns would not present a problem. It was found, however, that the subjects were bothered somewhat by the additional pedal required to trim when turning in the heading hold mode. This difficulty was voiced stronger by the second group of subjects; therefore, in the interest of consistency, no changes were made. Aside from these two problems, the subjects all agreed that the simulator was quite acceptable and had many very favorable qualities.

The problems with the display took two forms. The first was a problem with perception. The first group of pilots felt that the attitude indicator was giving reversed cue, in that the artificial horizon moved up and down in pitch against a fixed pitch scale. Both pilot A and pilot B felt the scale should move and the artificial horizon bar should remain fixed in pitch on the display. In that they were the first group, and

because this seemed to frustrate them considerably, the change was made. The display thereafter remained unchanged throughout the tests. The second display-related problem was related to the motions of the marker star. This was a problem related to the physical understanding of what the star was supposed to do. Because of the novelty of the concept considerable time was spent with explanation and training in this area. Finally all subjects did learn to use the star effectively.

Another significant problem with the training was a problem of pilot fatigue. The steady concentration on a very difficult task contributed to this fatigue, as did the viewing of a CRT display. It was found during research prior to this test that, given a difficult task requiring strict concentration, 30 minutes is about the longest time a subject can stand in the cockpit. After that time his performance starts to deteriorate rapidly and he loses his ability to concentrate. This time limit was again confirmed during the tests. Even alternating the subjects every 30 minutes, the pilots were visibly tired at the end of a work day. In this respect it is felt that the work performed in these tests represents about the maximum that should be exacted. Anymore than this could have resulted in degradation of data due to fatigue factors.

At the end of the training period, the pilots were briefed on the pilot rating scheme. They were asked to use the standard Cooper-Harper rating scale shown in Table III-2. The subjects were required to perform in at least two but not more than three test cells per sitting, with the guideline that only display configurations would change in a given sitting and not the control. In this way the pilot could provide system ratings based on one variable per sitting instead of two. Pilots were encouraged to make notes between test runs, and could use the time between sittings to perform detailed evaluations. In addition to the

numerical rating for each cell, the pilots were asked for specific verbal comment about each cell. These ratings and comments constituted the subjective data for the tests.

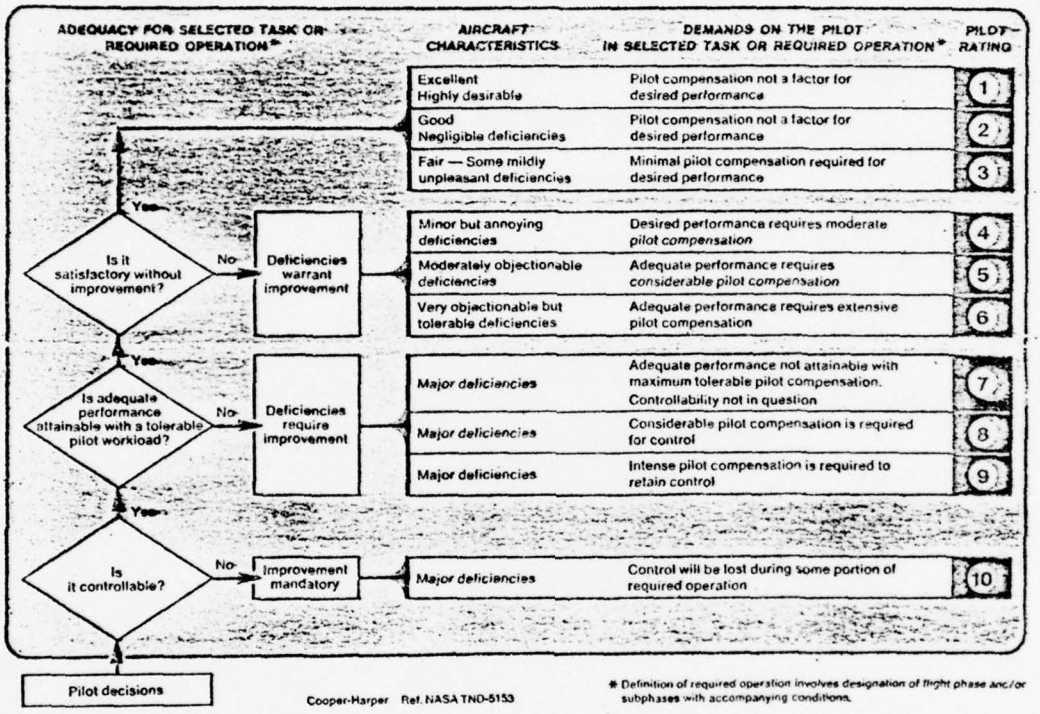

Table III-2

Cooper-Harper Pilot Rating System

Test Phase

The test phase involved recording data in each cell of the test matrix as the test pilots performed the task in that cell. The intent here is to describe the method used to obtain these data. The

data consisted of raw and reduced flight and control variables which were determined to be indicative of pilot workload and system performance. In this section the conduct of the individual test run will be described, followed by a discussion of the sequencing of subjects through the test matrix. Finally, a brief account is given of the record-keeping methods.

In order to minimize the possibility of error, four individuals were employed to conduct the test, to monitor and record the data, and to provide the maximum crosschecking of the data runs. However, one individual conducted the test and communicated with the subject under test in order to minimize pilot distraction. This operator acted essentially as an air traffic controller in radar contact. He gave takeoff clearances and monitored the test flight to insure that initial conditions were met prior to initializing the approach. The approach was initialized when this operator turned off the landing pad blanking circuits, causing the pad to appear in the pilots display; and activated the motion integrators which started the landing pad moving in accordance with aircraft flight variables. At this point of "Runway in Sight", the data run was initialized. During the remainder of the approach phase the same operator continued to monitor the approach and determined the termination point of the maneuver. The pilots were allowed to continue an approach as long as they were moving toward the hover point. An approach was terminated when the subject arrived near the nominal hover point, ceased to progress toward that point, or lost control. From the pilots viewpoint, the run started on the ground with the rotor turning, lifting off to a hover, taking off on a heading of 360^{o}, and flying to the initial altitude (120 ft), airspeed (60 kts), and heading (360^{o}). The landing pad appeared randomly right or left of

the course, always the same amount. At this point the approach task was initiated.

The second operator assisted the first in configuration changes but was primarily responsible for data recording. His equipment consisted of an eight channel strip chart recorder and a TR48 analog computer which had been programmed to perform mean absolute and root mean square data reduction on selected flight variables. This operator initialized the computer and recorder at "Runway in Sight", and recorded values and labeled the charts following run termination. In addition, the second operator was responsible for collecting pilot rating and comments, and cataloging them by run number.

The third individual acted as a data monitor. He was responsible for the proper operation of test equipment and recorders. He constantly checked supply voltages, and system fail indicators to insure that an equipment malfunction would not go undetected. The data monitor also crosschecked and labeled the strip chart recordings during the approach phase of each run, and assisted the second operator after run termination.

The fourth individual functioned as test coordinator. He was responsible for the continuity of the tests. During the test runs he operated a 10 channel magnetic tape recorder and made verbal record on the tape of events and peculiarities. In addition, he also observed the first operators visual display monitor during the run as a situational crosscheck.

One of the most important considerations involved with conducting

the test runs was how to order the presentation of test cells to the subjects. Several factors were relevant to this determination, each of which had to be weighed in order of its significance. The first and governing consideration is that of insuring reliability in the data resulting from the tests. It was not at all safe to assume that some learning effects would not manifest themselves as the testing progressed. The subjects were exposed to about 50 runs each, not counting practice runs, between the beginning and the end of testing. It could be expected that even after adequate training, some performance improvement might take place. In addition to learning effects on objective data, the effect of cell sequence on pilot rating had to be considered. The subjects might tend to compare a cell configuration with the one that preceded it. In order to minimize this effect, some alteration in sequence had to be included in the testing. Also, it was desirable as indicated earlier to change only one of the test variables per sitting to afford the subject a more controlled comparison base. Finally, the sitting time for the subjects could not exceed 30 minutes.

The result of the above considerations was a test run sequence, which had the following features. It allowed for a total of three test runs per pilot in each cell, alternated the order of cell presentation, did not change stability configuration during a sitting, and maintained the sitting time at less than 30 minutes. The first sequence through the test matrix began immediately after training and started each subject with the most augmented cell. That is test cell (5,3) in Fig. II-9. In that first sitting the subject performed in two cells (5,3) and (5,2). In the next sitting this subject performed in cells (4,4) and (4,3).

The third sitting was cells (4,2) and (4,1). This sequence continued until each pilot had made a test run in each cell down to (1,2). Following each sitting, the subject evaluated the configurations just tested. During this first sequence a practice run preceded each test run in each cell. In the second sequence the order of cell presentation was reversed and the subjects received only one practice run at the beginning of each sitting. This time the sequence began with cell (1,2) and progressed (1,3)(2,1)(2,2)(2,3), and so on through the matrix. In this sequence, however, two test runs were made in each cell. This procedure for sequencing the subjects through the test gave the maximum consideration to the factors discussed earlier, and offered the advantage of separating the data of the first and second test days. This separation afforded the opportunity to observe the presence of learning effects on objective data and sequence effects on the pilot rating.

The mechanics involved with record keeping involved assignment of an alpha numeric designation for each test run. This number identified the pilot, the test cell, and the run number. The special form shown in Figure III-1, was used to record computer reduced data, pilot rating, and pilot comment for each run. The run number was also inscribed on each of the strip chart recordings and verbally recorded on the 10 channel magnetic tape. The strip chart was used to show visual comparisons of control activity and attitude rates, while the tape recorder was used to provide records for future data reduction. The philosophy behind this approach to the data taking was that gross trends would be unveiled by the strip chart recorder, and the computer reduced data would provide immediately accessible material for the quantitative comparison of cells.

CONTROL, DISPLAY, SEQUENCE, PILOT

	APPROACH	HOVER
Position Error Longitudinal (MAV) Lateral (MAV) Height (MAV)		
Controls Stick Longitudinal (MS) Lateral (MS) Collective (MS) Rudder (MS)		
Rates Attitude (MS) Roll (MS) Yaw (MS)		
Pilot Rating		
Remarks		

FIGURE III-1. DATA RECORDING FORM

CHAPTER IV

Data Analysis and Results

Introduction

This chapter describes the variables which were measured during the test and discusses the methods used to obtain those measures. Not all of the variables recorded are analyzed here. Rather, certain variables have been selected which are primarily indicative of pilot workload. These variables are each analyzed in terms of significant differences among the cells of the test matrix. The "t" statistic is used as a vehicle for comparing pairs of cells because of the small sample sizes within each cell. The test cells are then compared to determine control configurations or display configurations which differ significantly in terms of the measures established. The discussion of the results is based on this comparison. In this test Cooper-Harper ratings were solicited from each pilot in each cell. As was indicated in the preceding chapter, the test pilots were sequenced through the test matrix twice. The first progression resulted in one data run per pilot in each cell. On the second progression two data runs were made in each cell. It was apparent during the testing of both groups of test pilots that learning effects were still present during the first progression through the matrix. For this reason the data analyzed consisted on only that data taken during the second progression through the test matrix. The data taken during the first progression was retained for further study.

Variables Analyzed

Pilot rating is one of the most significant indicators of relative "goodness" of systems. The test pilots made two subsequent data runs

in each cell but only one pilot rating was taken for each cell. The remainder of the data, however, contained two data points per variable from each pilot in each cell. The pilot ratings in each cell were averaged to produce mean Cooper-Harper ratings in each cell, and the standard deviation was calculated based on that mean.

The objective measures of pilot workload consisted of aircraft angular rate measurements and measurements of control deflections. Since the decelerating descent task required significant changes in stick deflection which varied from one control configuration to another, a high pass filter was used to eliminate the effect of these low frequency control deflections. The filter was chosen to pass only frequencies above .3 rad/sec. The mean square values of angular rates and of filtered control deflections were calculated on line during each data run and recorded at the termination of the run. Figure IV-1 shows the computer diagram of the mean square computation used for each of the variables. A separate integrator was used to provide the time of integration, and that value of time was used to determine the variable's mean square value.

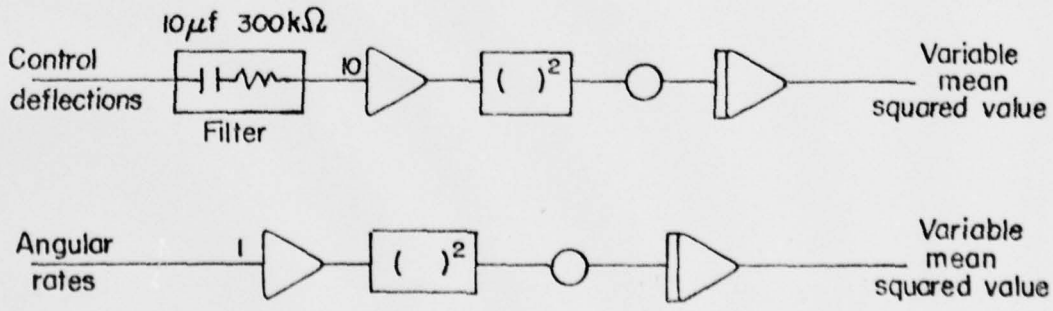

FIGURE IV-1. COMPUTER DIAGRAM OF ON-LINE MEAN SQUARE COMPUTATION

Since there were four test pilots, each performing two data runs in each cell of the test matrix, and there were four control deflection variables and three aircraft angular rate variables in each run, there were a total of eight observations of the seven objective variables in each test cell. The root mean squared value of each of the variables recorded was averaged for the eight observations and that value was recorded as the mean of the variable measured for that particular test cell. Also the standard deviation of the eight observations from the mean was calculated and recorded.

In summary, these data points to be analyzed are the mean value and standard deviation of each of the seven objective measures and of the pilot ratings, taken over the eight observations in each cell. The statistical analysis of these data points is the subject of the following section.

Statistical Analysis

One method of evaluating statistically significant differences between cells is the "t" statistic for two means. This essentially invokes the assumption that the two cells being compared are samples of two normally distributed populations having population means μ_1 and μ_2 and the same variance σ^2. The "t" statistic is used to test the null hypothesis that both samples were taken from the same population. For the two cells compared to be statistically significantly different the "t" value for those two cells must be less than the "t" value at the level tested. For example, if the sample size in each cell is n=4 the "t" value for testing the null hypothesis at the 5% level is 2.45, the "t" value for the two cells compared must be greater than 2.45 in order to reject the null hypothesis. If the hypothesis is rejected at the 5% level, one can say with 95% assurance that the two cells came

from different populations, hence are significantly different. One of the weaknesses of the "t" statistic is that estimates of the parent population mean and standard deviation are normally made based on two small samples. In this case, however, since it was desired to compare all test cells in pairs, the estimate of parent population parameters was based on the entire test matrix. This procedure implies the assumption that the standard deviation is not a function of display or control. No such function was observed during the tabulation of standard deviations by test cells. The computations of the population parameters and the "t" statistic for each measure in each cell of the test matrix was performed as follows:

let n_i = number of observations where i = number of the test cell ($1 \leq i \leq k$)

m_i = mean of a given measure in test cell i

m_j = mean of the same measure in some other test cell j

"t" is defined:

$$t = \frac{|m_i - m_j|}{s\sqrt{\frac{1}{n_i} + \frac{1}{n_j}}}$$

where s = estimate of parent population standard deviation estimated as follows:

let s_i = standard deviation of the given measure in cell i for the n_i observations

then:

$$s^2 = \frac{(n_1 - 1)\, s_1^2 + (n_2 - 1)\, s_2^2 + \ldots (n_k - 1)\, s_k^2}{(n_1 + n_2 + \ldots n_k - k)}$$

The values of "t" required to reject the null hypothesis at the 5% level

and 10% level for samples of 4 and 8 observations are:

	5%	10%
$(n_i + n_j - 2) = 6$	$t \geq 2.45$	$t \geq 1.94$
$(n_i + n_j - 2) = 14$	$t \geq 2.14$	$t \geq 1.76$

Table IV-1

Data

The following Tables IV-2 through IV-9 each give the "t" statistic for one of the measures analyzed. The chart in the lower right shows the mean value of the measures in each test cell, and the standard deviation of that measure over the eight observations. In the "horizontal" charts on the left the number shown on each cell indicates the "t" statistic of that cell with respect to the corresponding cell of the same row of the numbered column. In the "vertical" charts on the right the number in each cell indicates the "t" statistic of that cell with respect to the corresponding cell in the same column of the numbered row. Cells which are statistically significantly different (those cells in which the null hypothesis is rejected) are shaded. Diagonal shading indicates difference at the 10% level and crosshatched shading indicates difference at the 5% level.

T STATISTICS FOR TWO MEANS

Horizontal with respect to column ( )

	n.d.	n.d.	n.d.	n.d.
	1.1	4.5	1.7	1.6
	2.1	4.3	1.1	3.4
	1.4	3.3	.2	n.d.

(1)

	3.7	1.7	n.d.
	3.4	.6	2.7
	6.4	3.2	1.3
	4.7	1.6	n.d.

(2)

	1.9	n.d.
	2.8	6.1
	3.2	7.7
	3.1	n.d.

(3)

	n.d.
	3.3
	4.5
	n.d.

(4)

Vertical with respect to row ( )

					(1)
n.d	1.1	.8	.1	n.d.	
n.d.	.8	2.0	.7	n.d.	
n.d.	.3	.8	.4	n.d.	

					(2)
1.3	1.9	1.1	.7	.5	
1.1	1.4	.1	.4	n.d.	

					(3)
.2	.5	1.2	1.1	n.d.	

Scale factor 1 unit = .023 rad/sec

MEANS AND STANDARD DEVIATIONS

n.d.	.6 .1	.9 .3	.7 .2	n.d.
.6 .2	.7 .3	1.0 .3	.7 .3	.4 .2
.7 .2	.5 .1	1.1 .3	.8 .2	.4 .1
.7 .2	.6 .2	1.0 .3	.7 .2	n.d.

TABLE IV-2. PITCH RATE

T STATISTICS FOR TWO MEANS

Horizontal with respect to column ( )

	n.d.	n.d.	n.d.	n.d.
	.8	3.9	5.6	1.4
	1.5	4.8	6.3	.8
	1.1	5.7	6.9	n.d.

(1)

	3.6	3.8	n.d.
	4.8	6.4	.6
	3.3	4.8	.7
	4.6	5.8	n.d.

(2)

	.3	n.d.
	1.6	5.4
	1.4	4.0
	1.3	n.d.

(3)

	n.d.
	7.0
	5.5
	n.d.

(4)

Vertical with respect to row ( )

					(1)
n.d	1.7	.5	.8	n.d.	
n.d.	1.0	1.2	.0	n.d.	
n.d.	.9	.1	1.1	n.d.	

					(2)
1.6	.8	.7	.9	.6	
1.1	.8	.6	.3	n.d.	

					(3)
.5	.1	1.3	1.1	n.d.	

Scale factor 1 unit = 6.2% FS

MEANS AND STANDARD DEVIATIONS

n.d.	.4 .0	.2 .1	.2 .1	n.d.
.4 .2	.4 .1	.2 .1	.2 .1	.4 .1
.5 .2	.4 .1	.3 .1	.2 .1	.4 .1
.4 .2	.4 .1	.2 .1	.2 .1	n.d.

TABLE IV-3. LONGITUDINAL STICK

T STATISTICS FOR TWO MEANS

Horizontal with respect to column ( )

	n.d.	n.d.	n.d.	n.d.
	.4	1.0	1.3	.0
	.5	.3	.0	.4
	.4	.3	.2	n.d.

(1)

	1.8	2.3	n.d.
	1.4	1.8	.5
	.8	.5	.8
	.1	.7	n.d.

(2)

	.5	n.d.
	.3	1.0
	.3	.1
	.5	n.d.

(3)

	n.d.
	1.3
	.3
	n.d.

(4)

Vertical with respect to row ( )

n.d	.0	.3	.5	n.d.
n.d.	3.4	.8	.5	n.d.
n.d.	2.7	1.1	1.1	n.d.

(1)

2.4	3.3	1.1	1.1	2.0
2.7	2.7	1.4	1.6	n.d.

(2)

.3	.6	.3	.5	n.d.

(3)

Scale factor 1 unit = 2.3% FS

MEANS AND STANDARD DEVIATIONS

n.d.	1.1 .3	.9 .4	.8 .1	n.d.
1.1 .3	1.1 .4	1.0 .2	.9 .3	1.1 .4
.8 .1	.7 .1	.8 .1	.8 .2	.8 .3
.7 .3	.8 .1	.8 .2	.7 .2	n.d.

TABLE IV-4. COLLECTIVE

T STATISTICS FOR TWO MEANS

Horizontal with respect to column ( )

	n.d.	n.d.	n.d.	n.d.
	5.0	.2	3.6	4.4
	3.3	.2	4.1	3.9
	1.2	1.1	2.7	n.d.

(1)

	3.0	.1	n.d.
	5.2	1.5	.6
	3.1	.8	.6
	2.3	1.5	n.d.

(2)

	2.9	n.d.
	3.8	4.6
	3.9	3.7
	3.8	n.d.

(3)

	n.d.
	.9
	.2
	n.d

(4)

Scale factor 1 unit = 4.2% FS

Vertical with respect to row ( )

					(1)
n.d	.9	3.2	2.3	n.d.	
n.d.	1.1	1.3	.2	n.d.	
n.d.	1.4	.8	.1	n.d.	

					(2)
1.5	.2	1.9	2.0	1.0	
3.2	.5	2.3	2.4	n.d.	

					(3)
1.8	.3	.4	.3	n.d.	

MEANS AND STANDARD DEVIATIONS

n.d. n.d.	.4 .2	.8 .4	.4 .2	n.d.
1.2 .4	.5 .2	1.2 .5	.7 .3	.6 .3
1.0 .3	.5 .4	1.0 .4	.4 .3	.4 .2
.7 .3	.6 .3	.9 .4	.4 .1	n.d.

TABLE IV-5. RUDDER

T STATISTICS FOR TWO MEANS

Horizontal with respect to column ( )

	n.d.	n.d.	n.d.	n.d.
	-3	.3	.8	4.2
	.0	.6	.7	5.1
	.0	1.5	.9	n.d.

(1)

	1.0	1.1	n.d.
	.1	.5	3.8
	.6	.7	5.1
	1.5	.9	n.d.

(2)

	2.1	n.d.
	.5	3.9
	.2	4.5
	.6	n.d.

(3)

	n.d.
	3.4
	4.4
	n.d

(4)

Vertical with respect to row ( )

n.d	1.3	.4	1.9	n.d.
n.d.	2.3	.8	2.7	n.d.
n.d.	.6	3.1	.5	n.d.

(1)

.7	1.0	.3	.7	.3
2.3	2.0	3.5	2.4	n.d.

(2)

3.0	2.9	3.9	3.1	n.d.

(3)

Scale factor 1 unit = .023 rad/sec

MEANS AND STANDARD DEVIATIONS

n.d.	1.1 .2	1.2 .4	.9 .4	n.d.
1.4 .1	1.3 .3	1.3 .4	1.2 .5	.7 .3
1.5 .3	1.5 .2	1.4 .2	1.3 .5	.6 .2
1.0 .2	1.0 .5	.7 .2	.8 .2	n.d.

TABLE IV-6. ROLL RATE

T STATISTICS FOR TWO MEANS

Horizontal with respect to column ( )

	n.d.	n.d.	n.d.	n.d.
	.8	.2	.9	2.9
	.0	.3	1.8	3.7
	.6	1.0	1.1	n.d.

(1)

	1.2	1.0	n.d.
	1.0	.2	2.2
	.2	1.9	3.7
	1.6	1.7	n.d.

(2)

	2.2	n.d.
	1.2	3.1
	2.1	4.0
	.1	n.d.

(3)

	n.d.
	2.0
	1.9
	n.d.

(4)

Scale factor 1 unit = 2.8% FS

Vertical with respect to row ( )

					(1)
n.d	2.0	1.8	2.8	n.d.	
n.d.	3.2	2.2	2.3	n.d.	
n.d.	.3	2.6	.4	n.d.	

					(2)
.4	1.2	.4	.5	.4	
3.1	1.7	4.3	3.2	n.d.	

					(3)
3.5	2.9	4.8	2.7	n.d.	

MEANS AND STANDARD DEVIATIONS

n.d.	.6 .1	.7 .3	.5 .2	n.d.
.9 .4	.8 .3	.9 .5	.8 .3	.6 .2
.9 .3	.9 .2	1.0 .4	.7 .3	.5 .2
.5 .1	.6 .2	.4 .1	.4 .1	n.d.

TABLE IV-7. LATERAL STICK

T STATISTICS FOR TWO MEANS

Horizontal with respect to column ( )

	n.d.	n.d.	n.d.	n.d.
	1.2	1.5	.6	1.6
	1.4	.4	1.9	2.1
	.4	.0	.9	n.d.

(1)

	3.3	.1	n.d.
	2.7	.6	.5
	1.7	.5	.8
	.4	.5	n.d.

(2)

	3.2	n.d.
	2.1	3.2
	2.3	2.5
	.9	n.d.

(3)

	n.d.
	1.1
	.2
	n.d.

(4)

Vertical with respect to row ( )

					(1)
n.d	.8	.2	1.3	n.d.	
n.d.	.6	1.0	.1	n.d.	
n.d.	.5	2.5	.2	n.d.	

					(2)
.0	.2	1.2	1.4	.5	
1.1	.3	2.7	1.5	n.d.	

					(3)
1.1	.1	1.5	.1	n.d.	

MEANS AND STANDARD DEVIATIONS

n.d.	.3 .1	.7 .5	.3 .1	n.d.
.5 .1	.4 .1	.7 .3	.5 .4	.3 .1
.5 .1	.4 .1	.6 .2	.3 .1	.3 .0
.4 .1	.4 .1	.4 .1	.3 .1	n.d.

Scale factor 1 unit = .023 rad/sec

TABLE IV-8. YAW RATE

T STATISTICS FOR TWO MEANS

Horizontal with respect to column ( )

	n.d.	n.d.	n.d.	n.d.
	1.4	.7	1.4	3.2
	1.4	.4	1.4	2.2
	1.8	.7	.7	n.d.

(1)

	.0	1.1	n.d.
	.7	.0	1.8
	1.1	2.9	3.6
	1.1	2.5	n.d.

(2)

	1.1	n.d.
	.7	2.5
	1.8	2.5
	1.4	n.d.

(3)

	n.d.
	1.8
	.7
	n.d

(4)

Vertical with respect to row ( )

					(1)
n.d	.7	.0	.4	n.d.	
n.d.	.4	.7	1.4	n.d.	
n.d.	1.1	2.2	2.5	n.d.	

				(2)
1.8	1.1	.7	1.8	.7
3.6	.4	2.2	2.9	n.d.

				(3)
1.8	1.4	1.4	1.1	n.d.

MEANS AND STANDARD DEVIATIONS

n.d.	6.2 .8	6.2 1.5	5.5 1.4	n.d.
6.8 .6	5.8 .6	6.2 .2	5.8 .5	4.5 .4
5.5 1.1	6.5 1.3	5.8 1.1	4.5 .4	4.0 .7
4.2 1.0	5.5 1.6	4.8 1.1	3.8 .8	n.d.

TABLE IV-9. PILOT RATING

Results

Based on the data presented, several trends were noted. In order to present these trends graphically, the significant differences between the cells were evaluated and plotted in the test matrix. Each of the significant differences was evaluated to determine whether that difference represented an improvement or a degradation. Figure IV-2a shows significant improvements based on control augmentation and should be read from left to right by columns. Figure IV-2b shows significant improvements based on display augmentation and should be read from top to bottom by rows. The blocks shaded in Fig. IV-2 indicate significant improvements of the variables within a test cell with respect to the configuration in the reference column or row. For example, Figure IV-2a shows four significant improvements for test cell 32, two improvements in $\dot{\theta}$ and two in δ_{B1s}. Noting that each of these improvements occurs either in reference column 1 or reference column 2, indicates that test cell 32 shows significant improvement in pitch rate and longitudinal cyclic over test cells 12 and 22. Redundant improvements have been eliminated from the figures to simplify interpretation. Once a significant improvement was noted in a test cell with respect to a lower numbered cell, it was not repeated in higher numbered test cells. For example, test cell 42 does not show improvements in $\dot{\theta}$ or δ_{B1s} in reference columns 1 and 2 which have already been noted in cell 32. Test cell 52, however shows improvements in the variables $\dot{\phi}$ and δ_{A1s} with respect to columns 1 (cell 12) and 2 (cell 22), because significant improvements in those variables with respect to the first two columns were not previously noted.

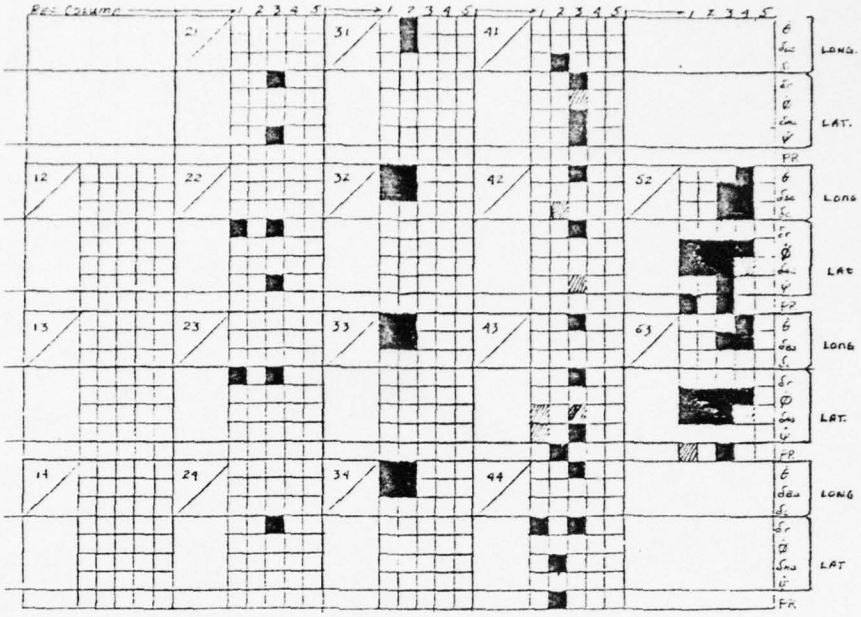

(a)

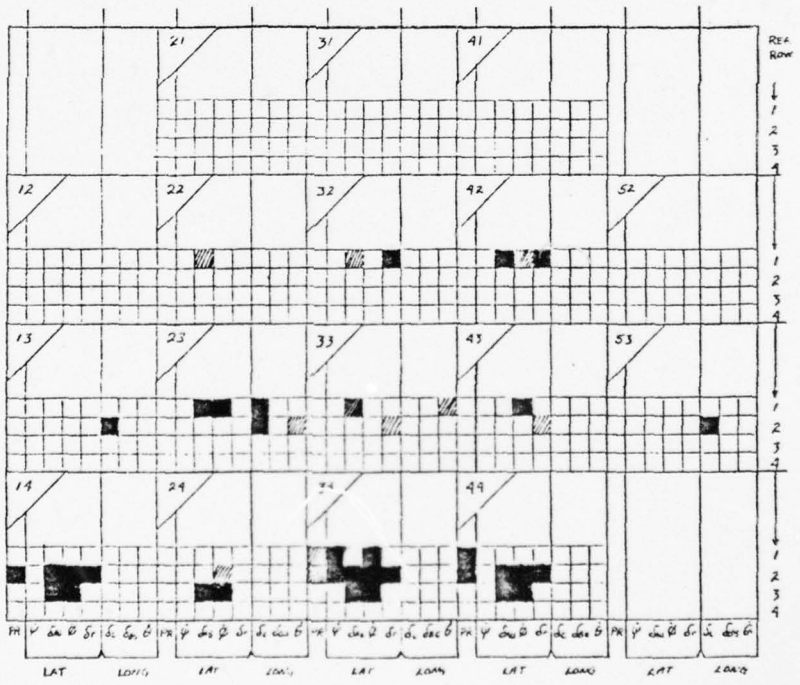

(b)

FIGURE IV-2. SIGNIFICANT REDUCTIONS IN PILOT WORKLOAD RESULTING FROM CONTROL AND DISPLAY AUGMENTATION

Hence, reduced pilot workload, indicated by the above described significant improvements, can be related to the control configuration or display configuration which effects the improvement. Further information concerning the aircraft axis in which the improvement occurs can be derived by observing the group of pertinent variables as shown in Figure IV-2.

The first noteworthy result illustrated by Figure IV-2a, as one reads left to right, is in column 2. All test cells in this column show improvements in δ_r and cells 21 and 22 show improvements in $\dot{\psi}$ as well. In most cases these improvements are shown w.r.t. column 3. This is the one instance where a higher numbered test cell represented an increase in workload. This exception can be accounted for by the fact that column 2 cells had heading-hold as did columns 4 and 5, while cells in columns 1 and 3 did not have heading-hold. As might be expected, the addition of the heading-hold appeared as an improvement in the lateral directional degrees of freedom.

A somewhat stronger result is noted in column 3. In all four display configurations a significant decrease in pilot workload is observed in terms of pitch rates and longitudinal cyclic control. This improvement is significant with respect to both of the lower numbered columns (1 and 2). Column 3 represents the rate command/attitude hold system, with no heading-hold. As might be expected, no improvement is noted in the yaw channel. One would expect, however, to observe some improvement in the roll channel. This improvement does not appear until column 4 (same control configuration as 3, but with heading-hold added). Column 4 basically shows only the significance of the heading-hold. An interesting disparity in this trend occurs in cell 44. Only one improvement in the lateral directional degrees of freedom is noted in the fourth row

until column four. This fourth row represents display configuration 4 (quickened velocity vector). It will become evident from display related results discussed later that the test subjects derived considerable lateral directional cues from the quickened vector. In the lower numbered control configurations in row 4 and to a lesser extent row 3, the vector is observed to be the predominant source of lateral cues. Not until cell 44 is the control augmentation enough to show strong improvement in this row. This improvement in cell 44, due to control augmentation, is further supported by pilot rating.

The most dramatic reductions in pilot workload occurred in control configuration 5 (attitude and attitude rate feedback system with heading-hold). Test cells 52 and 53 both show significant improvements in longitudinal and lateral directional degrees of freedom. This result is strongly supported by pilot rating.

The display related results are illustrated in Figure IV-2b. No strong improvement in pilot workload is observed in row 2, due to the addition of the Marker Star, although slight improvement in the lateral degrees of freedom is observed. This is not, however, an indication that the marker star did not improve performance, only an indication that it had no appreciable effect on workload. Row 3 shows the workload reduction resulting from addition of the velocity vector. The improvements are observed in the lateral directional degrees of freedom, although these improvements are again not strongly supported. The most interesting effect of the vector is the significant effect it has on collective control activity. This effect is observed in both of the least augmented configurations (columns 1 and 2). It also appears in control configuration 5. The vector was intended to provide course and glideslope cues, and these results indicate some reassurance that it

did.

Again the most dramatic improvements were noted in the most augmented display configuration (row 4). Here the effect of adding vector quickening on the lateral directional degrees of freedom is strongly supported in all control configurations. Pilot rating lends additional support to this observation.

Finally, an observation concerning the sensitivity of the pilot ratings compared to the objective variables is noted. In all cases, given any particular display configuration, pilot rating does not show a significant decrease in pilot workload as control augmentation increases until at least 8 improvements are observed in the objective variables at the 5% level. In the case of any aprticular control configuration, as display augmentation is increased, pilot rating does not improve significantly until at least 6 objective variables show significant reduction in pilot workload at the 5% level. In all cases, however, the pilot ratings appear to support the trends established by the objective variables.

CHAPTER V

Conclusions and Recommendations

Conclusions

Based on the results as interpreted from the data, several conclusions were drawn concerning the significance of the increments of control augmentation.

1. The heading hold system significantly reduced pilot workload in the task. The attitude hold system was effective in reducing pilot workload in the pitch attitude axis, but was not a significant improvement in the lateral directional degrees of freedom. When these two systems were combined with a display containing the vector, however (test cells 43 and 44), dramatic workload reduction occured in all axis. In the most augmented control configurations, the same dramatic workload reduction occured, but in this case, the reduction was nearly independent of display configuration.

2. The test subjects were deriving the most significant lateral attitude cues from the quickened vector which acted for them as a bank indicator. No such cue was available in the pitch axis, however, and as a result, no improvement in this axis was noted as display augmentation increased. Since pitch axis workload did decrease with control augmentation, it is concluded that the display failed to provide sufficient pitch attitude cues.

3. The vector was an effective display element in reducing pilot workload in this task. It was shown to be effective in reducing collective control activity and in providing lateral attitude cues,

especially when quickening was added.

4. The marker star was not strongly shown to be effective in reducing pilot workload. The results concerning the marker star, however, are inconclusive since this display element can be expected to show improvement in performance.

5. Finally, it is concluded that using no higher level of control augmentation than that presented in this test, display configurations can be designed which will reduce pilot workload to a satisfactory level even in the performance of the low level decelerating approach.

Recommendations

In view of the conclusions drawn above, it is recommended that further analysis be conducted on the data obtained in this test, to establish a measure of the marker star's effectiveness. It is further recommended that this analysis be extended to include flight path deviations and position errors as a measure of task performance. Regarding future testing in this area, it is recommended that the existing display format be modified to provide improved attitude information to the test subjects. This new format could be used as a baseline display for future study in this area. If this were accomplished, a new test matrix could be defined with a core centered on the most interesting portion of the present test matrix. With the addition of improved attitude cues to the display, the size of the test matrix could be reduced significantly.

APPENDIX A

Development of the Helicopter Model

a. Background

The model developed in the following pages satisfied the requirement for a reasonably accurate helicopter simulator in which the Superimposed Integrated Trajectory Error Display could be installed and evaluated under the various conditions specified in the task.

Since the nature of low-level decelerating approaches is essentially non-linear, a non-linear model was developed. The tradeoffs involved in mechanizing the model were largely those of enabling the model to perform over the range of flight conditions encountered in the low-level, low-speed approach while constraining it to operation on existing equipment. This equipment consisted of two TR48 analog computers, a fixed-base simulator cockpit with controls and instrument panel, multiple channel pen and tape recorders, and a limited amount of hard-wired auxiliary equipment fabricated in the laboratory.

Work done previosuly at Princeton by Born, Carico, and Durbin (Ref. 3); and later used by Tsoubanos (Ref. 33) demonstrated a non-linear dynamic performance and control model for the low speed regime. These works invoked the fundamental methods developed in Gessow & Meyers (Ref. 14). This model was proven to be readily mechanized on the analog computer providing a quite reasonable reproduction of the single rotor helicopter flight characteristics with no serious loss of fidelity in the cockpit. Another distinct advantage of this model is its simplicity which starts with the static performance of the helicopter treated as an accelerating point mass. The vehicle trajectory can then be determined by

rotating the axis into the inertial frame and integrating the accelerations to obtain rate and position information in the Earth fixed system.

Basically then, the model used in Ref.3 consists of a set of performance equations (force balance, power, momentum) and a set of control equations (pitching/rolling/yawing moment, rotor aerodynamic, and longitudinal/lateral cyclic-flapping relationships). These relationships determine the accelerations produced by the control inputs.

This model was used as a framework upon which a few modifications were made enabling it to perform the task at hand. Primarily those modifications were a.) expansion to include the lateral degrees of freedom, and b.) conversion to the shaft axis systems to ease manipulation of large inflow angles. Also, the assumptions were made that the shaft goes through the CG, and that the thrust vector is perpendicular to the tip path plane.

b. Nondimensionalization

The equations used in this model were nondimensionalized wrt hover conditions. Parameters of force such as thrust, T, are nondimensionalized wrt weight W, velocities wrt hover induced velocity v_h, angles wrt 1 radian, and inflow/advance ratios, λ/μ, wrt tip speed ΩR. For the purposes of this work the rotor tip speed is assumed held constant by a governor as is generally the case in turboshaft aircraft.

The nondimensionalization produces quantities such as:

Nondimensional thrust $\quad \frac{T}{W} = 1 + \frac{\Delta T}{W}$

Nondimensional velocities $\quad \bar{v}_i, \bar{u}, \bar{v}, \bar{w} = \frac{v_i}{v_h}, \frac{u}{v_h}, \frac{v}{v_h}, \frac{w}{v_h}$

$$\frac{\dot{x}}{x_g}, \frac{\dot{y}}{y_g}, \frac{\dot{z}}{z_g} = \dot{x}_{g/120}, \dot{y}_{g/120}, \dot{z}_{g/120}$$

where:

$$v_h = \sqrt{\frac{W}{2\rho\pi R^2}} \qquad \begin{pmatrix} u = 0 \\ T = w \end{pmatrix}$$

Mechanization of the nondimensionalized equations can then be accomplished on the analog computer by unity scaling each variable to its maximum value. It is of interest to note here that change in aircraft design parameter such as rotor radius or blade chord involves merely a change in scaling on the analog model.

c. Axis System and Sign Conventions

Throughout the following derivations a standard right hand axis is used in the shaft frame of reference. The accelerations resulting from the force balance equations are rotated into the earth fixed frame and integrated to produce inertial axis velocities. This rotation facilitates the addition of earth referenced wind and gust components. The resulting airspeed components are then rotated back into the shaft frame for use in the momentum equation as inflow and advance parameters. All angles, rate and accelerations are measured positive with respect to the right hand axis system except the angles affected by the angle of attack convention. Most of the literature assigns positive angle of attack to autogyros; helicopters therefore normally operate at negative angles of attack. In this work cyclic inputs B_{ls} and inclinations of the thrust vector a_{ls} which tend to produce negative angle of attack will be considered positive in a convention

which opposes the right hand axis system (See Fig. A-1). Then the flapping motions with respect to the shaft will have the following relationships.

$$a_1 = a_{1s} + B_{1s} \tag{A-1}$$

$$b_1 = b_{1s} - A_{1s} \tag{A-2}$$

The performance and control equations are derived with these basic conventions.

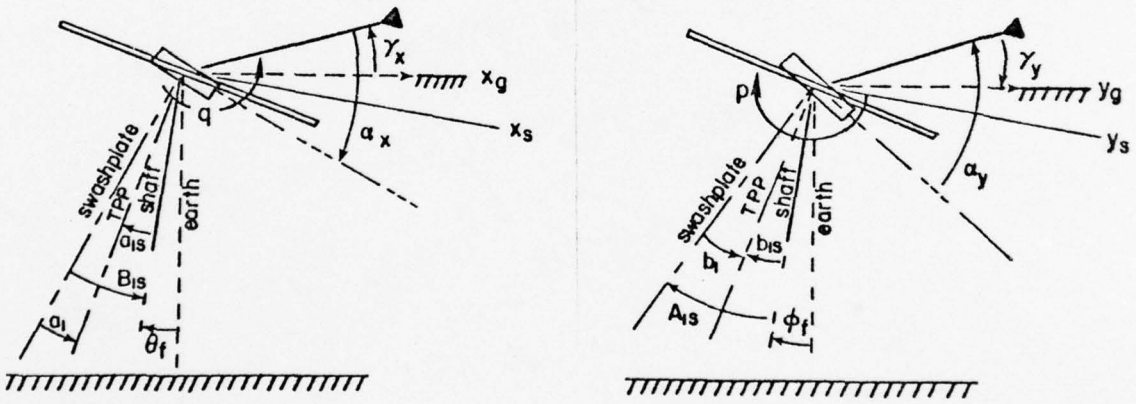

a. Longitudinal

b. Lateral

FIGURE A-1. AXIS SYSTEMS AND SIGN CONVENTION

d. Force Balance Equations

The longitudinal and lateral force balance equations are determined here in terms of the magnitude and inclination of the thrust vector. The forces produced by the horizontal stabilizer are small relative to the thrust of the main rotor and the side thrust generated by the tail rotor is considered only to counter the torque of the main rotor. The total drag of the vehicle is assumed to be a flat plate type drag proportional to (velocity)^2. Figure A-2 shows the geometrical relationship of the forces acting on the helicopter in the shaft axis.

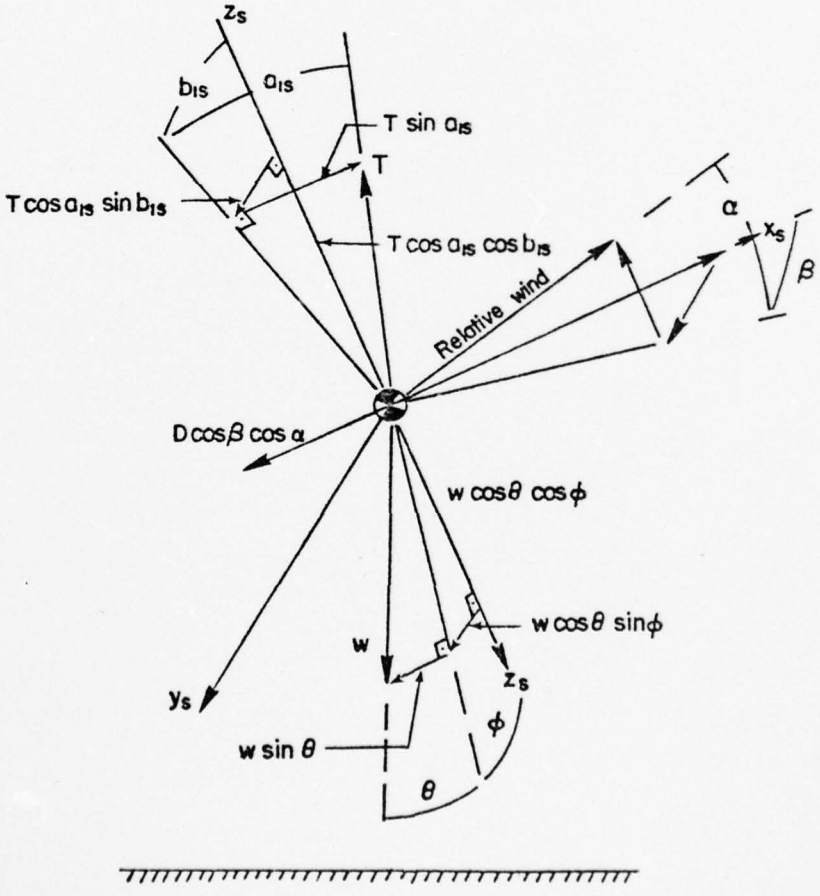

FIGURE A-2. FORCE BALANCE

The sum of the considered forces in the Z,X and Y directions is:

$$-T\cos a_{ls} \cos b_{ls} + W\cos\theta_f \cos\phi_f - m\dot{w} = 0 \qquad \text{(A-3)}$$

$$T\sin a_{ls} - W\sin\theta_f - D\cos(\theta_f - \gamma) - m\dot{u} = 0 \qquad \text{(A-4)}$$

$$T\cos a_{ls} \sin b_{ls} + W\cos\theta_f \sin\phi_f = mV\dot{\psi}\cos\phi_f = m\dot{v} = 0 \qquad \text{(A-5)}$$

where:

$$V = \sqrt{u^2 + v^2 + w^2}$$

and the flat plate drag along the x axis is the only drag term considered, primarily because of its significance in determining aircraft pitch attitude.

The H force as defined in the control axis results from the blade element lift and profile drag components reflected in the ANF when the blades flap in forward flight; this force is assumed equal to Ta_1. The thrust vector, as defined here, is the resultant vector which would be resolved in the ANF as thrust and H force. The centrifugal force terms which arises when curved flight paths are considered have been neglected here, with the exception of the lateral case. The assumption here is that the products of angular rates and lateral and vertical velocities are negligible compared with the products of angular rates and longitudinal velocity. Of the two terms in this category, only the lateral term given above has a noticeable affect in the flight conditions of this study. The radius of curvature encountered upon entering the 8^o-10^o glideslopes used in this task is considered negligible and the associated centrifugal force has no appreciable affect on the handling

qualities of the simulator. The terms involved in this approximation are shown in the axis rotation at the end of this section.

Nondimensionalizing the forces in equations A-4, A-4, and A-5, wrt W and using second order small angle approximations for a_{1s}, θ_f, and ϕ_f, one obtains:

$$-\frac{T}{W} + \frac{T}{W}\ \frac{a_{1s}^2}{2} + 1 - \frac{\theta_f^2}{2}\ - \frac{\phi_f^2}{2} = \frac{\dot{w}}{g}$$

$$\frac{T}{W}\, a_{1s} - \theta_f - \frac{D}{W}\cos(\theta_f - \gamma) = \frac{\dot{u}}{g}$$

$$\frac{T}{W}\, b_{1s} + \ _f - \frac{f}{2} - \frac{V}{g}\,\dot{\psi} + \frac{\phi^2}{2} = \frac{\dot{v}}{g}$$

or substituting $\frac{T}{W} = 1 + \frac{\Delta T}{W}$, and neglecting higher than second order terms

$$-\frac{\Delta T}{W} + \frac{a_{1s}^2}{2} - \frac{\theta_f^2}{2} - \frac{\phi_f^2}{2} = \frac{\dot{w}}{g} \qquad \text{(A-6)}$$

$$\frac{\Delta T}{W}\, a_{1s} + a_{1s} - \theta_f - \frac{D}{W}\cos(\theta_f - \gamma) = \frac{\dot{u}}{g} \qquad \text{(A-7)}$$

$$\frac{\Delta T}{W}\, b_{1s} + b_{1s} + \phi_f - \frac{\theta_f^2}{2} - \frac{V}{g}\,\dot{\psi} + \frac{\phi_f^2}{2} = \frac{\dot{v}}{g} \qquad \text{(A-8)}$$

The above equations, A-6, A-7, and A-8 express the normalized accelerations in the shaft axes. Figure A-3 shows the analog mechanization of these relationships. These shaft axes accelerations are transformed to earth fixed accelerations before integration. The rotations, assuming θ_f, ϕ_f, and ψ_f are small angles, are derived from the standard axis transformation in Table A-1.

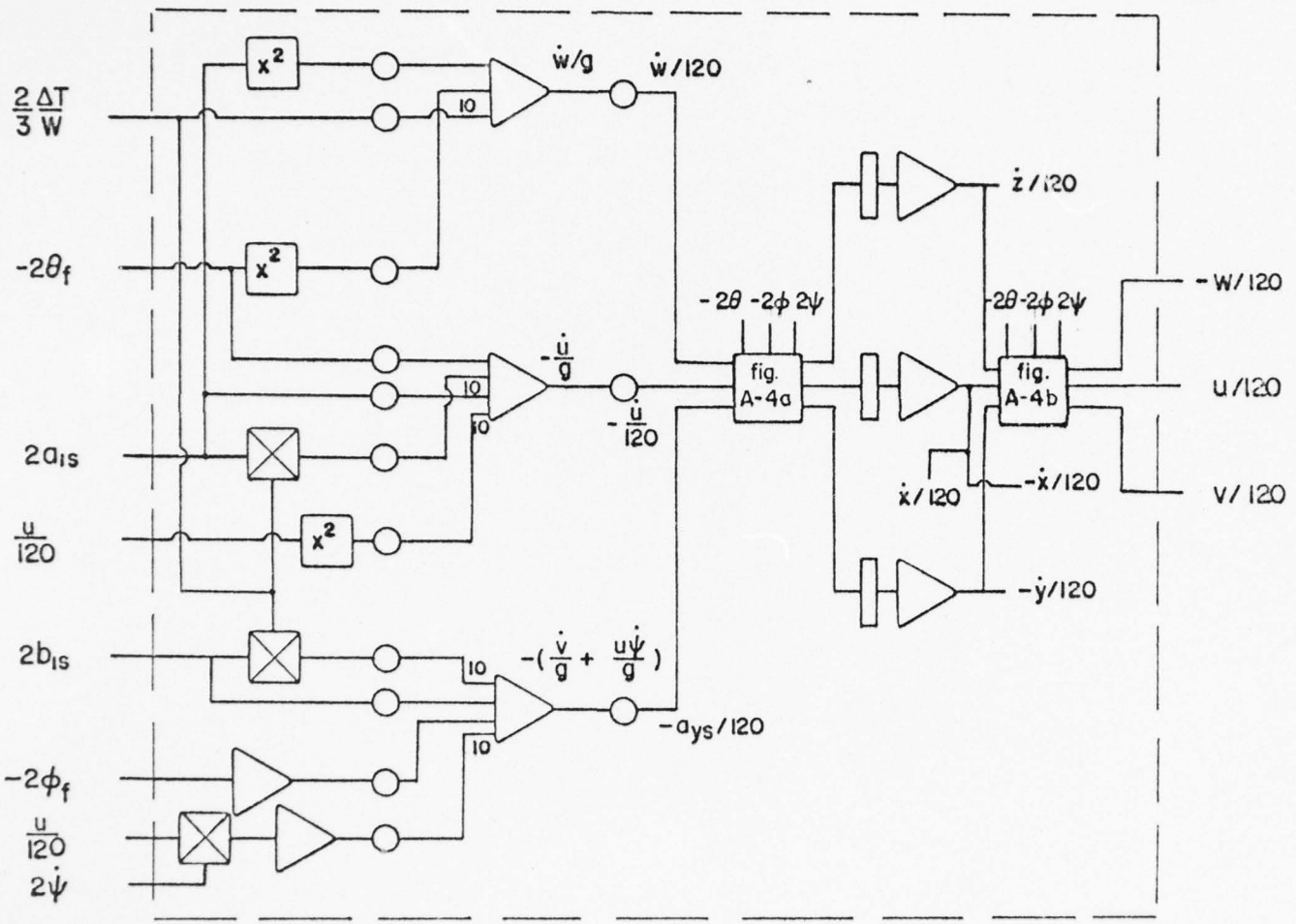

FIGURE A-3. COMPUTER DIAGRAM OF FORCE BALANCE EQUATIONS

	SHAFT AXIS COORDINATES		
	x	y	z
Earth fixed coordinates x_g	$\cos\theta \cos\psi$	$\sin\phi \sin\theta \cos\psi - \cos\phi \sin\psi$	$\cos\phi \sin\theta \cos\psi + \sin\phi \sin\psi$
y_g	$\cos\theta \sin\psi$	$\sin\phi \sin\theta \sin\psi + \cos\phi \cos\psi$	$\cos\phi \sin\theta \sin\psi - \sin\phi \cos\psi$
z_g	$-\sin\theta$	$\sin\phi \cos\theta$	$\cos\phi \cos\theta$

TABLE A-1

AXIS CONVERSION TABLE

The matrix for the transformation is used in the equation below:

$$\begin{bmatrix} \ddot{x}_g \\ \ddot{y}_g \\ \ddot{z}_g \end{bmatrix} = \begin{bmatrix} 1 & -\psi_f & 0 \\ \psi_f & 1 & 0 \\ 0 & 0 & 1 \end{bmatrix} \begin{bmatrix} 1 & 0 & \theta_f \\ 0 & 1 & 0 \\ -\theta_f & 0 & 1 \end{bmatrix} \begin{bmatrix} 1 & 0 & 0 \\ 0 & 1 & -\phi_f \\ 0 & \phi_f & 1 \end{bmatrix} \begin{bmatrix} a_{xs} \\ a_{ys} \\ a_{zs} \end{bmatrix}$$

where:

$$a_{xs} = \dot{u} + w\dot{\theta}_f - v\dot{\psi}_f \simeq \dot{u}$$

$$a_{ys} = \dot{v} + u\dot{\psi}_f - w\dot{\phi} \simeq \dot{v} + u\,\dot{\psi}_f$$

$$a_{zs} = \dot{w} + v\dot{\phi}_f - u\dot{\theta} \simeq \dot{w}$$

As previously indicated, all products of angular rate and velocity, with the exception of $u\dot{\psi}$, have been considered negligible for the purpose of this simulation.

Neglecting products of small angles, the equations become:

$$\ddot{x}_g = a_{xs} - a_{ys}\,\psi_f + a_{zs}\,\theta_f$$

AD-A051 242 PRINCETON UNIV N J DEPT OF AEROSPACE AND MECHANICAL--ETC F/G 1/3
A HELICOPTER SIMULATOR STUDY OF CONTROL DISPLAY TRADEOFFS IN A --ETC(U)
MAY 77 J C ADAMSON

UNCLASSIFIED NL

2 OF 2
AD
A051242

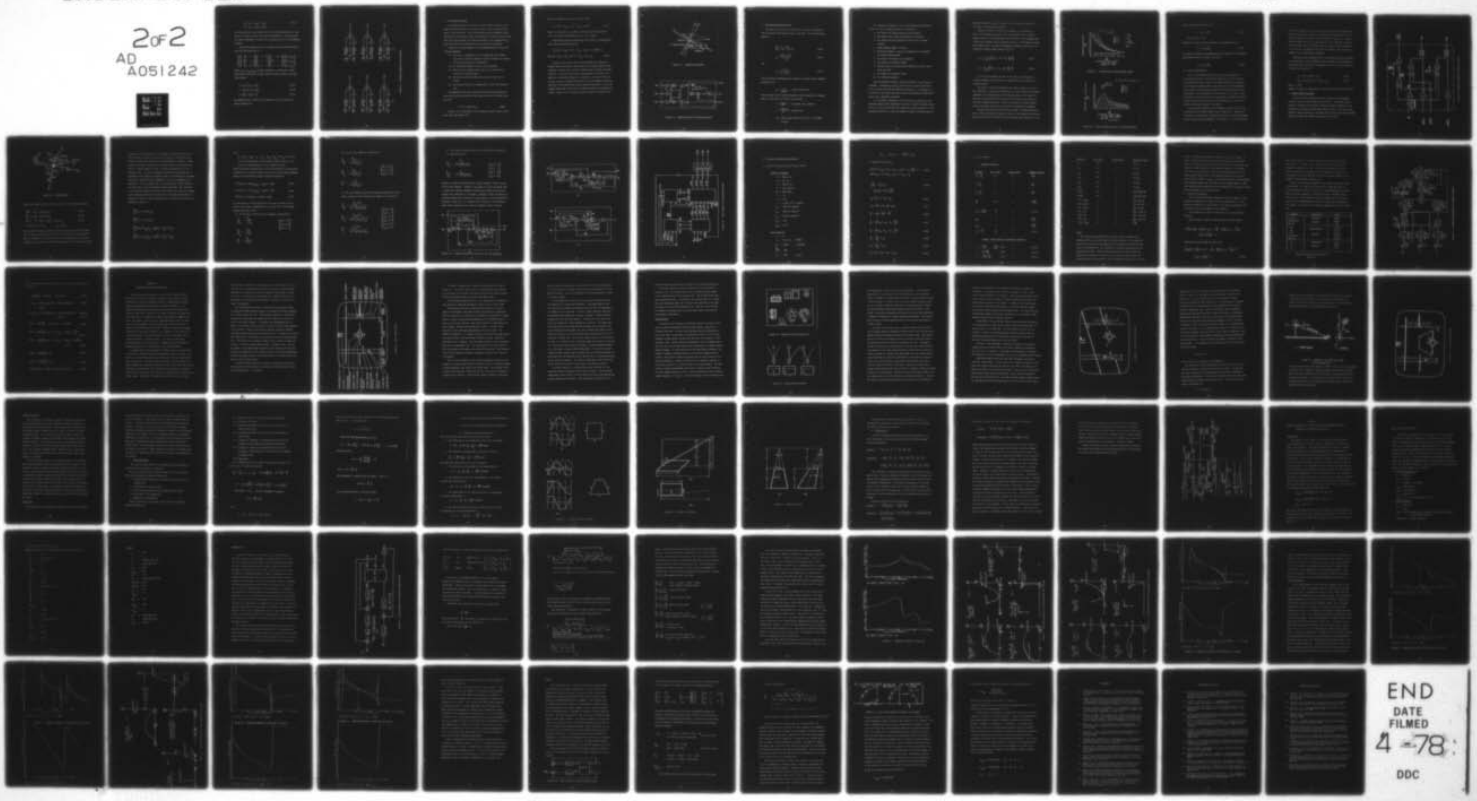

END
DATE FILMED
4-78
DDC

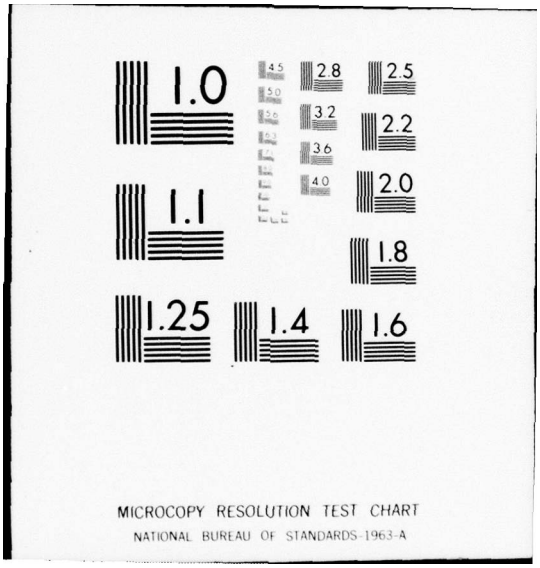
1.0
1.1
1.25
1.4
1.6
1.8
2.0
2.2
2.5
2.8
3.2
3.6
4.0
4.5
5.0
5.6
6.3
7.1
8.0
9.0
10
11
12
14
16
18
20
22
25
28
32
36
40
45
50
56
63
71
80
90
100
MICROCOPY RESOLUTION TEST CHART
NATIONAL BUREAU OF STANDARDS-1963-A

$$\ddot{y}_g = a_{ys} + a_{xs}\psi_f - a_{zs}\phi_f \qquad \text{(A-11)}$$

$$\ddot{z}_g = a_{zs} - a_{xs}\theta_f + a_{ys}\phi_f$$

The accelerations, thus rotated into earth fixed parameters, are integrated to produce velocity and position information. The velocities are again transformed to shaft axis velocities for use in the momentum equation.

The matrix equation used for rotating the earth fixed velocities back into the shaft axis is:

$$\begin{bmatrix} u \\ v \\ w \end{bmatrix} = \begin{bmatrix} 1 & 0 & 0 \\ 0 & 1 & \phi_f \\ 0 & -\phi_f & 1 \end{bmatrix} \begin{bmatrix} 1 & 0 & -\theta_f \\ 0 & 1 & 0 \\ \theta_f & 0 & 1 \end{bmatrix} \begin{bmatrix} 1 & \psi_f & 0 \\ -\psi_f & 1 & 0 \\ 0 & 0 & 1 \end{bmatrix} \begin{bmatrix} \dot{x}_g + u_{w/g} \\ \dot{y}_g + v_{w/g} \\ \dot{z}_g + w_{w/g} \end{bmatrix}$$

where: $u_{w/g}$, $v_{w/g}$, $w_{w/g}$ are gust components in earth axes. Again, neglecting the products of small angles and with no gusts, the equations become:

$$u = \dot{x}_g + \dot{y}_g \psi_f - \dot{z}_g \theta_f \qquad \text{(A-13)}$$

$$v = -\dot{x}_g \psi_f + \dot{y}_g + \dot{z}_g \phi_f \qquad \text{(A-14)}$$

$$w = \dot{x}_g \theta_f - \dot{y}_g \phi_f + \dot{z}_g \qquad \text{(A-15)}$$

The mechanization of both sets of equations for axis rotation is shown in Figure A-4.

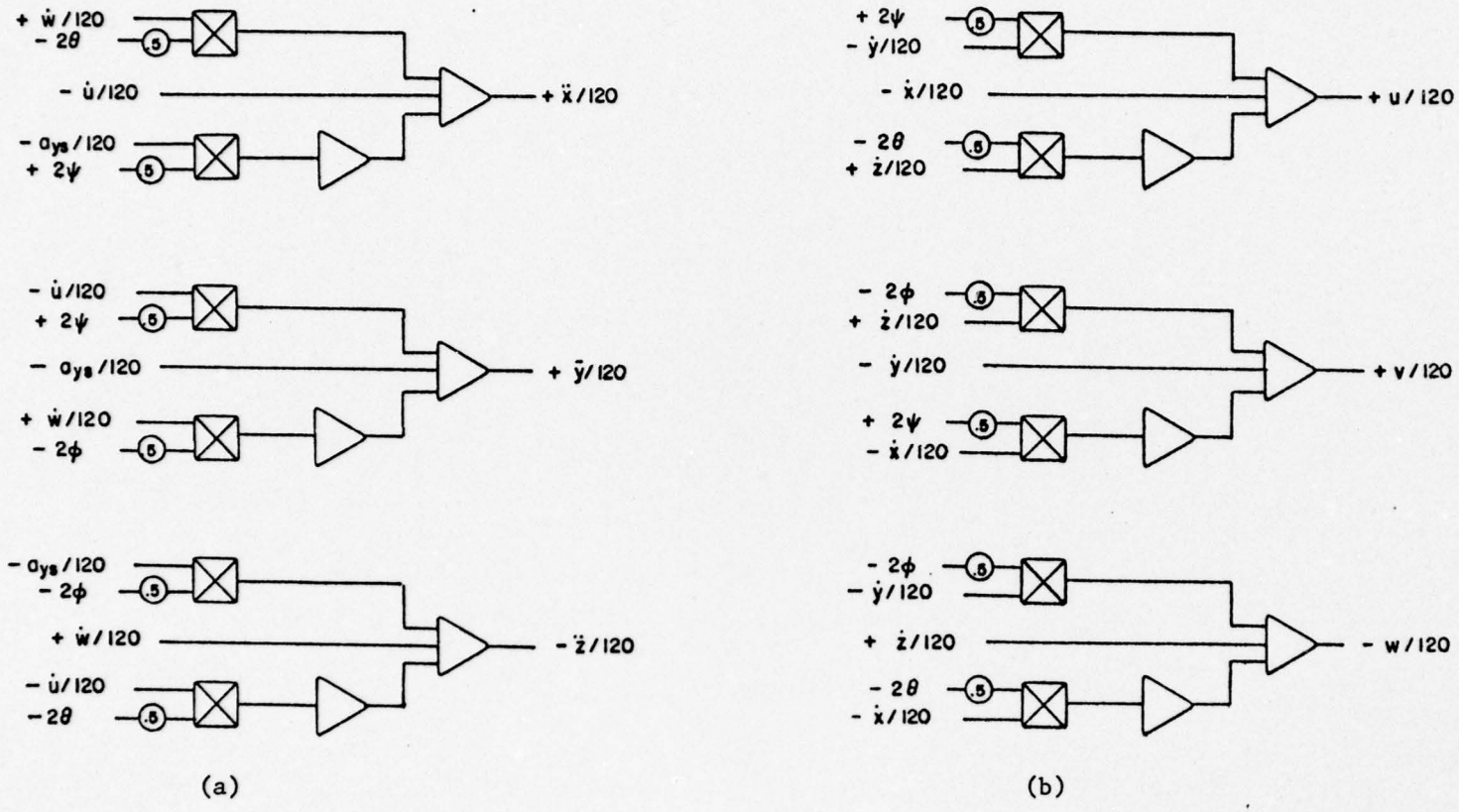

FIGURE A-4. COMPUTER DIAGRAM OF AXIS ROTATIONS

e. The Momentum Equation

The momentum equation was used to relate induced velocity to the magnitude and incidence of the thrust vector, and the velocity components in the shaft axis. Since the induced velocity parameter is perpendicular to the plane of tips, the resolution of shaft axis velocities into this plane produces the inflow and advance ratio parameters (λ_{TP}, μ_{TP}) which were later converted for use in the rotor equations.

Inherent in the development of the momentum equation are the following assumptions:

(a) The rotor is considered to be an infinitely thin actuator disc with an infinite number of blades allowing it to accelerate the air mass with no periodicity.

(b) No rotational energy is lost to the slipstream.

(c) The air is an inviscid fluid; that is, no losses are incurred due to profile drag.

(d) The flow is uniform through the rotor disc with no tip losses.

(e) The induced velocity is perpendicular to the rotor plane of tips.

The momentum theory then states that the thrust produced by the rotor disc equals the mass flow rate times the velocity change across the disc.

$$T = \dot{m}\Delta v = (\rho A V')(2v_i) \qquad \text{(A-16)}$$

where V' is the magnitude of the resultant velocity vector at the rotor disk (See Figure A-5).

With the assumption that a_{ls} is a small angle.

$$V' = [(\bar{u} + \bar{w}\, a_{ls})^2 + (\bar{w} - \bar{u}\, a_{ls} - \bar{v}_i)^2]^{\frac{1}{2}} \qquad \text{(A-17)}$$

where all velocities in the above relation have been normalized w.r.t. the hover induced velocity (e.g., $\bar{v}_i = v_i/v_h$).

Substituting the above expression into (A-16) in nondimensional form, and using $2\rho\pi R^2 v_h = W$ yields

$$\bar{v}_i^2\, [(\bar{u} + \bar{w}\, a_{ls})^2 + (\bar{w} - \bar{u}\, a_{ls} - \bar{v}_i)^2] - (1 + \frac{\Delta T}{W})^2 = 0$$

$$\text{where } \bar{u} + \bar{w}\, a_{ls} = \mu_{TP} \text{ and } \bar{w} - \bar{u}\, a_{ls} - \bar{v}_i = \lambda_{TP} \qquad \text{(A-18)}$$

Because of the quartic form of the equation, this method of finding induced velocity is well suited to the analog computer where nonlinear circuitry can be used in closed loops to produce real-time solutions. The time lag in such a mechanization is virtually nil, making it an excellent choice for a simulator. Using the values of v_i, λ_{TP}, and μ_{TP} in Equation A-18 above, the blade element theory provides the rotor dynamics and control equations necessary to close the computational loops around the force balance relations previously described. Figure A-6 is the analog computer diagram of Equation A-18.

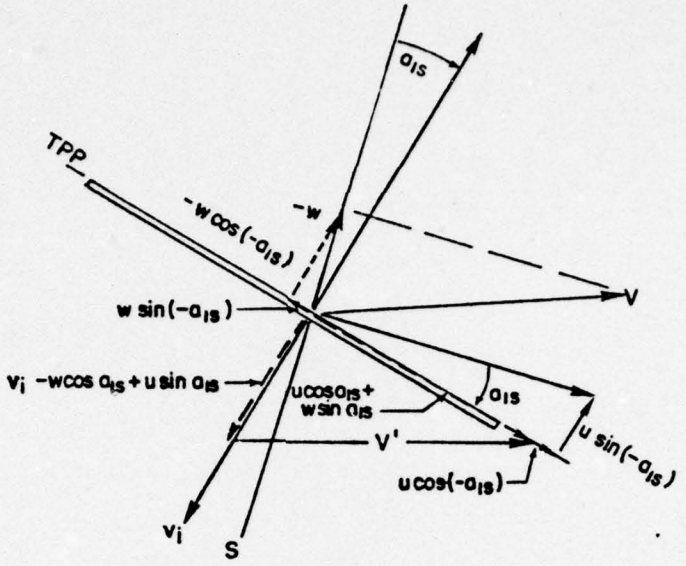

FIGURE A-5. MOMENTUM RELATIONSHIP

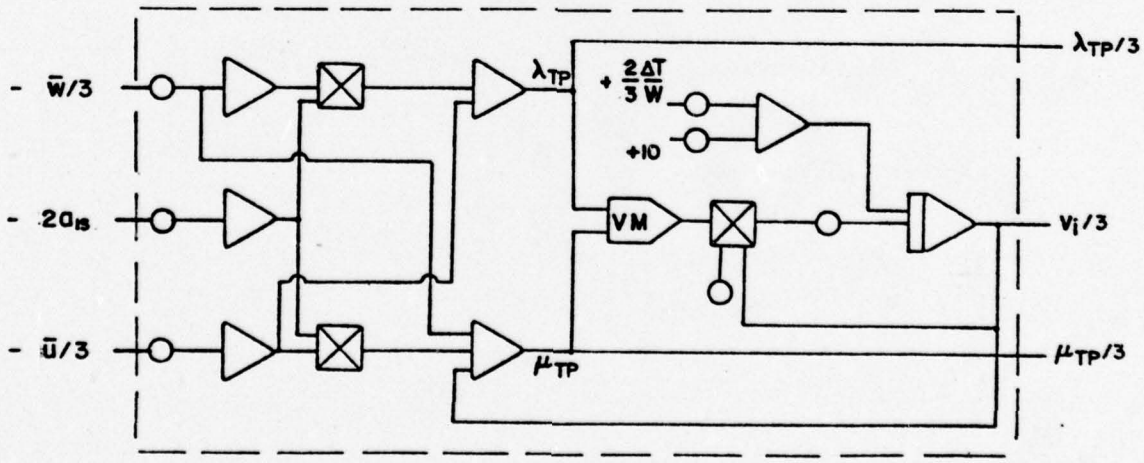

FIGURE A-6. COMPUTER DIAGRAM OF MOMENTUM EQUATION

f. Helicopter Control Equations

Reference 14 derives the expressions for thrust and flapping from the simple blade element theory in the ANF. For forward flight these are

$$\frac{2C_T}{a\sigma} = \frac{\theta_c}{3} + \frac{\mu^2\theta_c}{2} + \frac{\lambda}{2} \qquad \text{(A-19)}$$

$$a_1 = \frac{\mu(\frac{8}{3}\theta_c + 2\lambda)}{1 - \frac{1}{2}\mu^2} \qquad \text{(A-20)}$$

and

$$b_1 = \frac{4\mu a_o}{3(1 + \frac{1}{2}\mu^2)} \qquad \text{(A-21)}$$

Since the above relationships are derived in the ANF, their component parameters are:

$$C_T = \frac{T}{\rho A(\Omega R)^2} = \text{thrust coefficient}$$

where, based on small angle assumptions, thrust magnitude is assumed equal in shaft axis and control axis systems.

$$\mu = \frac{v\cos\alpha}{\Omega R} = \text{tip speed ratio (advance)}$$

$$\lambda = \frac{v\sin\alpha - v_i}{\Omega R} = \text{inflow ratio}$$

a_o = coning angle, which for the UH-1 is assumed constant

The assumptions embodied in these relationships are discussed in Ref. 14 but are summarized here for convenience.

1. The blades are assumed untwisted and untapered.
2. The radial flow at each blade element is neglected.
3. The induced velocity through the rotor disk is assumed constant.
4. Blade flapping angles are small.
5. Second and higher harmonics are neglected in calculating the blade flapping angle.
6. No reverse flow effects are considered.
7. The blades are centrally hinged.
8. Average values for profile drag coefficient and lift curve slope are used.
9. The blades are infinitely rigid.
10. Tip losses are ignored.

From the momentum equation, derived previously, λ_{TP} and μ_{TP} are available. Although λ_{TP} and μ_{TP} differ from the control axis λ and μ by a rotation through the flapping coefficient a_1. The angle a_1 is so small for this study that this rotation was ignored and these parameters were considered equivalent.

It is, however, important to note here that λ_{TP} and μ_{TP} in the momentum equation were normalized by the hover induced velocity; whereas, λ and μ in (A-19)-(A-21) were normalized by the tip speed. It was necessary therefore to scale the computer variables obtained from the

momentum equation by $3v_i/\Omega R$ in order to get the correct values for the thrust and flapping expressions.

Equations (A-20) and (A-21) are incomplete. The dynamics require a pitch damping term and a roll rate coupling term in (A-20). Equation (A-21) is not dynamically correct without a roll damping term, a pitch rate coupling, and an additional term, λ_1, which might be called the blow-back term. Writing the flapping coefficient equations to include all of these dynamic terms results in:

$$a_1 = \frac{1}{1 - \frac{\mu^2}{2}} \left\{ \mu\left(\frac{8}{3}\theta_c + 2\lambda\right) + \frac{p}{\Omega} - \frac{16}{\gamma\Omega} q \right\} \qquad \text{(A-22)}$$

$$b_1 = \frac{1}{1 + \frac{\mu^2}{2}} \left\{ \frac{4}{3}\mu a_o + \lambda_1 - \frac{q}{\Omega} - \frac{16}{\gamma\Omega} p \right\} \qquad \text{(A-23)}$$

In a later development it will be seen that the pitching and rolling responses of this model were simulated using a stability derivative scheme.

The effect of the Bell Stabilizer Bar, which is that of a lagged rate feedback to control, was simulated by a viscous damper in the moment equations. The contributions of the damping terms in A-22 and A-23, however, were separated from the M_q and L_p derivatives and fed back to the above flapping equations. As far as the vehicle response simulation is concerned, this did not constitute a compromise in handling.

The blow-back effect λ_1 predicted by Coleman in a NACA Wartime Report (L-126) represents the change in slope of the induced velocity curve when the rotor wake blows back with forward speed (See Figures A-7, A-8).

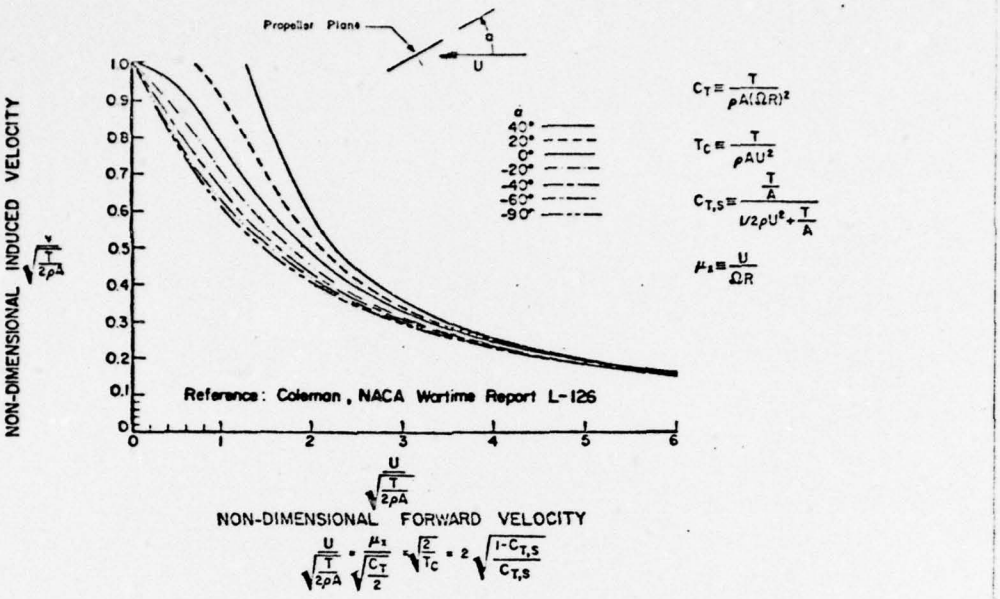

FIGURE A-7. INDUCED VELOCITY FROM MOMENTUM THEORY

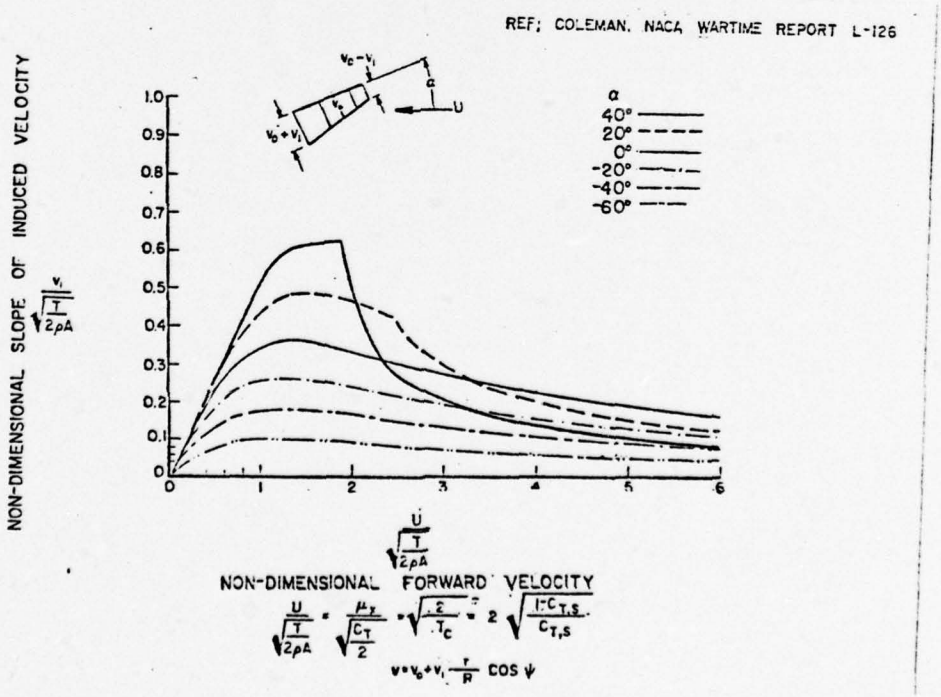

FIGURE A-8. SLOPE OF INDUCED VELOCITY VS FORWARD VELOCITY

Coleman quantified this effect as:

$$\lambda_1 = \bar{v}_i \tan \frac{X}{2} \qquad \text{(A-24)}$$

where $\tan X = (-\frac{\mu}{\lambda})$

Comparison of the two curves suggests an approximation for λ_1

$$\lambda_1 = \bar{v}_i \frac{V}{V + 2\bar{v}_i} \qquad \text{(A-25)}$$

but Harris concluded from experimental data presented to the American Helicopter Society in January, 1972 that:

$$\lambda_1 = \bar{v}_i \frac{V}{V + \bar{v}_i} \qquad \text{(A-25a)}$$

is a closer approximation.

All of this indicates that the λ_1 term is significant at low speeds near hover, and the pilot would have to move the cyclic stick forward and left at about a 45^o angle initially to translate his helicopter straight ahead. Near the end of a decelerating approach, however, with other non-uniform flow effects caused by wake interactions, the significance of this term is not as clear. Since the effect occurs near the end of the maneuver considered, and principally affects only the lateral stick deflections, it was not included in the final version of the model.

The preceding discussion of the flapping coefficients has been restricted to the forward flight case for simplicity. Expansion of the model to allow lateral translation involves a parallel development using a lateral advance parameter, ν, instead of μ. The contribution

of lateral translation to the inflow was neglected in this simulation. The important effect achieved by including the flapping equations for lateral flight was realistic rolling response of the model. Since in this work there was no real requirement to hover laterally at any significant speed, and it was assumed that the tasks would be performed at or close to a coordinated trim point in sideslip, this was not considered to be a significant compromise.

Combining these considerations of the handling qualities desirable in the simulator, and the assumption that the blades flap instantly to the steady state flap angle, the equations for the rotor flap angles in the shaft axis system are:

$$a_{1s} = 8/3\ \theta_c\ \mu + 2\lambda\mu - B_{1s} \qquad \text{(A-26)}$$

$$b_{1s} = 8/3\ \theta_c\ \nu + 2\lambda\nu + 4/3\ \mu a_o + A_{1s} \qquad \text{(A-27)}$$

where $\nu = v/\Omega R$

Figure A-9 shows the mechanization of equations (A-19)(A-26) and (A-27).

g. Moment Balance Equations

The force balance equations and the coordinate transformations involve the three aircraft angles θ_f, ϕ_f and ψ_f. The moment balance equations determine the pitching, rolling and yawing responses of the fuselage to the rotor and antitorque control inputs. For ease in mechanization these responses are decoupled in the rolling and pitching modes. Figure A-10 shows the moments considered in this model.

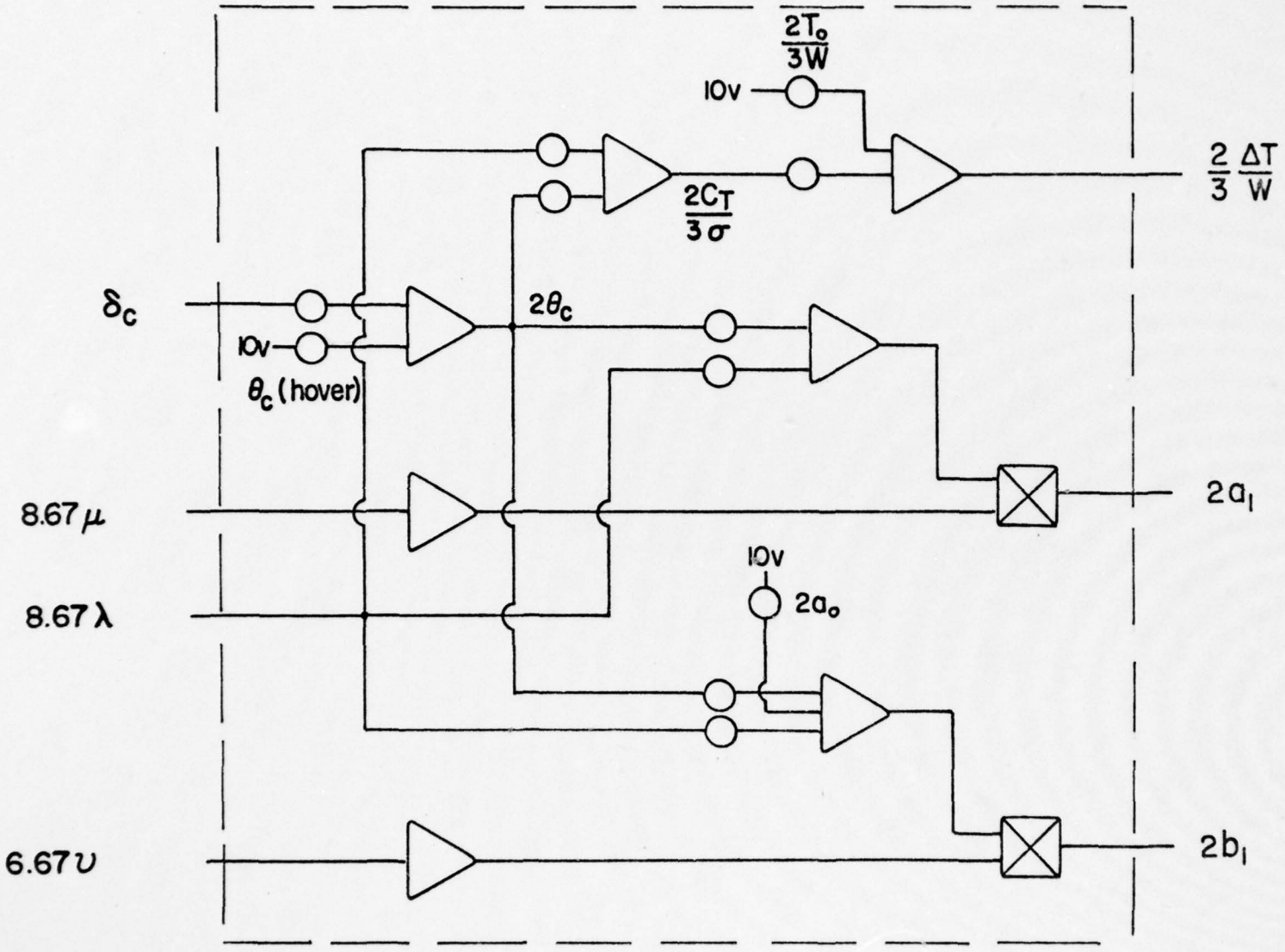

FIGURE A-9. COMPUTER DIAGRAM OF CONTROL EQUATIONS

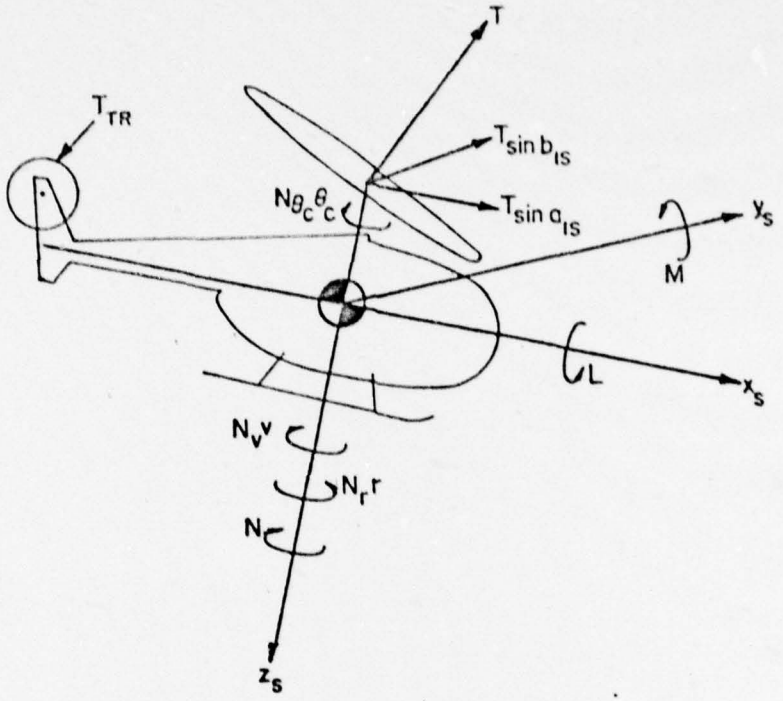

FIGURE A-10. MOMENT BALANCE

Summing the moments about each axis results in the following equations:

$$\sum M = I_{yy}\ddot{\theta}_f = h_{cg}T(a_1 - B_{1s}) \qquad \text{(A-28)}$$

$$\sum L = I_{xx}\ddot{\phi}_f = h_{cg}T(b_1 + A_{1s}) \qquad \text{(A-29)}$$

$$\sum N = \ddot{\psi}_f = N_{\delta r}\delta_r + N_{\theta c}\theta_c + N_v v + N_r r \qquad \text{(A-30)}$$

where: $a_{1s} = a_1 - B_{1s}$, $b_{1s} = b_1 + A_{1s}$

These equations assume a centrally hinged rotor, and that the shaft goes the CG. They assume that the tail rotor contribution to the rolling moment is negligible, as is the horizontal tail contribution to the speed stability, M_u. In order to rewrite these equations in a form which permits

flexibility in the construction of automatic stabilization sytems, it was desirable to replace the controls B_{ls} and A_{ls} in the above equations with forms more suitable to the development of feedbacks. Additionally, the UH-1 stabilizer bar transfer function was replaced with that of a viscous damper in order to simplify mechanization of the feedback loops. The loss in frequency response resulting from the replacement of the lagged rate feedback with a rate feedback was warranted because the aircraft was not intended for use in its unaugmented configuration. If the simulator was to be used without further stabilization this lag in the rate feedback should be included. The remainder of the inherent damping in the UH-1 is the $16/\gamma\Omega$ term, which is included in the flapping coefficient for each axis. Expanding the flapping coefficient in terms of their component parts, including the terms for the feedbacks, results in:

$$\frac{Th_{cg}}{I_{yy}} a_1 = M_u u + M_{a_1} \dot{\theta}_f$$

$$\frac{Th_{cg}}{I_{xx}} b_1 = L_v v + L_{b_1} \dot{\phi}_f$$

$$\frac{Th_{cg}}{I_{yy}} B_{ls} = M_{B_{lp}} \delta_{B_{ls}} + M_{BAR} \dot{\theta}_f + M_{s_q} \dot{\theta}_f + M_{s_\theta} \theta_f$$

$$\frac{Th_{cg}}{I_{xx}} A_{ls} = L_{A_{lp}} \delta_{A_{ls}} + L_{BAR} \dot{\phi}_f + L_{s_q} \dot{\phi}_f + L_{s_\phi} \phi_f$$

where

$M_q = (M_{a_1} + M_{BAR})$, $L_p = (L_{b_1} + L_{BAR})$, $M_{B_{lp}}$ and $L_{A_{lp}}$ are pilots control effectiveness, and derivatives subscripted sq, sθ, sp and sφ are feedback gains for the augmented systems.

Substituting these expanded forms into the pitching and rolling moment equations, and including feedback terms in the yawing moment equations results in the following Laplace transformed equations:

$$[s^2 - M_q s]\ \theta_f = M_u u + M_{B_{lp}} \delta_{B_{ls}} + M_{sq} s\theta_f + M_{s\theta} \theta_f \qquad \text{(A-31)}$$

$$[s^2 - L_p s]\ \phi_f = L_v v + L_{A_{lp}} \delta_{A_{ls}} + L_{sp} s\phi_f + L_{s\phi} \phi_f \qquad \text{(A-32)}$$

$$[s^2 - N_r s]\ \psi_f = N_v v + N_{\delta_r} \delta_r + N_{sr} s\psi_f + N_{s\psi} \psi_f \qquad \text{(A-33)}$$

For the purpose of characterizing the attitude responses to pilot input in the various configurations, let u and v↦0. The following transfer functions result.

1) For the basic aircraft with no automatic stabilization:

$$\frac{\theta_f}{\delta_{B_{ls}}} = \frac{M_{B_{lp}}}{s^2 - M_q s}$$

$$\frac{\phi_f}{\delta_{A_{ls}}} = \frac{L_{A_{lp}}}{s^2 - L_p s}$$

$$\frac{\psi_f}{\delta_r} = \frac{N_{\delta_r}}{s^2 - N_r s}$$

$$\begin{bmatrix} M_q \simeq -.50 \\ L_p \simeq -1.23 \\ N_r \simeq -1.1 \end{bmatrix}$$

2) For the rate augmented configuration:

$$\frac{\theta_f}{\delta_{B_{ls}}} = \frac{M_{B_{lp}}}{s^2-(M_q+M_{sq})s}$$

$$\frac{\phi_f}{\delta_{A_{ls}}} = \frac{L_{A_{lp}}}{s^2-(L_p+L_{sp})s}$$

$$\frac{\psi_f}{\delta_r} = -\frac{N_{\delta_r}}{s^2-(N_r+N_{sr})s}$$

$$\begin{bmatrix} M_{sq} \simeq -2.0 \\ L_{sp} \simeq -5.0 \\ N_{sr} \simeq -4.4 \end{bmatrix}$$

3) The rate command attitude hold system incorporated an integrator and lead circuit between the cockpit and the control.

$$\frac{\theta_f}{\delta_{B_{ls}}} = \frac{M_{B_{lp}}(s+1)}{s[s^2-(M_q+M_{sq})+M_{s\theta}]}$$

$$\frac{\phi_f}{\delta_{A_{ls}}} = \frac{L_{A_{lp}}(s+1)}{s[s^2-(L_p+L_{sp})s+L_{s\phi}]}$$

$$\frac{\psi_f}{\delta_r} = \frac{N_{\delta_r}(s+1)}{s[s^2-(N_r+N_{sr})s+N_{s\psi}]}$$

$$\begin{bmatrix} M_{sq} \simeq -1.0 \\ L_{sp} \simeq -\ 0 \\ N_{sr} \simeq -3.4 \\ M_{s\theta} \simeq 10 \\ L_{s\phi} \simeq 10 \\ N_{s\psi} \simeq 10 \end{bmatrix}$$

4) The attitude command system for the pitch and roll channels is characterized by:

$$\frac{\theta_f}{\delta_{B_{ls}}} = \frac{M_{B_{lp}}}{s^2-(M_q+M_{sq})s+M_{s\theta}}$$

$$\frac{\phi_f}{\delta_{A_{ls}}} = \frac{L_{A_{ip}}}{s^2-(L_p+L_{sp})s+L_{s\phi}}$$

$$\begin{bmatrix} M_{sq} \simeq -1.0 \\ L_{sp} \simeq 0 \\ M_{s\theta} \simeq 10 \\ L_{s\phi} \simeq 10 \end{bmatrix}$$

Figure A-11 shows the mechanization of these feedback systems in each of the three channels. Appendix C discusses in detail the method used to design the complete automatic stabilization systems using the most complex case considered as an example. Appendix C shows the effects of coupling whereas those effects have been avoided in this simplified presentation. Figure A-12 is a complete block diagram of the helicopter model which incorporates the computer diagrams already discussed.

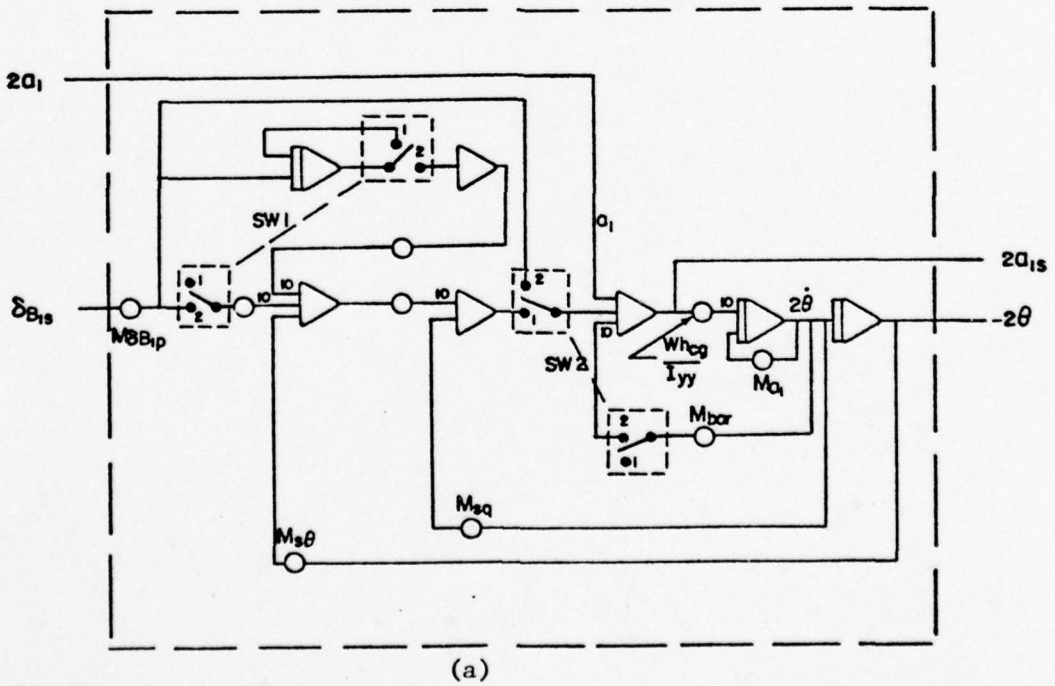

(a)

FIGURE A-11. COMPUTER DIAGRAM OF PITCH, ROLL, AND YAW EQUATIONS

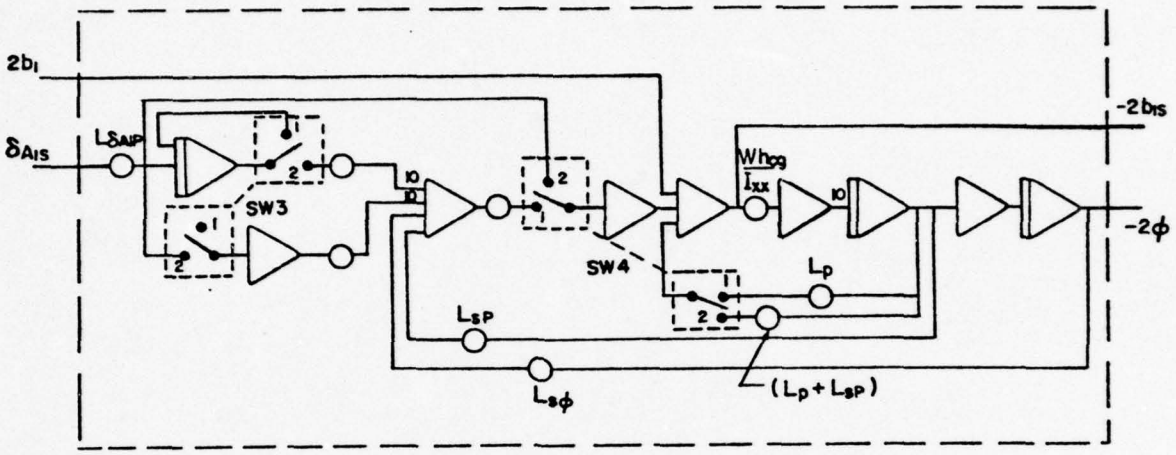
2b1
δAIS
LδAIP
SW3
SW4
Whpg
Ixx
-2bIS
-2φ
Lp
LsP
Lsφ
(Lp + LsP)

(b)

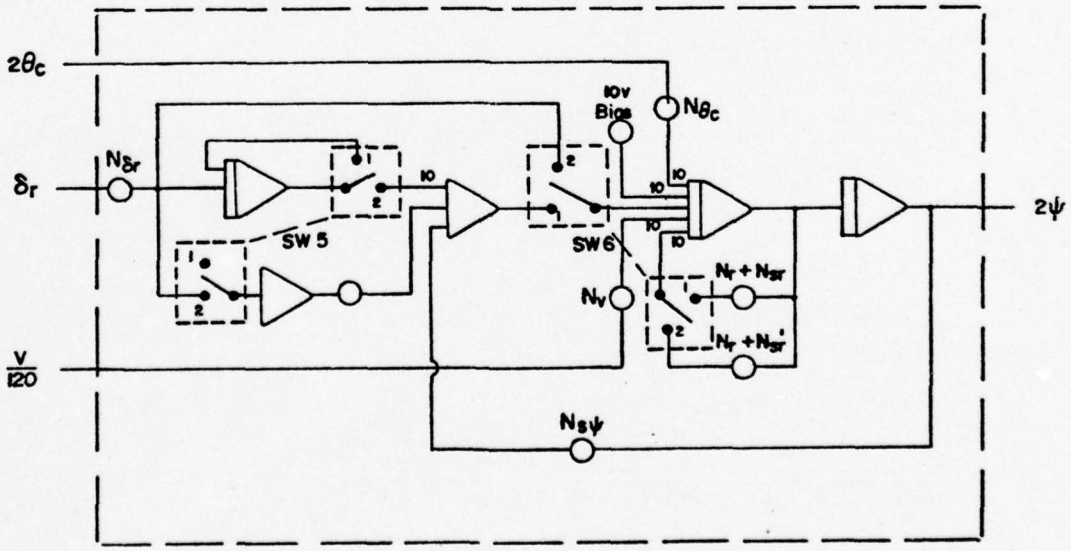
2θc
10V
Bias
Nθc
Nδr
δr
SW5
SW6
Nr + Nsr
Nv
Nr + Nsr'
V/120
Nsψ
2ψ

(c)

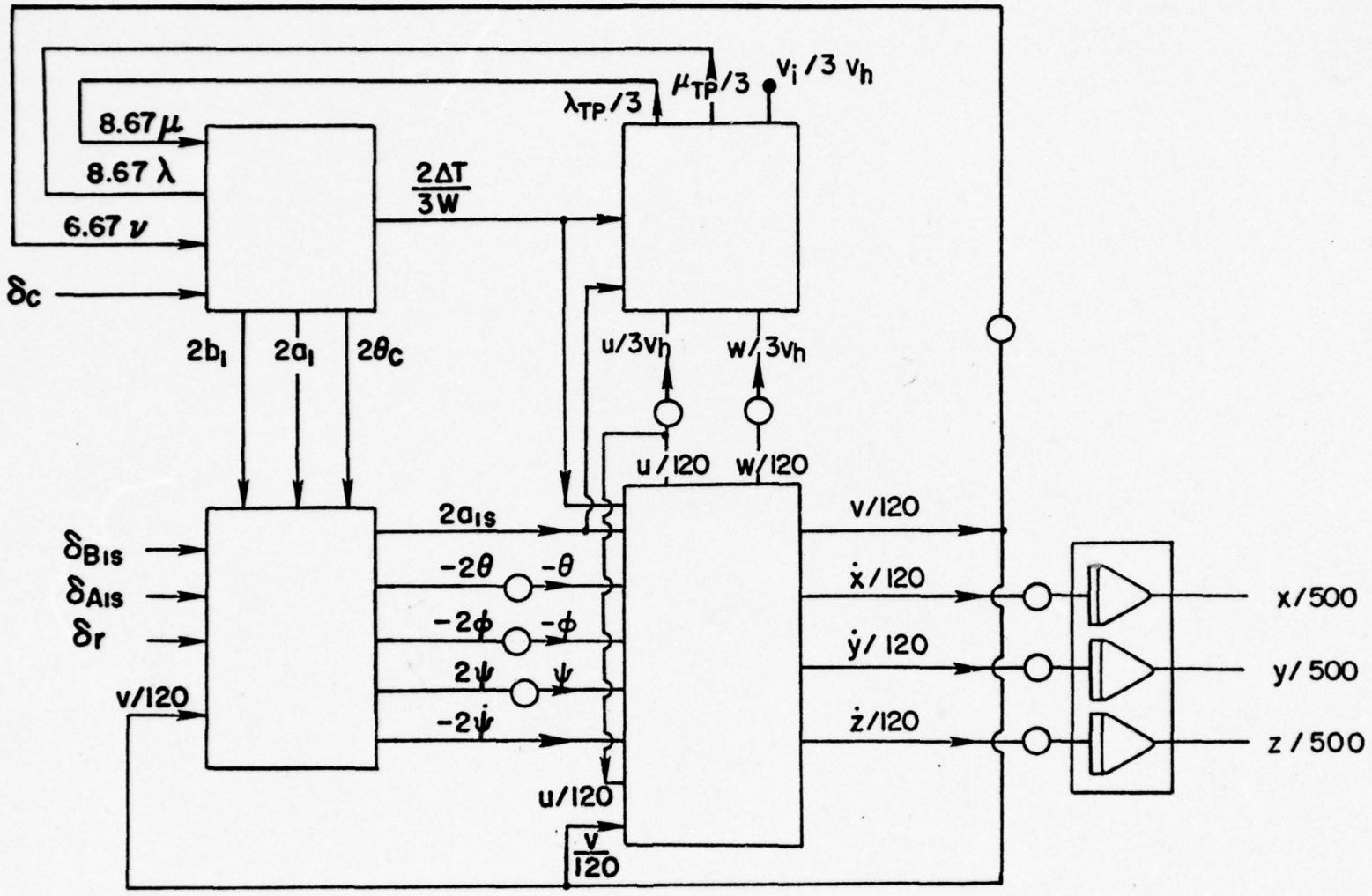

FIGURE A-12. BLOCK DIAGRAM OF THE HELICOPTER MODEL

h. Scaling of Variables and Equations

1. Aircraft Configuration and Constant Values.

CONSTANT PARAMETERS

$W = 8012.2$ lbs

$R = 24.1$ ft

$A = 1824.67$ ft^2

$\Omega = 33.2$ rad/sec

$\Omega R = 800$ ft/sec

$\sigma = .05$

$a = 5.73$

$\rho = 2.3769 \times 10^{-3}$ slugs/ft^3

$I_{xx} = 3256.724$ slugs/ft^2

$I_{yy} = 10095.37$ slugs/ft^2

$I_{zz} = 8183.752$ slugs/ft^2

$h_{cg} = 6.56'$

$\ell_{TR} = 27.31'$

HOVER CONDITION

$T = W$

$v_h = 30.77$ fps $= \sqrt{W/2\rho A}$

$C_{Th} = .00289 = W/\rho A(\Omega R)^2$

$\frac{2C_{Th}}{a\,\sigma} = .0202$

$\lambda_h = .0385 = -\dot{v}_h/\Omega R$

$$\theta_{ch} = .118 \text{ rad} = 3\left(\frac{2\,C_{Th}}{a\,\sigma} - \frac{1}{2}\,\lambda_h\right)$$

2. Equations To Be Scaled

$$\bar{v}_i^{\,2}\left[(\bar{u} + \bar{w}\,a_{1s})^2 + (\bar{w} - \bar{u}\,a_{1s} - \bar{v}_i)^2\right] - \left(1 + \frac{\Delta T}{W}\right)^2 = 0 \qquad \text{(A-18)}$$

where $\mu_{TP} = \bar{u} + \bar{w}\,a_{1s}$, $\lambda_{TP} = \bar{w} - \bar{u}\,a_{1s} - \bar{v}_i$

$$\frac{2\,C_T}{a\,\sigma} = \frac{\theta_c}{3} + \frac{1}{2}\,\lambda \qquad \text{(A-19a)}$$

where $\frac{T}{W} = 49.63\left(\frac{2\,C_T}{a\,\sigma}\right)$

$$a_{1s} = \frac{8}{3}\,\theta_c\,\mu + 2\lambda\mu - B_{1s} \qquad \text{(A-26)}$$

$$b_{1s} = \frac{8}{3}\,\theta_c\,\nu + 2\lambda\,\nu + \frac{4}{3}\mu\,a_o + A_{1s} \qquad \text{(A-27)}$$

$$\frac{\dot{w}}{g} = -\frac{\Delta T}{W} + \frac{a_{1s}^2}{2} - \frac{\theta_f^2}{2} \qquad \text{(A-6a)}$$

$$\frac{\dot{u}}{g} = \frac{\Delta T}{W}\,a_{1s} + a_{1s} - \theta_f = \frac{D_{fp}}{W} \qquad \text{(A-7)}$$

$$\frac{\dot{v}}{g} = \frac{\Delta T}{W}\,b_{1s} + b_{1s} + \phi_f - \frac{V_T}{g}\,\dot{\psi} \qquad \text{(A-8a)}$$

$$\ddot{\theta}_f = \frac{h_{cg}}{I_{yy}}\,T\,a_{1s} \qquad \text{(A-28)}$$

$$\ddot{\phi}_f = \frac{h_{cg}}{I_{xx}}\,T\,b_{1s} \qquad \text{(A-29)}$$

$$\ddot{\psi}_f = N_{\delta r}r + N_r r + N_v v + N_{\theta c}\theta_c \qquad \text{(A-30)}$$

3. Scale Factors

1. MOMENTUM EQUATIONS

Variable	Max. Value	Computer Max.	Computer Variable
$\bar{v}_i = \frac{v_i}{v_h}$	3	1	$[\frac{\bar{v}_i}{3}]$
$\bar{u} = \frac{u}{v_h}$	3	1	$[\frac{\bar{u}}{3}]$
$\bar{w} = \frac{w}{v_h}$	3	1	$[\frac{\bar{w}}{3}]$
$\frac{\Delta T}{W}$	3/2	1	$[\frac{2}{3}\frac{\Delta T}{W}]$
$a_{1s} = \frac{a_{1s}}{1 \text{ rad}}$	1/2	1	$[2\ a_{1s}]$
μ_{TP}	3	1	$[\frac{\mu_{TP}}{3}]$
λ_{TP}	3	1	$[\frac{\lambda_{TP}}{3}]$
$\theta_c = \frac{\theta_c}{1}$	1/2	1	$[2\ \theta_c]$

CONTROL, FORCE BALANCE, AND DYNAMICS EQUATIONS

$\mu = [\frac{\mu_{TP}}{3}]$	$\frac{3v_h}{\Omega R} = .1154$	1	$[8.67\mu]$
$\nu = [\bar{v}] \frac{120}{\Omega R}$	.1500	1	$[6.67\nu]$
$\lambda = [\frac{\lambda_{TP}}{3}] \frac{3v_n}{\Omega R}$	.1154	1	$[8.67\lambda]$

Variable	Max. Value	Computer Max.	Computer Variable
a_1	1/2	1	$[2\ a_1]$
b_1	1/2	1	$[2\ b_1]$
a_{1s}	1/2	1	$[2\ a_{1s}]$
b_{1s}	1/2	1	$[2\ b_{1s}]$
A_{1s}	1/2	1	$[2\ A_{1s}]$
B_{1s}	1/2	1	$[2\ B_{1s}]$
$\theta,\dot{\theta},\ddot{\theta}$	1/2	1	$[2\phi],[2\dot{\phi}],[2\ddot{\phi}]$
$\psi,\dot{\psi},\ddot{\psi}$	1/2	1	$[2\psi],[2\dot{\psi}\ ,[2\ddot{\psi}]$
* $\bar{u} = u/120$	3	1	$[\bar{u}] = [u/120]$
* $\bar{v} = v/120$	1	1	$[\bar{v}] = [v/120]$
* $\bar{w} = w/120$	1	1	$[\bar{w}] = [w/120]$
* $\dot{\bar{u}} = u/g$	1	1	$[\dot{\bar{u}}] = [u/32.2]$
* $\dot{\bar{v}} = v/g$	1	1	$[\dot{\bar{v}}] = [v/32.2]$
* $\dot{\bar{w}} = w/g$	1	1	$[\dot{\bar{w}}] = [w/32.2]$
$\bar{V}_T = V_T/v_h$	4	1	$[\frac{V_T}{4}]$

*NOTE:

The accelerations generated in the force balance equations were normalized wrt g to produce computer variables whereas, in the momentum equation the velocities resulting from the integration of these accelerations are normalized wrt v_h. Elsewhere in the model velocities are normalized wrt 120 fps. These scaling variations were made to allow the computational equipment to operate over its entire voltage range. The momentum equation was hardwired, and its components operated on a ±15 volt

range. The TR48 analog computer operated on a ±10 volt range. In terms of mechanization this involved scale changes in the computer variables between the force balance equations and the integrators and between the TR48 computer and the momentum computer. For example, the computer variables $[\bar{u}] = u/120$ must be multiplied by the ratio $120/3v_h$ before being input to the momentum computer where the computer variable is $[\bar{u}/3] = u/3v_h$. All variables have been scaled against unity maximums rather than the TR48's 10 volt maximum range, so that the resulting scaled equations would be independent of voltage and could later be applied to any voltage range.

4. Scaling the Equations

Due to the nonlinearities in Equation A-18, for example, linear scaling techniques do not always result in optimum scaling. After scaling the equation via this method, it was indeed necessary to perform some local scaling changes on the computer.

The following is a sample calculation of the scaled momentum equation.

Using the above computer variables equation (A-18) becomes:

$$81[\frac{\bar{v}_i}{3}]^2[([\frac{\bar{u}}{3}] + \frac{1}{2}[\frac{\bar{w}}{3}][2\ a_{1s}])^2 + ([\frac{\bar{w}}{3}] - \frac{1}{2}[\frac{\bar{u}}{3}][2\ a_{1s}] - [\frac{\bar{v}_i}{3}])^2]$$

$$- \frac{9}{4}(\frac{2}{3} + [\frac{2}{3}\frac{\Delta T}{W}])^2 = 0$$

dividing by 81 and taking the square root

$$[\frac{v_i}{3}][([\frac{u}{3}] + \frac{1}{2}[\frac{w}{3}][2\ a_{1s}])^2 + ([\frac{w}{3}] - \frac{1}{2}[\frac{u}{3}][2\ a_{1s}] - [\frac{\bar{v}_i}{3}])^2]^{\frac{1}{2}}$$

$$- \frac{1}{6}(\frac{2}{3} + [\frac{2}{3}\frac{\Delta T}{W}]) = 0 \qquad \text{(A-18a)}$$

The above equation is scaled and ready for final voltage scaling on the computer. In order to save computer space in this model, and because this equation is such a versatile relationship, it was decided to hardwire this equation into an auxiliary box which could be rescaled as the user desired. The circuit of this equation in its hardwired form is shown in Figure A-13.

The six 741 operational amplifiers are wired to invert the signs of the inputs. Op. amps 1-3 are wired for a ciosed loop gain of 2, 4-6 are wired for a gain of 1, and 7 is a 725 instrumentation op. amp used as a leaky integrator. Essentially op amp 7 integrates the $\bar{v}_i$ error to zero. The multipliers and vector modules are self explanatory, and the potentiometers are used for scaling and for biasing in the op amps. The values of the remaining components are shown in Table A-2.

COMPONENT	DESCRIPTION	VALUE
R1,R3,R5	PRECISION	50KΩ±
R2,R4,R6-R17	RESISTOR	100KΩ±
R18,R19		10Ω±
R21	NON PRECISION	4.7KΩ±5%
R22		27Ω±5%
R23	RESISTOR	270Ω±5%
R20,R24,R25		5.1KΩ±5%
R26-R31		47KΩ±5%
C1	ELECTROLYTIC	.047μf
C2	CONTROL	.0015μf
C3		.10μf

Momentum Computer Component Values

TABLE A-2

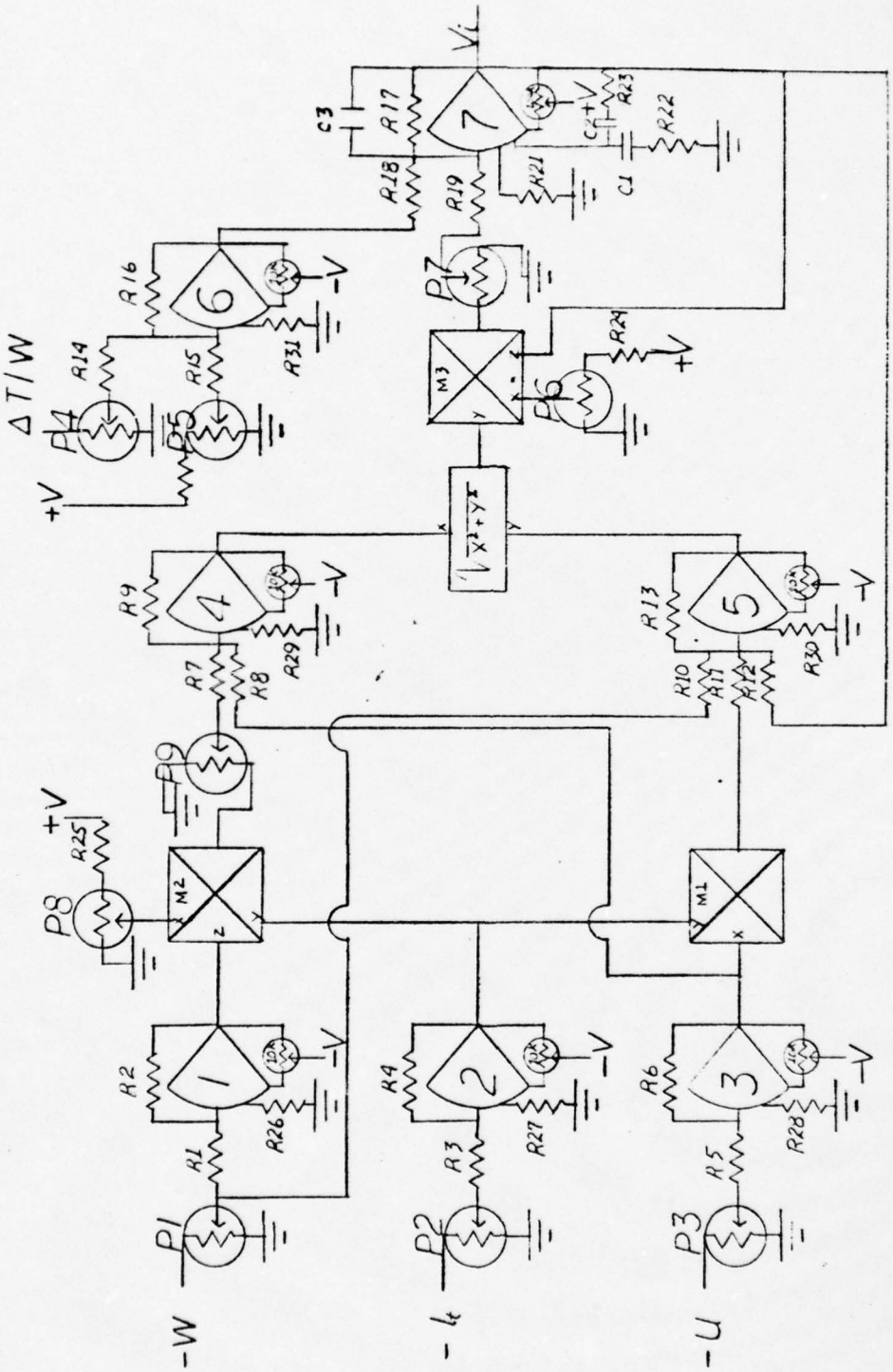

FIGURE A-13. DIAGRAM FOR HARDWIRING THE MOMENTUM EQUATION

The remaining equations are listed here in their scaled form, without development.

$$.3022[\tfrac{2}{3}\tfrac{T}{W}] = .1667[2\theta_c] - .0567[8.67\lambda] \qquad \text{(A-19b)}$$

$$[2\,a_{ks}] = .3076[2\theta_c][8.67\mu] + .0532[8.67\mu][8.67\lambda] - [2B_{1s}] \qquad \text{(A-26a)}$$

$$[2b_{1s}] = .3076\,[2\theta_c][6.67\nu] + .0532\,[6.67\nu][8.67\lambda] + .01[8.67\mu] + [2A_{1s}] \qquad \text{(A-27a)}$$

$$[\dot{\bar{w}}] = -1.5[\tfrac{2}{3}\tfrac{\Delta T}{W}] + .125\,[2\,a_{1s}]^2 - .125[2\theta_f]^2 \qquad \text{(A-6b)}$$

$$[\dot{\bar{u}}] = .75[\tfrac{2}{3}\tfrac{\Delta T}{W}][2\,a_{1s}] + .5[2\,a_{1s}] - .5[2\theta_f] - [\tfrac{D_{fp}}{W}] \qquad \text{(A-7a)}$$

$$[\dot{\bar{v}}] = .75[\tfrac{2}{3}\tfrac{\Delta T}{W}][2\,b_{1s}] + .5[2\,b_{1s}] + .5[2\phi_f] - .062[\tfrac{V_T}{4}][2\dot{\psi}] \qquad \text{(A-8b)}$$

$$[2\ddot{\theta}] = 7.809[\tfrac{2}{3}\tfrac{T}{W}][2\,a_{1s}] \qquad \text{(A-28a)}$$

$$[2\ddot{\phi}] = 24.21[\tfrac{2}{3}\tfrac{T}{W}][2\,b_{1s}] \qquad \text{(A-29a)}$$

$$[2\ddot{\psi}] = N_{\delta r}[\delta_r] + N_r[2\dot{\psi}] + 120\,N_v[\bar{v}] + N_{\theta c}[2\theta_c] \qquad \text{(A-30a)}$$

APPENDIX B

Description of the S-ITED Display

The Superimposed-Integrated Trajectory Error Display (S-ITED), developed at Princeton University and used in this simulator study, evolved from a series of studies directed at enhancing pilot performance by improving the presentation of flight information. It is generally accepted that pilots control aircraft by perceiving errors and error rates from a desired "trim" flight condition, and apply control deflections in proportion to these errors either in magnitude or time. The degree to which the pilot minimizes these errors is a measure of his performance, and if averaged over a number of pilots, a measure of the difficulty of the task. Efforts to present this needed information to the pilot originated in an analysis of the actual loop closures involved. The detailed history of this development and the rationale behind it is given in Refs. 4, 10, and 12; and, while not pertinent here in its entirety, is summarized for the purpose of understanding the use of the display in the task simulation.

A simple model of the helicopter in flight consists of three angular degrees of freedom and three translational degrees of freedom. Six variables are controlled by the pilot using four controls; longitudinal and lateral cyclic, collective pitch, and rudder. The hierarchy of the symbol augmentation required is derived from this basic model and from the knowledge that essentially four integrations are required to derive position from cyclic inputs while only two are required from collective and rudder inputs. Regardless of whether some of these loops are closed

automatically or whether the pilot must act to close them, it is clear that the job is accomplished with more facility when the positioning information is displayed in the most "natural" way possibly in terms of errors. It should also be mentioned that attention was given to providing only the essential information to perform the task so as to reduce "cluttering".

The S-ITED has been termed an "abstract analog display" because it generates various abstract symbols to represent the flight variables in an analog format on a CRT. These abstract symbols are formed from lissajous patterns which are displaced on the CRT by the analog voltage of the motion variable. The symbols are superimposed over an image of the actual terrain as seen by a forward looking camera mounted in the aircraft. Early in the display research, methods to improve the symbol-image integration were pursued as well as methods of utilizing this capability in the absense of ground-based position measuring equipment. From this work the present display format as shown in Figure B-1 evolved, as did the terrain marking symbol or "marker star". The improvements in the symbol-image integration were derived primarily from studies and comparisons of the various levels of the symbol augmentation hierarchy discussed earlier, and through choices of variables and references at each of these levels.

The display modes used in this study are derivatives of this earlier research and in particular are versions of Display Format I which is described in Ref. 4 as follows:

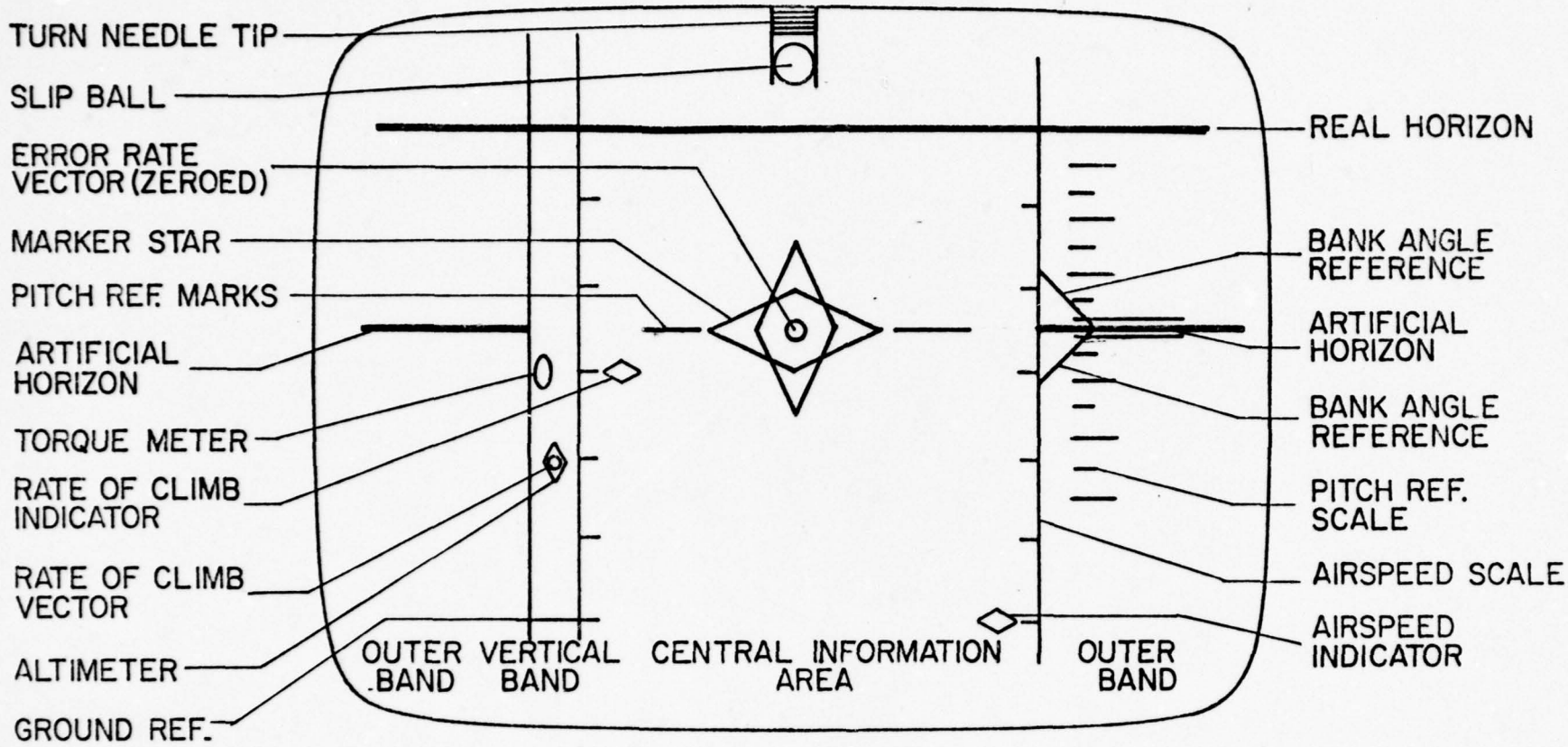

FIGURE B-1. BASIC DISPLAY FORMAT

"The basic configuration of symbols in this format is shown in Figure B-1. The entire display area is subdivided into four regions as indicated at the bottom of the Figure: Horizon Left, Horizon Right, Vertical Information Band, and Central Information Area."

On the following pages the rest of the description and Figure B-1 were modified to describe the display format as used in this study.

The artificial horizon is shown only in the areas on the two sides of the display; zero pitch and zero bank angle are illustrated. The zero position of the horizon on the display corresponds to an image seen by a camera looking down approximately 8 to 10 degrees with respect to zero pitch altitude. Bank angle reference is provided by the long triangle moving with the horizon in pitch. Its cusp is referenced for zero bank angle independent of the pitch angle. Its length corresponds to $\pm$ 15 degrees so that the horizon bar going through the opposite ends of the bank angle reference triangle indicates a bank angle of $\pm$ 15 degrees. The bank angle reference on the right-hand side plays an additional role. Its cusp points at the pitch scale so that the absolute pitch angle can be read off this scale. The spacings on this scale represent 2½ degree increments in pitch, for a total of $\pm$ 15 degrees.

There are four symbols in the vertical information band and on its boundary: an altitude and climb rate reference line, an altitude diamond, a ground reference line, and an oval torque meter. The spacings on the altitude scale represent 25 feet so that the scale shown corresponds to a range of 0 to 150 feet. The situation shown in Figure B-1 indicates

that the pilot is hovering at an altitude of 50 feet (the ground line is 75 feet below the altitude reference) and the helicopter is at the desired altitude. In low level flight, the altitude diamond is driven by a radar altimter.

In the middle and at the top of the central information area is the symbology of a needle-ball indicator. The displacement of one full width of the needle tip represents the turn rate corresponding to a 2-minute turn (3.0 deg/sec). A pair of pitch reference lines and a star-shaped marker symbol and a vector are shown in nominal position aligned with the artificial horizon. In Figure B-1, the error rate vector is shrunk into a point showing zero velocity. The marker symbol always moves up and down with the TV image and the horizon. The pitch reference and the marker star can be biased with respect to the horizon by means of the vertical thumb wheel control shown on the left-hand side in Figure B-2. This control enables the pilot to use the marker star as a "pointer" with a selectable angle with respect to horizontal. The pointer may be used to represent a desired glideslope angle or, in hovering, a steeper down-looking angle. As stated, the pitch reference lines, rather than coinciding with the artificial horizon, are moved down with the symbology in the central area for improved proximity of the attitude reference. The vertical thumb wheel control moves the entire marker star portion of the display, including the vector.

A terrain feature or a nominal descent path laterally off the helicopter plane of symmetry can be chosen by means of the horizontal thumb wheel control (Fig. B-2) which shifts the entire superimposed symbology sideways on the display. This adjustment is needed only in a

crosswind approach and has not been used in the study presented here.

Three more symbols are shown in Figure B-1 in the central information area. An airspeed scale and an airspeed indicator appear on the right-hand side of the central area. The airspeed scale spacings represent 10 knots. Accordingly, the airspeed shown is 0 knots. The third additional symbol is a rate-of-climb indicator on the left-hand side of the central information area. The short lines serving as altitude scale serve also as rate-of-climb scale; their spacing corresponds to 500 ft/min.

Terrain Marker

The marker star was given an additional function in order to help extract position information from the image display, especially in precision hovering. In hover, the horizontal position components can be derived from a visual image by watching the motions of two terrain elements straight ahead, one near,the other far, with respect to fixed reference lines. During lateral displacements, the near element moves more than the one far away, whereas this relationship is opposite during heading changes. For the extraction of the longitudinal component, the change in apparent spacing between the two terrain elements must be watched. This kind of mental processing does not result easily in sensitive information. Figure B-3 illustrates the ambiguity inherent in the relative motion of a terrain feature on an image display. The same relative lateral displacement occurs with no change in hover position, but with changed heading, as with a lateral displacement and no heading change (Figure B-3, b and c). A similar ambiguity arises involving pitch

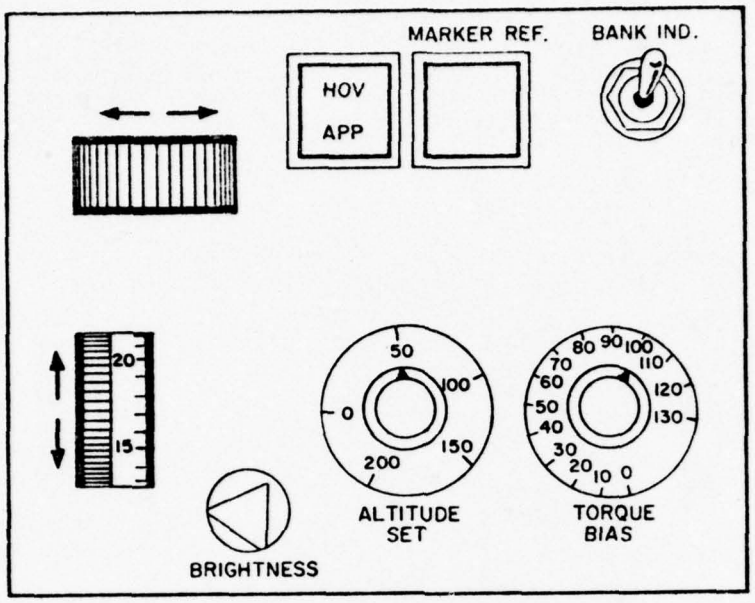

FIGURE B-2. MARKER STAR MODE SELECTOR UNIT

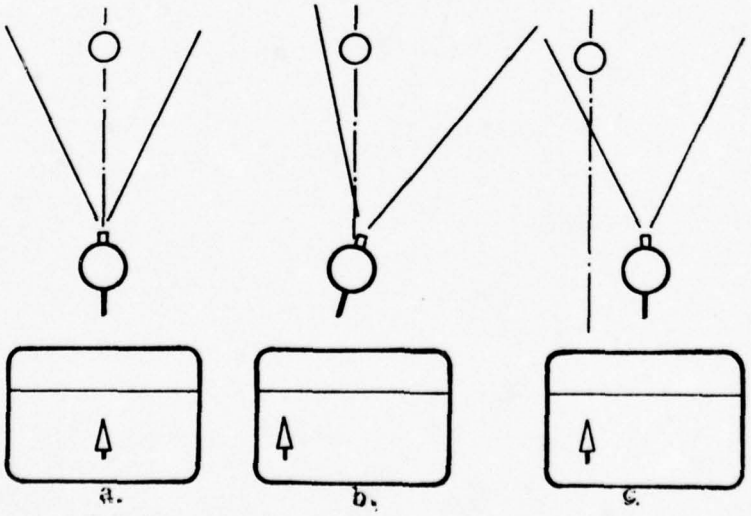

FIGURE B-3. IMAGE DISPLAY AMBIGUITY

and longitudinal as well as vertical displacements. A considerable improvement can be expected if a terrain element at some subtended angle is "marked" by a symbol that stays with it during angular motions of the helicopter. In this case, the terrain element leaving the marker is an easily interpreted indication of deviations from a virtual attitude-stabilized light beam extending from the helicopter to the ground. The marker representing this beam can also be used effectively to enhance the display for unaided approach and landing. The longitudinal accuracy at hover depends greatly on the accuracy with which altitude is held.

In order to create the visual stabilized light beam, the role of the star-shape symbol is somewhat modified when the pilot activates the "Marker Reference" pushbutton switch on the Control Unit. The heading angle at the time of activation serves as reference from this time on. The deviations from this refernce is shown by the star. Heading deviation is indicated by lateral motion of the star and terrain feature with respect to the center display position, while lateral position deviation is shown as a marker star displacement wrt the terrain feature; pitch deviation is shown by the deviations of the marker star with respect to the pitch reference lines which remain fixed at all times. In other words, the motion of the star is such that it stays with a chosen terrain feature while the aircraft is pitching, rolling and yawing if there is no translation. Therefore, when the Reference switch is on, the symbol serves as a terrain marker or glideslope indicator. The marker symbol also provides quantitative pitch and yaw angle information

because the half-widths of the diamonds are adjusted to represent 2½ degrees. Accordingly, the situation in Figure B-4 shows a nose-up pitch angle deviation of 2½ degrees. Thus, the terrain marker plays a dual role: in order to keep the heading as desired, the marker star should remain centered in the display. In order to keep the helicopter position stationary, with respect to the chosen terrain feature, this feature should remain inside the marker star. The larger the down-looking angle chosen by the pilot, the easier it is to perceive longitudinal deviations from a desired position.

Essentially, with the terrain marker, the positioning task amounts to "illuminating" a chosen terrain feature while maintaining close altitude control at the same time. The star shape was chosen for two reasons: in order to avoid obscuring the reference feature with the superimposed symbology and to facilitate quantitative indication of pitch and heading deviations with the same symbol.

The rest of the symbology in Figure B-4 indicates the following flight situation: forward flight at 60 knots airspeed, an instantaneous turn rate of 3 deg/sec, a bank angle of approximately 15 degrees. The altitude is 75 feet, diminishing at a rate of approximately 500 ft/min.

Additional symbols which have been used throughout the tests include the torque symbol, a real horizon and a landing pad symbol to substitute the terrain video and the use of a color CRT. The symbology appears on the CRT in colors that were chosen to aid the pilot in discriminating among flight variable information, visual terrain information, and the static reference grid. The flight variable symbols appear yellow, the landing pad and horizon appear green, and the reference grid orange.

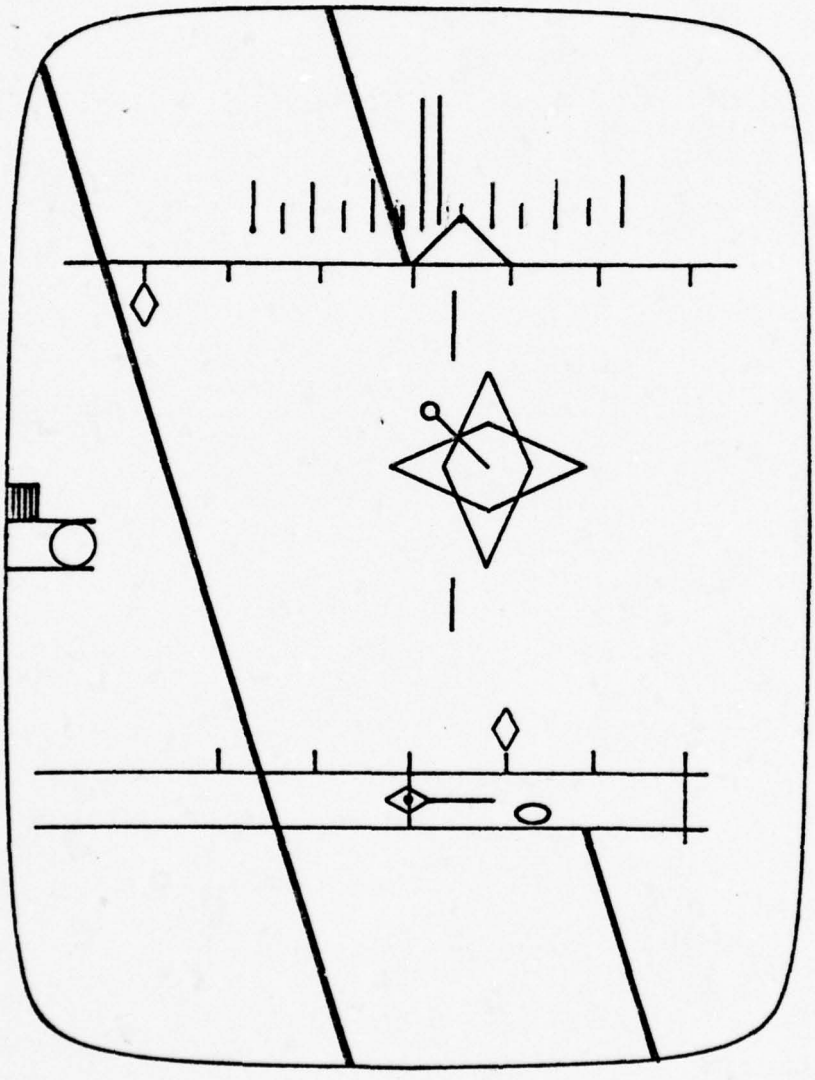

FIGURE B-4. DISPLAY FLIGHT SITUATION

Additionally, two of the display configurations for the experiment employ a vector. In one mode the vector indicates velocity information only. In the second mode the vector represents velocity quickened by added attitude information. This quickening is designed to aid the pilot by requiring less lead compensation than does the velocity information only. Based on exploratory work performed in decelerating approaches and hover, using this display, a significant modification was made to the error rate vector in the approach mode. The vector in the hover mode remained unchanged in that it was used to indicate x and y axis velocities with respect to an intended hover point on the earth. In the approach mode, however, the inputs to the vector were changed so that the vector would indicate flight path error rate with respect to the preselected glideslope or down-looking angle of the marker star. Figure B-5 shows the geometry involved in this modification. In the approach the aircrafts descent rate must satisfy the relationship,

$$\dot{x} \tan \gamma_o - \dot{Z} = 0$$

if the aircraft is to remain on the glideslope.

The left side of this relationship was used as the input to the vertical deflection circuits of the error rate vector. In this way the vector shrinks to zero length only when the above glideslope relationship is satisfied. In the lateral direction the vector was similarly modified to indicate course error rate. In this case the pertinent relationship is:

$$\dot{y} - \dot{x} \tan \psi_{ref} = 0$$

where, ψ_{ref} is the approach course selected by the pilot at the time the marker star is activated. After marker star activation, the lateral deflections of the vector indicate course error rate and the vertical deflections indicate glideslope error rate.

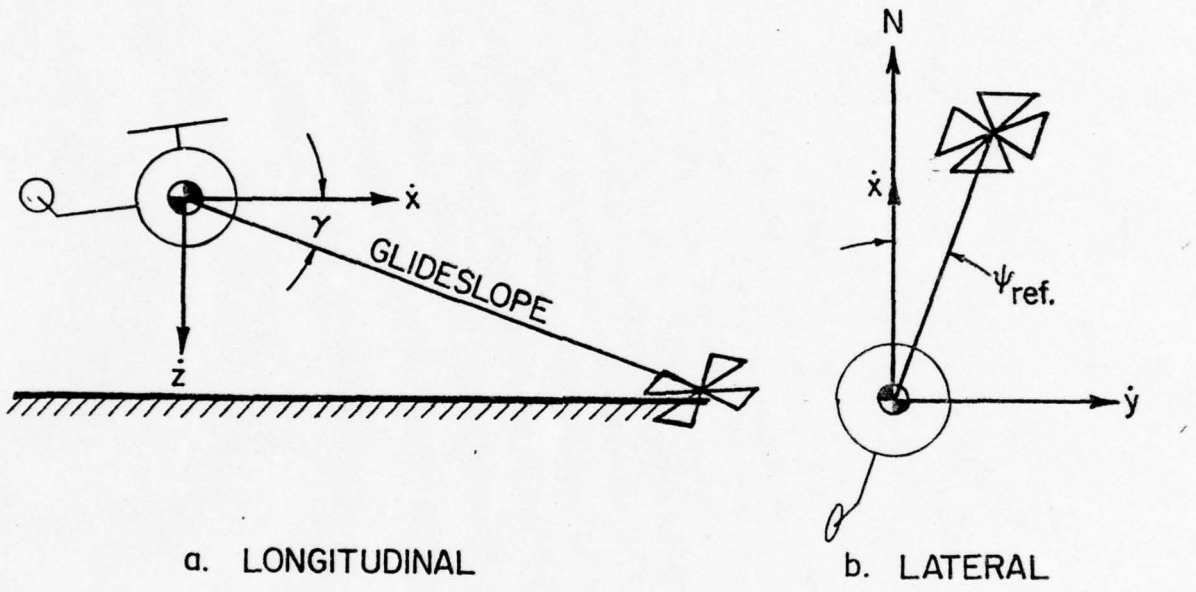

FIGURE B-5. GEOMETRY OF THE ERROR RATE VECTOR IN THE APPROACH MODE

In the hover mode the vector inputs are simply $\dot{x}$ and $\dot{y}$, and are independent of descent rate or heading. Figure B-6 shows the display in the hover mode. The vector indicates that the aircraft is translating in the direction of the vector. For hover, the vector must be kept zeroed, and the desired altitude must be maintained by referencing the vertical information band of the display.

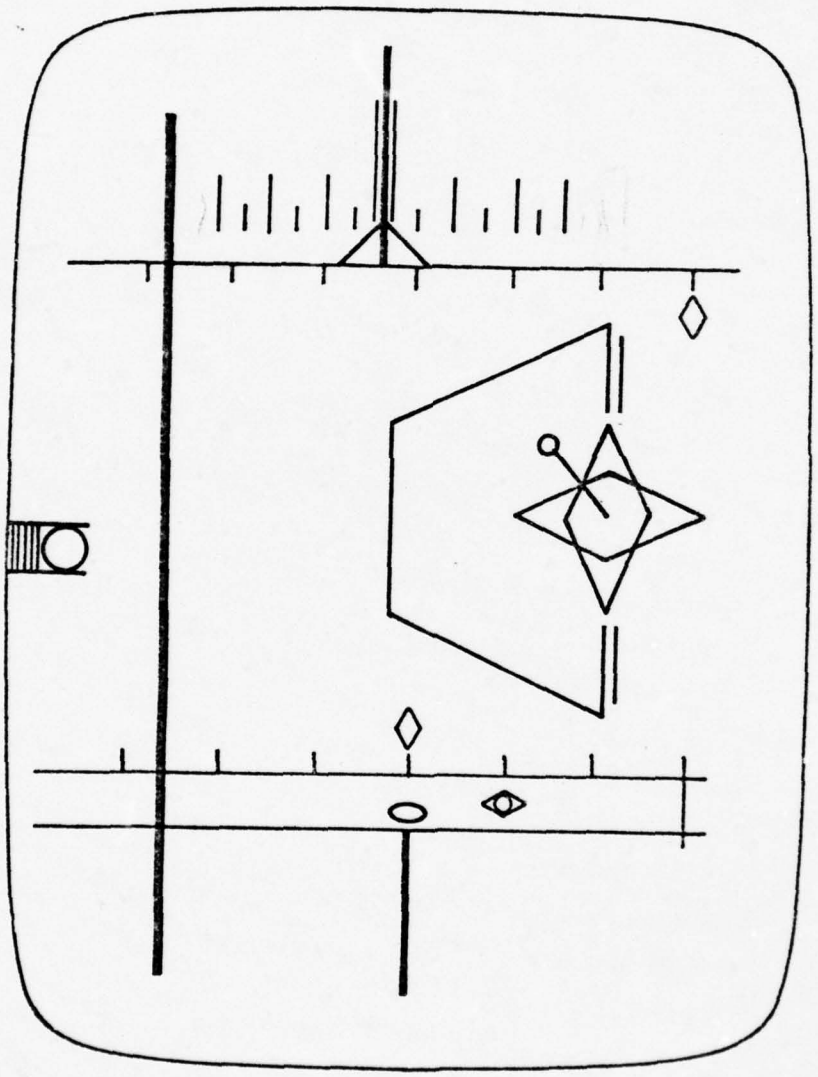

FIGURE B-6. DISPLAY HOVER SITUATION

Terrain Simulation

The S-ITED has been designed to enhance flight path control and hover positioning when the analog symbology previously discussed is superimposed on terrain features. This superposition is the key feature which allows the marker star to be used as a totally "on board" glideslope system. In the aircraft the terrain image is easily obtained by mounting a camera on the fuselage and projecting the camera image on the CRT. In the laboratory, this is not possible without an elaborate terrain belt and servo mounted camera system which is driven by the helicopter computer model. Even with such a system, problems of resolution and limitations on flight variables make realism difficult to achieve.

The most efficient answer to this problem seemed to be electronically generated symbols which would represent terrain features. This approach was used by Lemons in his hover simulation (Ref.19), and reflects a method conceived and developed by Dukes at Princeton to create a trapezoidal lissajous pattern which moves and contorts as the pilot's vantage point changes. Basically, the size of the landing pad is determined by the distance from the aircraft, and the shape is determined by the pilot's viewing angle. The landing pad and a real horizon bar constitute the terrain features simulated for this study, and the development that follows is a modification of the earlier work done by Dukes and Lemons.

Landing Pad

The generation of the landing pad symbol starts with a rectangular

lissajous pattern obtained by driving the horizontal and vertical deflection circuits of a CRT display with two square waveforms, 90^{o} out of phase. Figure B-7a shows these basic waveforms and the resulting pattern. The shape of this pattern may then be altered by summing additional waveforms to either the horizontal waveform X or the vertical waveform Y. For example, if W is a triangular wavefore of particular amplitude and is added to X, a trapizoidal pattern results (Fig. B-7b), which could represent the taper resulting from a given perspective viewing angle. As the amplitude of W varies, so does the taper of the two sides of the pattern. Other changes can be made in accordance with the observer's viewing angle and are derived from the basic geometry of the problem.

a. Basic Derivation

The work of Lemons (Ref.19) in documenting this derivation is reproduced in this section for convenience.

In order to quantify the required changes in the basic waveform, five runway variables are defined (Figure B-8):

x = distance from reference point (center of the far end of the landing pad)

h = altitude above reference point

y = lateral displacement from the landing pad center line

D = half width of the landing pad

L = length of the landing pad

These variables must be related to the following six display variables (Figure B-9).

ℓ_1 = displayed distance of reference point from horizon

ℓ_2 = displayed pad length

w_1 = displayed half-width of the pad at the center of the runway (Figure B-9a)

w_1' = displayed half-width at the far end of the landing pad (Figure B-9a)

w_2 = a measure of "skewing" as expressed by the lateral displacement of the landing pad mid-point (Figure B-9b)

w_2' = a measure of skewing as expressed by the lateral displacement of the mid-point of the far end of the landing pad (Figure B-9b)

From Figure B-8a

$\ell_1 = (SF)(\frac{h}{x})$ where (SF) is simply an appropriate constant, the scale factor. By similar triangles:

$$\frac{\ell_2}{L} = \frac{\ell_1}{x-L} \quad \ell_2 = \ell_1 \frac{L}{x-L} = (SF)\left[\frac{hL}{x(x-1)}\right] = (SF)\left[\frac{h}{x-1} - \frac{h}{x}\right]$$

$$w_1' = (SF)\frac{D}{\sqrt{y^2+h^2}} = (SF)(\frac{D}{x})(1 - \frac{1}{2}\frac{h^2}{x^2} + \ldots) \approx (SF)(\frac{D}{x})$$

From Figure B-9a, w_1' and ℓ_1 determine δ uniquely

$$\tan\delta = \frac{w_1'}{\ell_1} \approx \frac{D}{h}$$

and

$$w_1 = (\ell_1 + \frac{\ell_2}{2})\tan\delta \approx (\ell_1 + \frac{\ell_2}{2})\frac{D}{h}$$

The slope of sections 2 and 4 (amplitude of the triangular waveform, (Figure B-7b) is determined by

$$w_1 - w_1' \approx \frac{\ell_2}{2} \frac{D}{h}$$

Using the same approximation as for w_1'

$$w_2' = (SF) \frac{y}{\sqrt{x^2+h^2}} = (SF) \left(\frac{y}{x}\right) \left(1 - \frac{1}{2} \left(\frac{h^2}{x^2}\right) + \ldots\right) \approx (SF) \left(\frac{y}{x}\right)$$

From Figure B-9b

$$\tan \mu = \frac{w_2}{\ell_1} = \frac{(SF) \frac{y}{(x)}}{(SF) \left(\frac{h}{x}\right)} = \frac{y}{h}$$

and $w_2 \approx \left(\ell_1 + \frac{\ell_2}{2}\right) \frac{y}{h}$

The difference in slopes of the two sides, 2 and 4, is:

$$(w_2 - w_2') = \frac{\ell_2}{2} \frac{y}{h}$$

The following notation is used for brevity:

$$A = \frac{h}{x} \; ; \; B = \frac{h}{x-L} \; ; \; C = \frac{D}{h}$$

X = basic horizontal deflection waveform (Figure B-7)

Y = basic vertical deflection waveform (Figure B-7)

W = triangular waveform of Figure B-7

The total vertical deflection is made up of two parts:

1. The deflection of the landing pad center from the horizon:

$$\ell_1 + \frac{\ell_2}{2} = \frac{1}{2}(SF)\left(\frac{h}{x} + \frac{h}{x-L}\right) = \frac{(SF)}{2}(A+B)$$

2. The deflection corresponding to the size of the pad:

$$\frac{\ell_2}{2} Y = \frac{(SF)}{2}\left(\frac{h}{x-L} - \frac{h}{x}\right) Y = \frac{(SF)}{2}(B-A)\,Y$$

The horizontal deflection is the sum of 4 signals:

1. The deflection corresponding to the landing pad size:

$$w_1 X = \left(\ell_1 + \frac{\ell_2}{2}\right)\left(\frac{D}{h}\right) X = \left[\frac{(SF)}{2}(A+B)C\right]X$$

2. The deflection of the side corresponding to the distance from the pad reference point:

$$(w_i - w_i')\, W = \frac{\ell_2}{2}\left(\frac{D}{h}\right) W = \left[\frac{(SF)}{2}(B-A)C\right]W$$

3. The displacement of the landing pad pattern corresponding to lateral displacement, y:

$$w_2 = \left(\ell_1 + \frac{\ell_2}{2}\right)\frac{y}{h} = \left[\frac{(SF)}{2}(A+B)\right]\frac{y}{h}$$

4. The skewing deflection (change in slope of sides 2 and 4) corresponding to lateral displacement, y:

$$(w_2 - w_1')\, Y = \frac{\ell_2}{2}\left(\frac{y}{h}\right) Y = \left[\frac{(SF)}{2}(B-A)\left(\frac{y}{h}\right)\right] Y$$

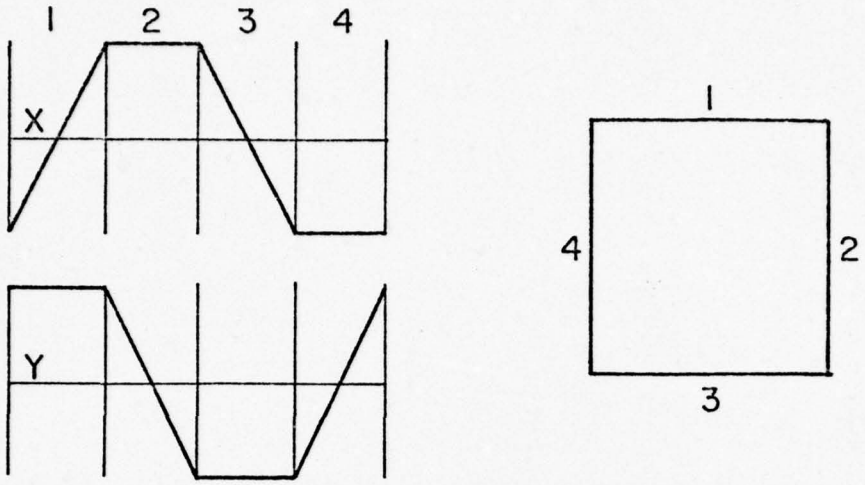

a.

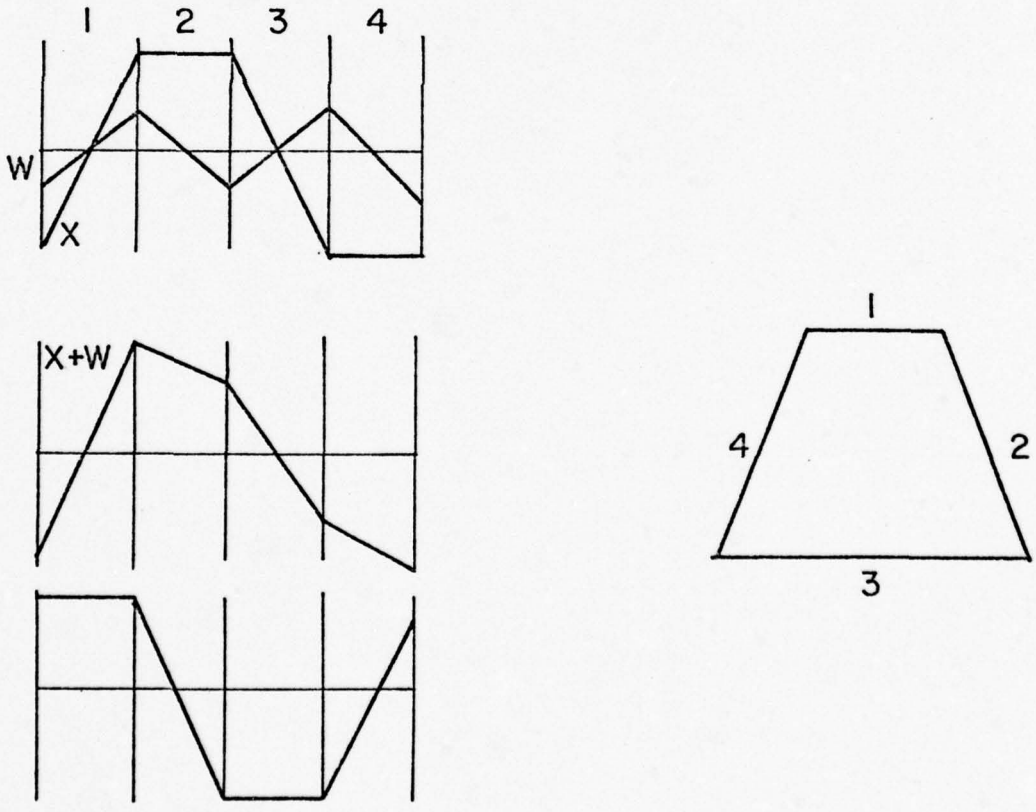

b.

FIGURE B-7. LANDING PAD BASIC WAVEFORMS

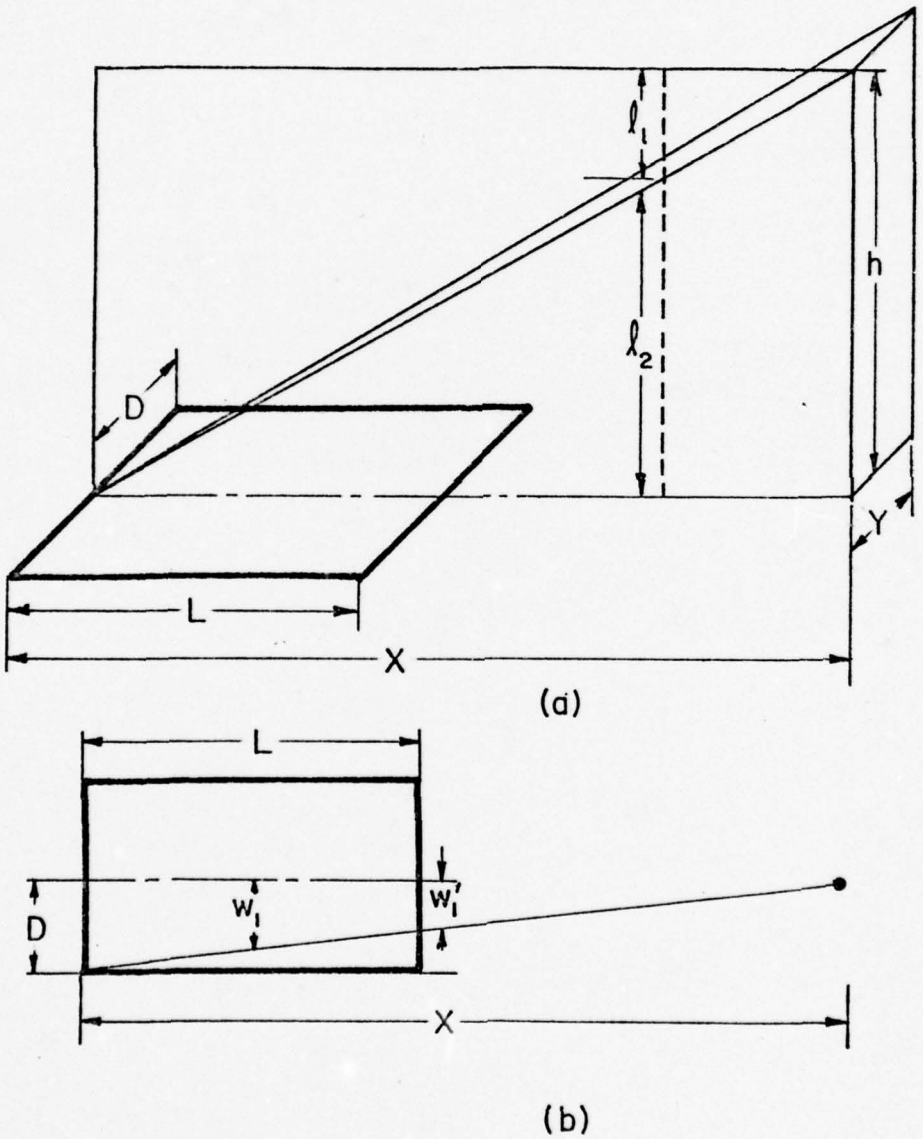

FIGURE B-8. LANDING PAD VARIABLES

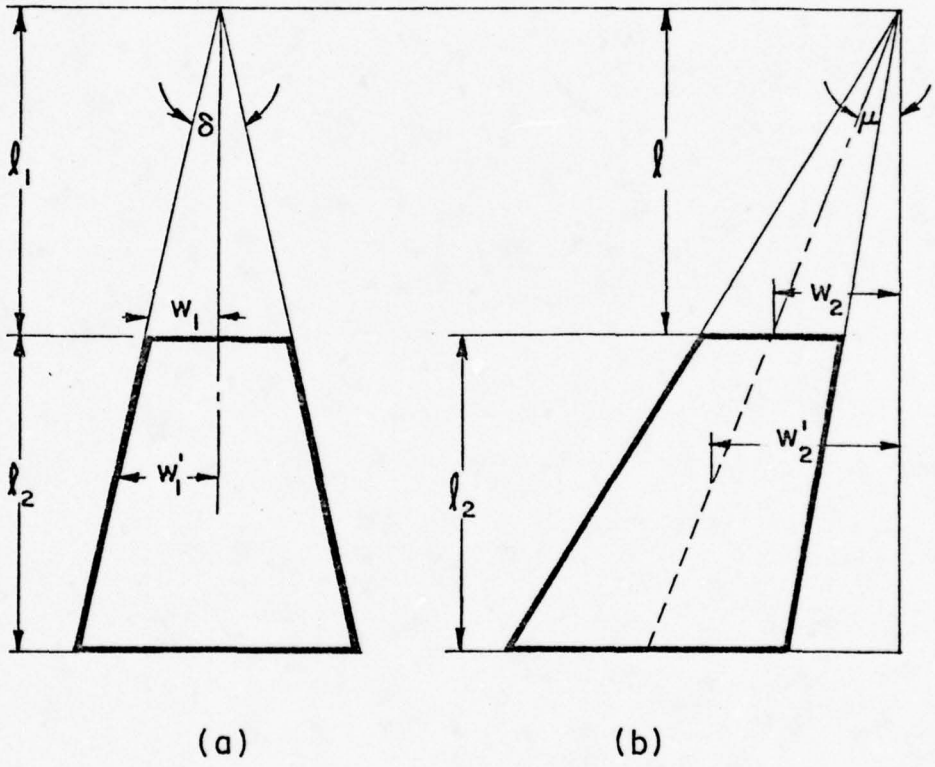

FIGURE B-9. DISPLAY VARIABLES

Angular motions of the aircraft, yaw, pitch, and roll, are represented by appropriate translations and rotation of the landing pad symbol on the cathode ray tube.

b. Modifications

In order to mechanize the deflection circuit suggested in the above derivation, the horizontal and vertical deflection voltages take the forms below:

$$\underline{\text{vertical}} = \frac{SF}{2}\left(\frac{h}{x-L} - \frac{h}{x}\right) Y + \frac{SF}{2}\left(\frac{h}{x-L} + \frac{h}{x}\right)$$

$$\underline{\text{horizontal}} = Y\left\{\frac{yx}{hr}\left[\frac{SF}{2}\left(\frac{h}{x-L} - \frac{h}{x}\right)\right]\right\} + \frac{yx}{hr}\left[\frac{SF}{2}\left(\frac{h}{x-L} + \frac{h}{x}\right)\right]$$

$$+W\left\{\frac{Dx}{hr}\left[\frac{SF}{2}\left(\frac{h}{x-L} - \frac{h}{x}\right)\right]\right\} + X\left\{\frac{Dx}{hr}\left[\frac{SF}{2}\left(\frac{h}{x-L} + \frac{h}{x}\right)\right]\right\}$$

Some advantage is enjoyed by mechanizing these equations as they appear above. The most significant advantage is that each geometrical aspect of the landing pad's appearance can be isolated in the circuit and adjusted independently. The greatest disadvantage of the above from is that it requires nearly twice as much nonlinear hardware as does a reduced form of the equations. For this study, the latter disadvantage was the overriding factor and the equations were reduced as follows:

Factoring out $\frac{h}{x}$ in the above expressions

$$\underline{\text{vertical}} = \left(\frac{SF}{2}\right)\left(\frac{h}{x}\right)\left(\frac{L}{x-L}\right) Y + \frac{SF}{2}\left(\frac{h}{x}\right)\left(\frac{2x-L}{x-L}\right)$$

$$\underline{\text{horizontal}} = \left\{\left[\left(\frac{y}{r}\right)\left(\frac{SF}{2}\right)\left(\frac{L}{x-L}\right)\right] + \left[\left(\frac{y}{r}\right)\left(\frac{SF}{2}\right)\left(\frac{2x-L}{x-L}\right)\right] + W\left[\left(\frac{D}{r}\right)\left(\frac{SF}{2}\right)\left(\frac{L}{x-L}\right)\right]\right\} Y$$

$$+\left[\frac{D}{r}\left(\frac{SF}{2}\right)\left(\frac{2x-L}{x-L}\right)\right] X$$

and again factoring out like terms and combining the remainder:

$$\underline{\text{vertical}} = \frac{SF}{2}\left(\frac{h}{x}\right)\left[Y\left(\frac{L}{x-L}\right) + \left(\frac{2x-L}{x-L}\right)\right]$$

$$\underline{\text{horizontal}} = \left(\frac{1}{r}\right)\left(\frac{SF}{2}\right)\left\{\left[\left(\frac{L}{x-L}\right)(Y\ y+WD)\right] + \left[\left(\frac{2x-L}{x-L}\right)(y+XD)\right]\right\}$$

These equations represent the complete deflection circuits required to distort the landing pad according to the observer's position changes. In order for the landing pad to move on the display with angular changes in aircraft attitude, these angles must be summed in the appropriate channel. Positive pitch, nose up, for example, will cause the landing pad to move down the display a distance equal to the angle θ times the display scale factor in centimeters on the CRT per degree of viewing angle. Likewise, a heading change will cause a lateral displacement. For these motions the attitude angles are used directly. Displacements caused by coupled angular deflections are somewhat more subtle. Rolling, for example, displaces vertically those elements of the landing pad which are laterally displaced from the center of the display. This is accomplished by summing the product of the roll angle and horizontal deflection with the vertical deflection and vice versa. This represents a "rolling" of the AC waveforms and makes the landing pad appear to rotate. There is an additional effect which is observable if a roll occurs when the aircraft is "off heading". In this case, the landing pad is laterally displaced on the CRT because of a heading deflection. Now, when a roll angle is present, the landing pad not only appears to roll, it also appears

to vertically move to maintain its distance from the real horizon. This effect is achieved by summing the scaled product of heading error from the reference and roll angle into the vertical deflection circuit. There are other effects stemming from the various possible angular deflections, but most are not very significant as long as the task is performed close to the nominal or reference heading.

Figure B-10 shows the analog computer diagram used to mechanize the landing pad deflection circuits described above, and the generation of the basic landing pad AC waveforms.

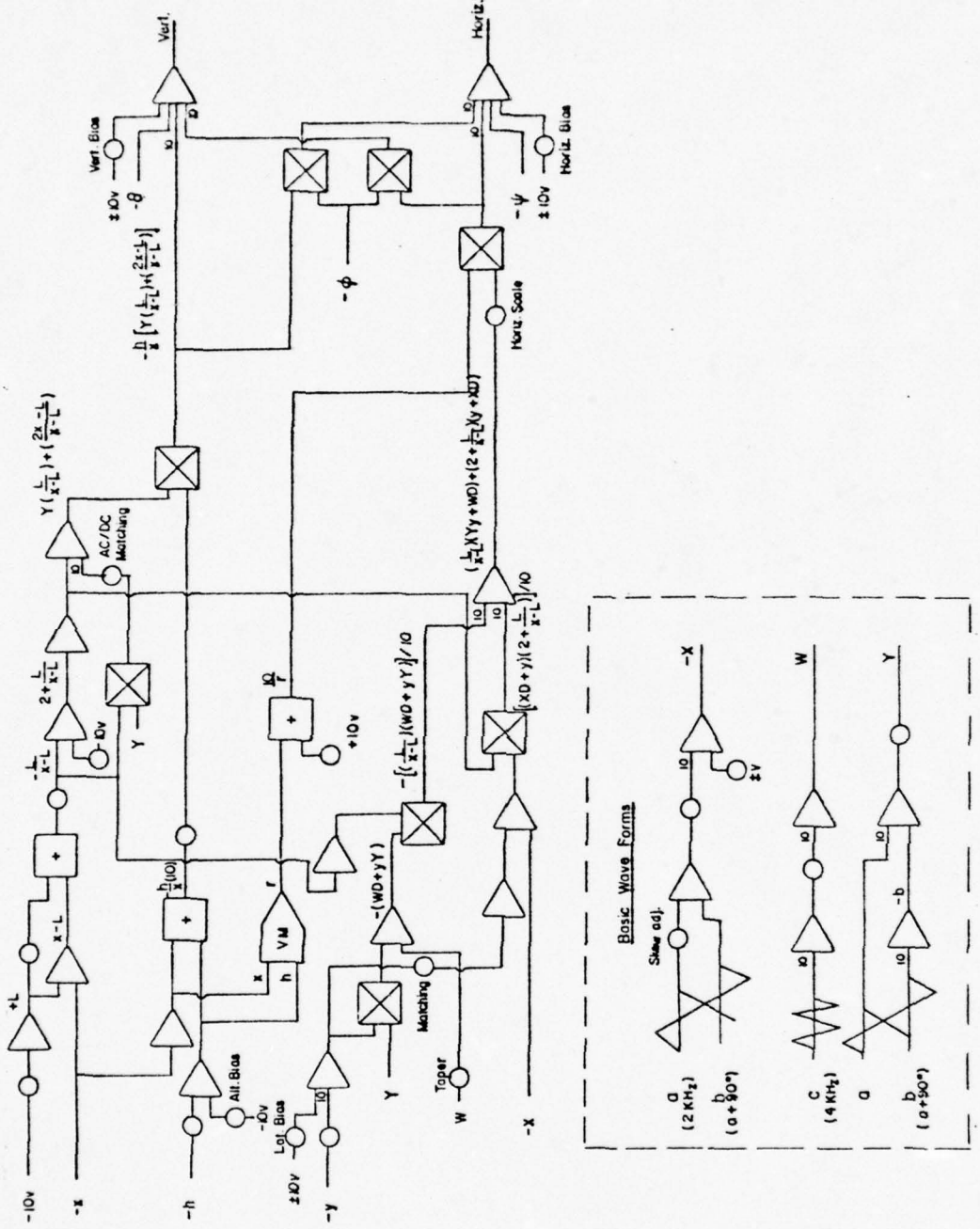

FIGURE B-10. COMPUTER DIAGRAM OF LANDING PAD SIMULATION

APPENDIX C

A Sample Calculation of the Feedback Gains and Compensation for Augmenting the Stability of the UH-1

Introduction

The purpose of this analysis is to outline the methods used in the development of the various stability augmentation configurations used in the simulator. The approach taken here is that of a complete multiloop analysis of the longitudinal degrees of freedom with the airspeed and altitude loops representing the outer loops normally closed by the pilot. In the lateral degrees of freedom, the coupling effects in the roll and yaw channels were dealt with and a simple attitude controller resulted. The development of this automatic stabilization system illustrates the coupling effects among the loops and also indicates the relative independence of the inner attitude loops. The assumption used here is that the inner pitch, roll and yaw loops which are designed here for the automated system will have the same good response characteristics when the pilot is closing them as outer loops. The feedback trans fer functions resulting from this analysis are:

$$G_{\delta_{Bls}\theta} = K_{\dot{\theta}}(s+K_\theta/K_{\dot{\theta}}),\ K_{\dot{\theta}} = .56 \quad K_\theta = 1.4$$

$$G_{\delta_{Als}\phi} = K_{\dot{\phi}}(s+K_\phi/K_{\dot{\phi}}),\ K_{\dot{\phi}} = .184\ K_\phi = .45$$

$$G_{\delta_r r} = K_r = 2.5$$

The values of the pitch and roll rate and position feedback gains shown above imply closed loop time constants on the order of .3 seconds. This response time is comparable with Calspan's work in their X22 simulation (Ref. 18).

Stability and Control Data

The aircraft parameters and flight condition for this analysis are those of a UH-1 Bell helicopter in forward flight at low altitude. The dimensional data was taken from the Army Operators manual (Ref. 9) and a Bell Helicopter Company report (Ref.31). The stability and control derivatives were taken from a Janair technical report (Ref.24). Some of the derivatives in the Janair report were found to be in error. Those derivatives were estimated by empirical means and compared with reasonable data on other single rotor helicopters. The aircraft configuration, flight condition and stability parameters for this analysis are as follows:

a. Aircraft Configurations

W = 8500 lbs

R = 24.13 ft

Ω = 320 RPM = 33.5 rad/sec

I_{xx} = 3455 slug ft^2

I_{yy} = 10,710 slug ft^2

I_{zz} = 8,682 slug ft^2

I_{xz} = 0 (∴ L', N' derivatives = L, N)

b. Flight Conditions

U_o = 146.67 fps

h = 200 ft

Winds - calm (turbulence not considered except where indicated in ride quality analysis)

Flight Path - straight and level

b. Stability and Control Derivatives

LONGITUDINAL (DIVIDED BY THEIR RESPECTIVE MASS OR INERTIAL TERM)

X_u = -.028

X_w = .0015 (X_α=.220)

X_q = 9.16

$X_{\dot{\beta}}$ = 0

$X_{\delta_{Bls}}$ = 31

X_{δ_c} = -3.0

X_β = -5.9

M_u = .00273

M_w = -.0167 (M_α=-2.449)

$M_{\dot{w}}$ = 0

M_q = -.495

$M_{\dot{\beta}}$ = 0

M_β = 7.22

$M_{\delta_{Bls}}$ = -7

M_{δ_c} = -2.005

Z_u = -.0005

Z_w = -.658 (Z_α=-06.507)

$Z_{\dot{\beta}}$ = 0

$Z_{\delta_{Bls}}$ = 95.0

Z_{δ_c} = -316.0

$(M_o - Z_q)$ = 144.8

LATERAL

$L_p = -1.228$

$L_r = 0$

$L_{\dot{v}} = -0.00634$ ($L_{\dot{\beta}}=-.930$)

$L_v = -.0376$ ($L_\beta=5.515$)

$L_{\delta_r} = 13.58$

$L_{\delta_{Als}} = 34.0$

$N_r = -.48$

$Y_v = -0.1467$ ($Y_\beta=-21.516$)

$(mV_o - Y_r) = 150.4$

$(W_o - Y_p) = -11.2$

$Y_{\delta_r} = 23.0$

$Y_{\delta_{Als}} = 27$

$Y^*_{\delta_r} = .156$

$Y^*_{\delta_{Als}} = .184$

$N_{\delta_{Als}} = 0$

$N_{\dot{v}} = .0098$ ($N_{\dot{\beta}}=1.437$)

$N_v = .0386$ ($N_\beta=5.661$)

$N_{\delta_r} = -18.28$

Longitudinal

An effort is made here to illustrate a reasonably detailed multiloop design for a longitudinal controller that will be effective for straight and level flight, and for shallow approach angles. For this reason collective pitch is used to control altitude and airspeed is controlled by cyclic pitch. While this sort of control is familiar to helicopter pilots, a simpler, conventional aircraft altitude controller might well close the altitude loop around the elevator or cyclic pitch. Use of the collective, however, eliminates the problems associated with "back-side" operation and may be modified to include a broader range of flight conditions. Furthermore, this system will stand more severe gust perturbations about the trim condition. Fig. C-1 illustrates the proposed system in block diagram form. Notice here that a pitch damper and altitude rate feedback are anticipated as compensators to tighten up the inner loops. It will be seen later that while the pitch damper is essential, the altitude rate feedback is not of much consequence, unless it becomes desirable to operate at much higher gains than are presented here. This is mentioned only because it is possible to operate this loop at higher gains without detrimental effects.

The transfer functions used in this design were derived from the equations of motion shown below in LaPlace form. The stability and control data was that explained previously, and the multiloop algorithms were taken from Ref. 21. The loop closure sequence in this two control problem was chosen to close the pitch loop first in both cases, then

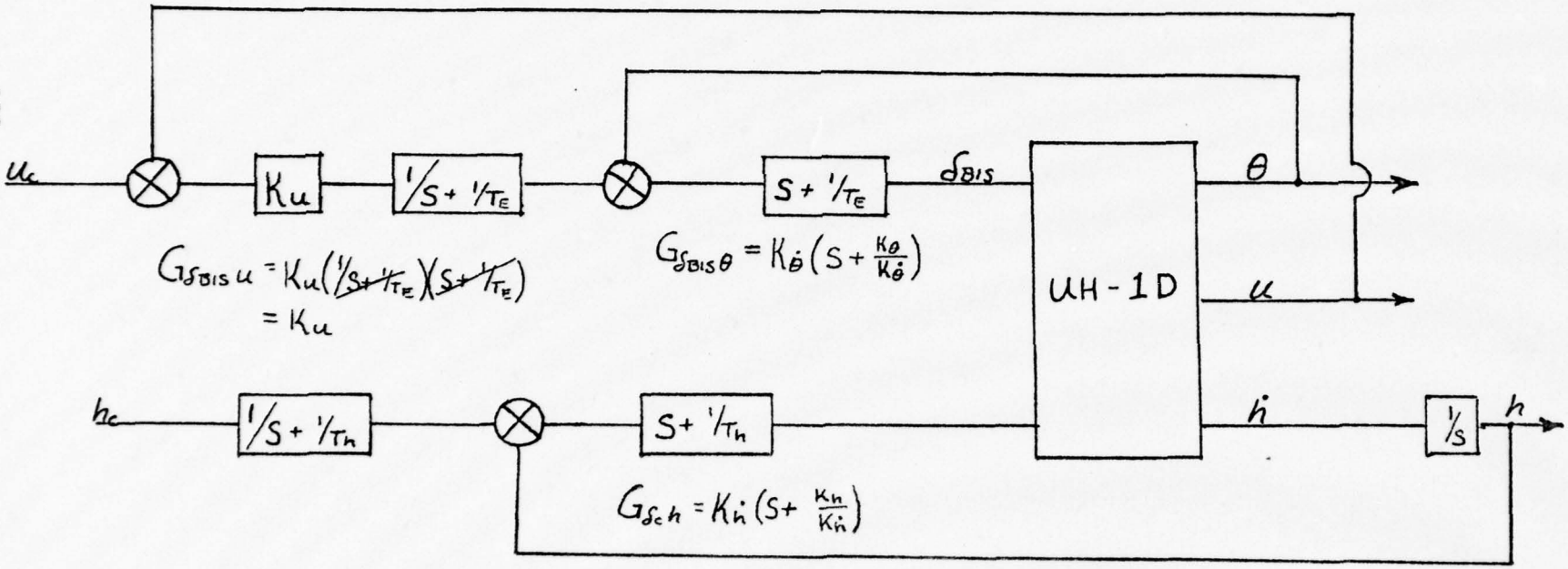

FIGURE C-1. BLOCK DIAGRAM OF LONGITUDINAL FEEDBACK SYSTEM

altitude and speed. To this end the h/h_c response was evaluated first.

$$\begin{bmatrix} s-X_u & -X_w & -X_q s+g\cos\gamma_o \\ -Z_u & s-Z_w & -(Z_q+U_o)s+g\sin\gamma_o \\ -M_u & -M_w s-M_w & s^2-M_q s \end{bmatrix} \begin{bmatrix} u \\ w \\ \theta \end{bmatrix} \begin{bmatrix} X_{\delta_{Bls}} & X_{\delta_c} \\ Z_{\delta_{Bls}} & Z_{\delta_c} \\ M_{\delta_{Bls}} & M_{\delta_c} \end{bmatrix} \begin{bmatrix} \delta_{Bls} \\ \\ \delta_c \end{bmatrix}$$

Note that γ_o was assumed hereafter to be a small angle, however this assumption does not invalidate the equations for shallow glideslopes. Also X_q and Z_q have not been neglected as is customary in conventional aircraft. This is because $g/X_q = 3.5$ which is within the frequency range of interest. Z_q was included solely because the stability derivative data available included values of (V_o+Z_q), and for no other reason.

Writing the h/h_c transfer function in the canonical form

$$\frac{C}{R} = \frac{G}{1+GH}$$

and knowing that $G = \frac{N}{D}$, the number of necessary loop closures to find the closed loop response can be reduced to 5.

h/h_c in the form $\frac{N}{D+HN}$ is:

$$\frac{h}{h_c} = \frac{\left(N_{\delta_c}^{h} + G_{\delta_{Bls}\theta} N_{\delta_c}^{h} \delta_{Bls}^{\theta} + G_{\delta_{Bls}u} N_{\delta_c}^{h} \delta_{Bls}^{u}\right)}{\left(\Delta_{long} + G_{\delta_{Bls}\theta} N_{\delta_{Bls}}^{\theta} + G_{\delta_{Bls}u} N_{\delta_{Bls}}^{u}\right) + G_{\delta_c h}\left(N_{\delta_c}^{h} + G_{\delta_{Bls}\theta} N_{\delta_c}^{h} \delta_{Bls}^{u} + G_{\delta_{Bls}u} N_{\delta_c}^{h} \delta_{Bls}^{u}\right)}$$

(1) (2) (3) (4) (5)

In other words, four loop closures are required to determine the open loop transfer function and the fifth closure determines $G_{\delta_c h}$ and the closed loop operating point.

The speed loop is developed in a manner similar to the altitude loop with the required inner loop closures indicated below.

$$\frac{u}{u_c} = \frac{N_{\delta_{Bls}}^{u} + G_{\delta_c h} N_{\delta_{Bls}}^{u} \delta_c^{h}}{\Delta_{long} + G_{\delta_{Bls}\theta} N_{\delta_{Bls}}^{\theta} + G_{\delta_c h} N_{\delta_c}^{h} + G_{\delta_{Bls}\theta} G_{\delta_c h} N_{\delta_{Bls}}^{\theta} \delta_c^{h} + G_{\delta_{Bls}u}}$$

(6) (7) (8) (9) (10)

$$\left(N_{\delta_{Bls}}^{u} + G_{\delta_c h} N_{\delta_{Bls}} \delta_c^{h}\right)$$

Again 4 loop closures are required to factor the transfer function, however, (6) has already been accomplished in the altitude control. (7), (8), and (9) must be closed using values previously determined in the h/h_c loop closures to obtain the open loop poles and zeros for the u/u_c analysis, which is loop closure (10). The characteristic equation and numerator factors are given below in polynomial and factored form. The third and fourth degree polynomials were factored using a Newton-Raphson digital subroutine.

$$\left[N_{\delta_{B1s}}^{u}\right] \qquad 31[s^3 + 1.158s^2 + 9.999s + .1998]$$
$$31[(s+.02003)(s+.56899\pm j3.1068)]$$

$$\left[s\, N_{\delta_{B1s}}^{\theta}{}^{h}_{\delta_c}\right] = -2402.475(s+.0172)$$

$$\left[-s\, N_{\delta_{B1s}}^{u}{}^{h}_{\delta_c}\right] = -9511[s^2+.495s+10.1089]$$

$$\left[s\, N_{\delta_{B1s}}^{u}{}^{h}_{\delta_c}\right] = 9511[s+.247s\pm j3.1697] \qquad \begin{cases} \omega = 3.1794 \\ \zeta = .14667 \end{cases}$$

$$\left[s\, N_{\delta_c}^{h}\right] = 316[s^3+523s^2+2.418s+.1667]$$
$$= 316[(s+.06986)[s+.22657\pm j1.52807]] \qquad \begin{cases} \omega = 1.54478 \\ \zeta = .14667 \end{cases}$$

$$\left[N_{\delta_{B1s}}^{\theta}\right] = -7[s^2+9s+.016]$$
$$= -7(s+.882)(s+.0185)$$

$$\left[\Delta_{long}\right] = s^4+1.181s^3+2.801s^2+.148s+.058$$
$$= [\omega_{sp}=1.652,\ \zeta_{sp}=.3438][\omega_p=.1458,\ \zeta_p=.1557]$$

In order to facilitate explanation, the loops to be analysed have been numbered in sequence 1 through 10. 1 through 5 define the altitude response and 7 through 10 the speed response. Loop 6 is the same as loop 1 and is therefore not considered again. Each time a design parameter was chosen (eg. a feedback gain K or a compensator) it was retained for use in successive loop closures of that design "trial". The number of the design trial is indicated by a subscript following the loop letter (eg. $5B_2$). The letter indicates the particular loop closure for a particular loop in a particular design trial. For example, $5B_3$ indicates the second closure of loop 5 during the third design trail.

In trial one, loop 1, a pitch damper was used to create well behaved pitching response in as tight a loop as possible. The better damping and higher frequencies for the short period mode were made possible by a compensator with a time constant equal to the ratio of the pitch rate to pitch feedback gains. In closure 1A, a compensator zero with an inverse time constant of 1.6 was selected. Fig. C-2 shows the frequency response of this system. The dc gain is at about 5.5db for a damping ratio of ζ=.74. $1B_1$ was an effort to squeeze a little more dc gain out of this system without compromizing the nicely damped second order response. In this case the compensator zero was moved out to an inverse time constant of 2.5. This loop was closed for a damping ratio of ζ=.81 at a dc gain of about 15db. The response is fairly flat out to a bandwidth of about 7 radians/sec.

Fig. C-3A shows that the closed loop roots of $1B_1$ become the open loop poles of $2A_1$; the design parameter being selected in loop 2 is K_u.

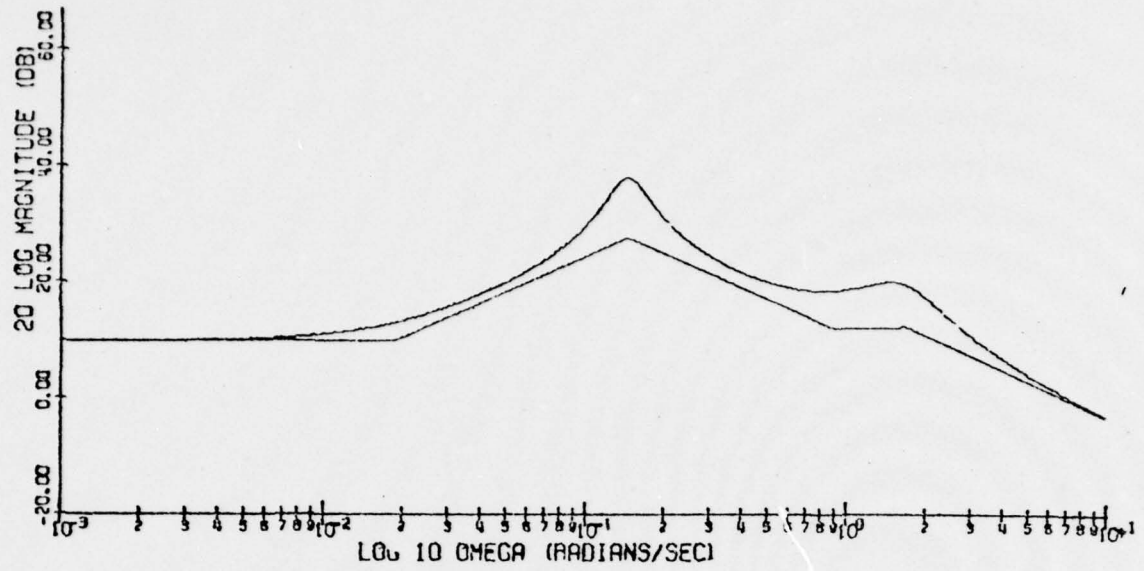

JW BODE MAGNITUDE PLOT $1A_1$

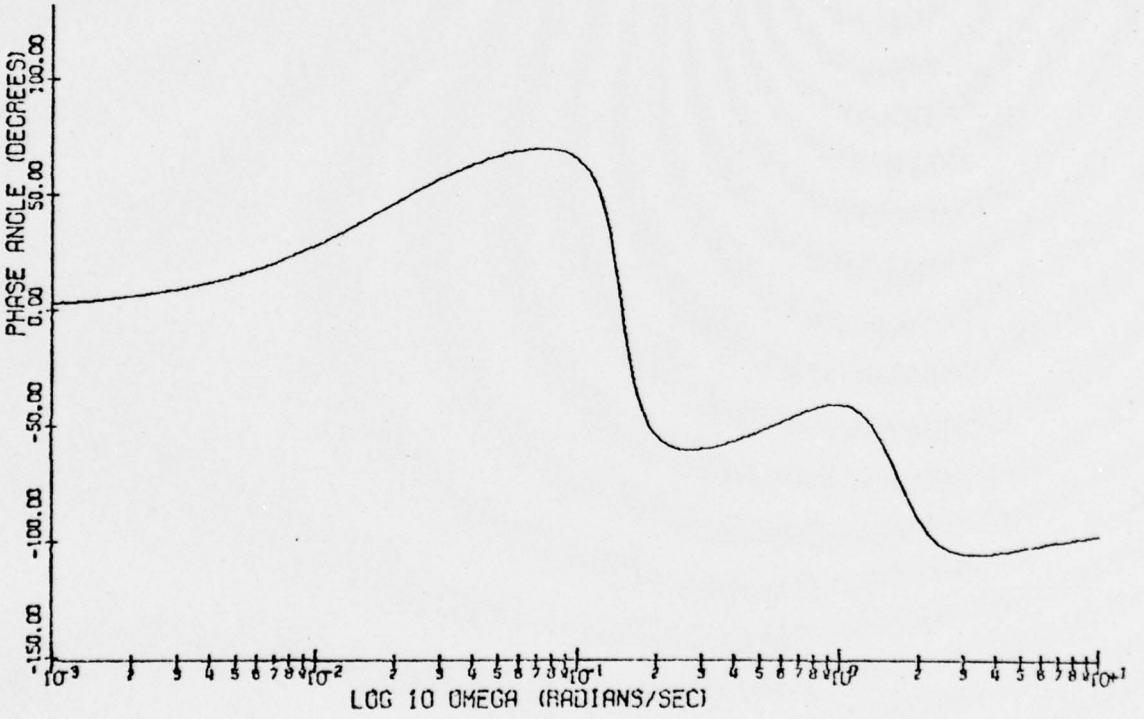

JW BODE PHASE PLOT $1A_1$

FIGURE C-2. FREQUENCY RESPONSE OF PITCH LOOP

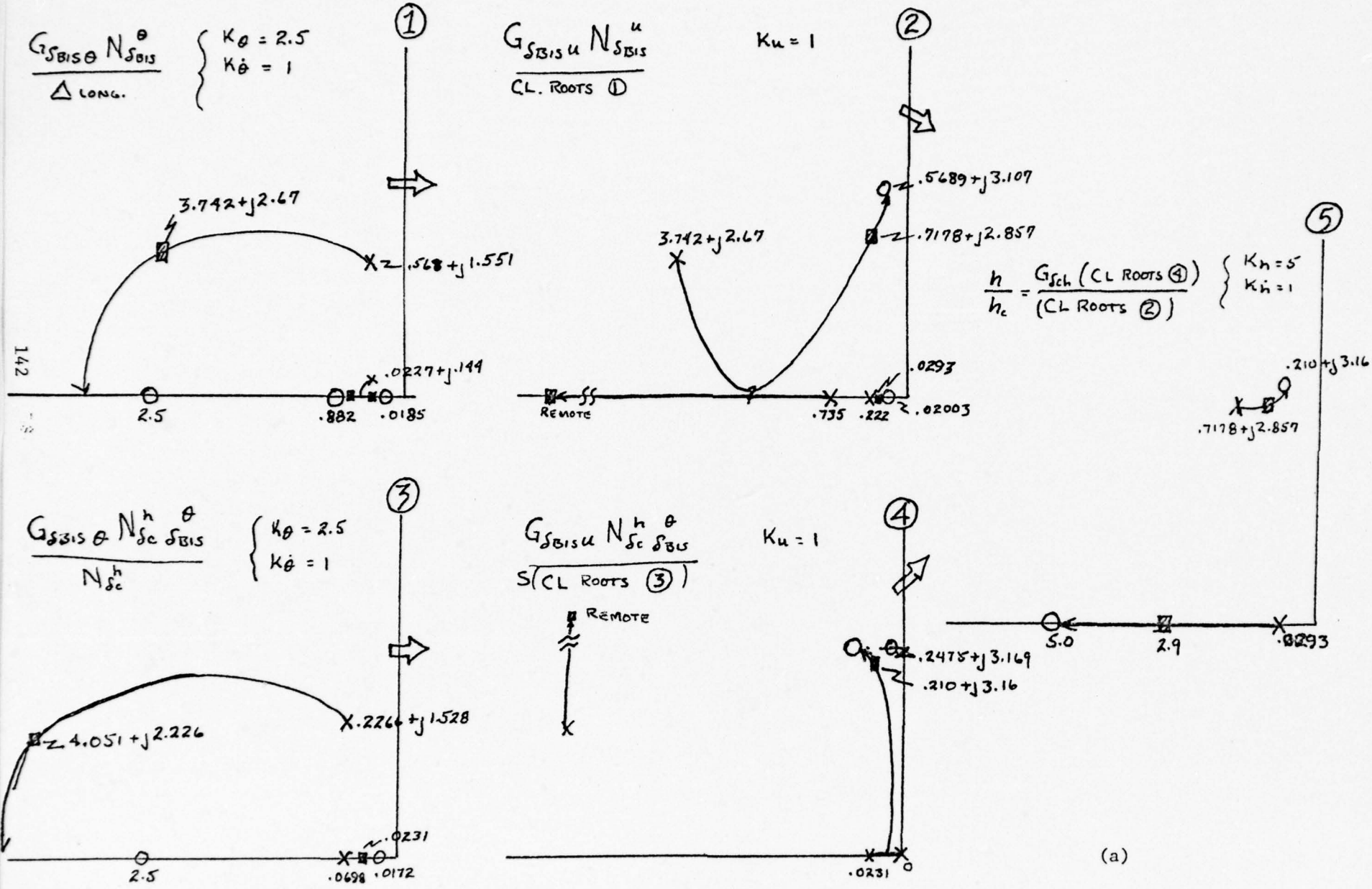

FIGURE C-3. ROOT LOCUS SKETCHES OF ALTITUDE CONTROL LOOP CLOSURES

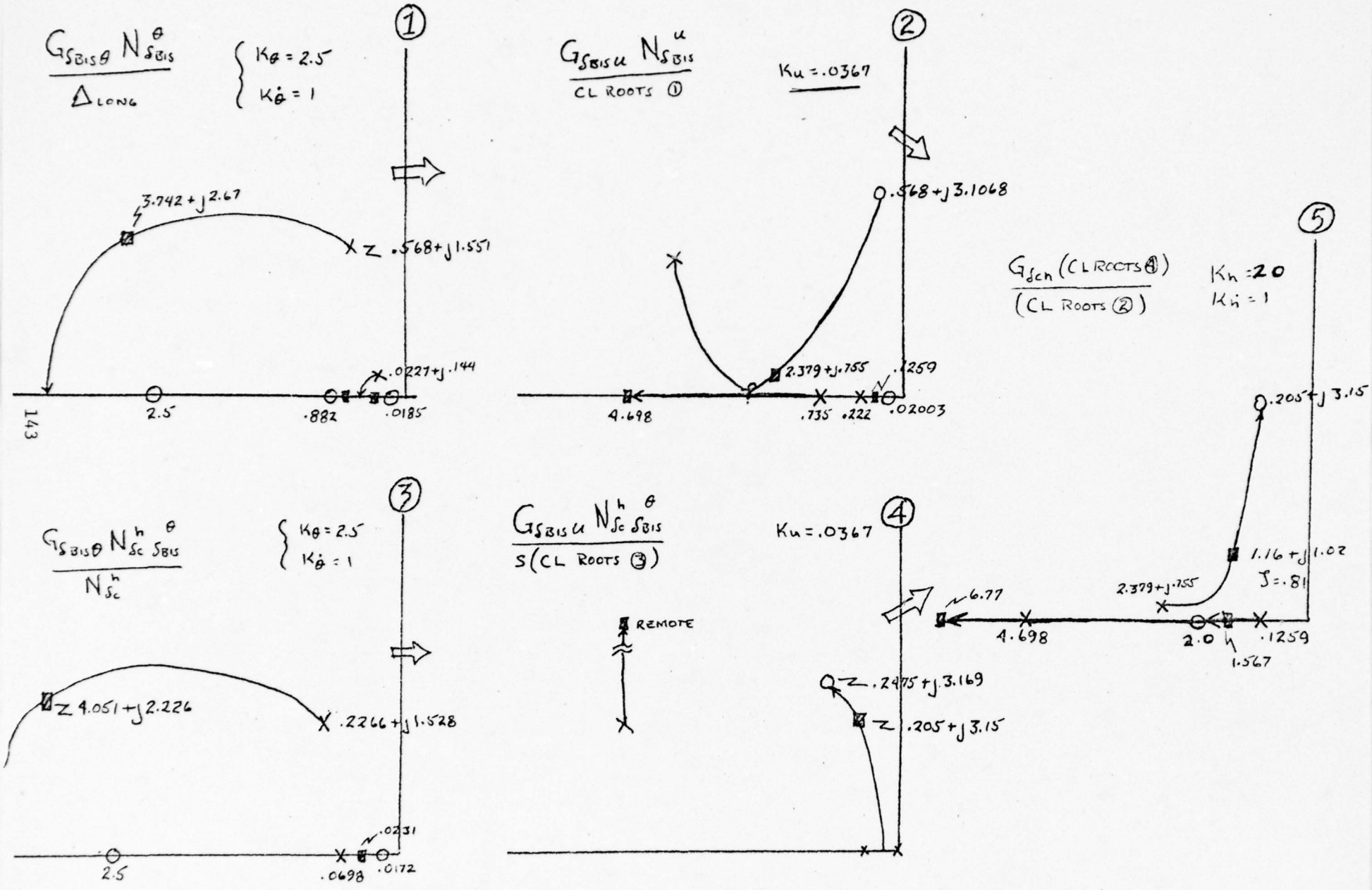

FIGURE C-3. ROOT LOCUS SKETCHES OF ALTITUDE CONTROL LOOP CLOSURES

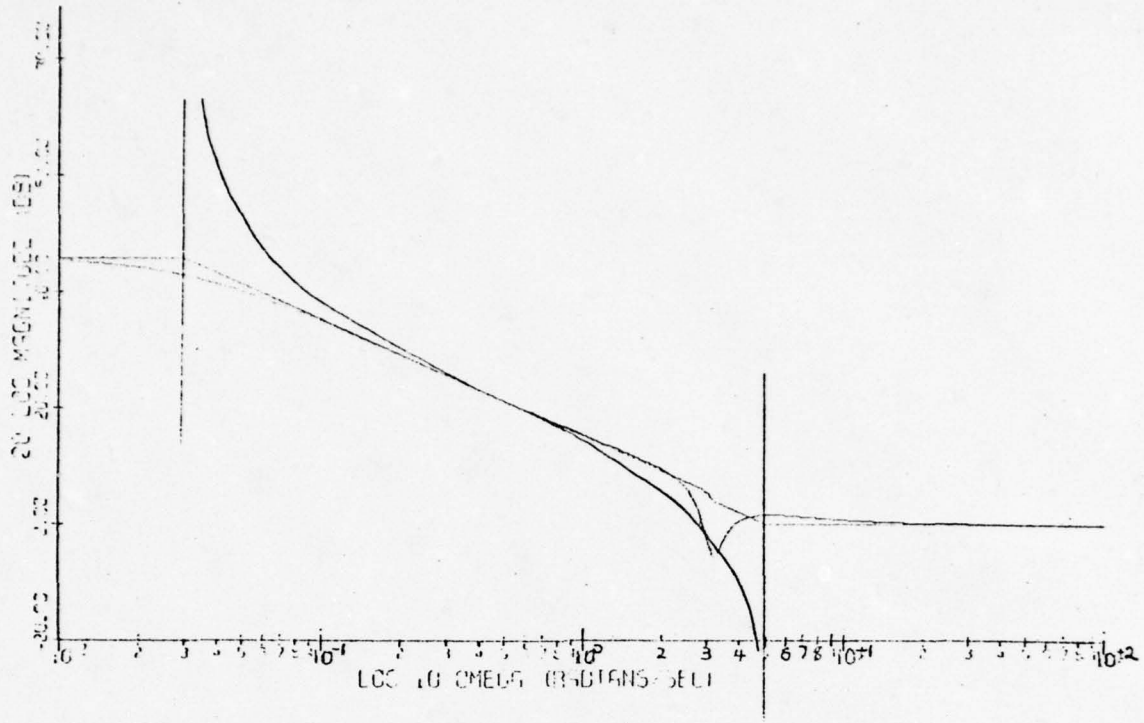

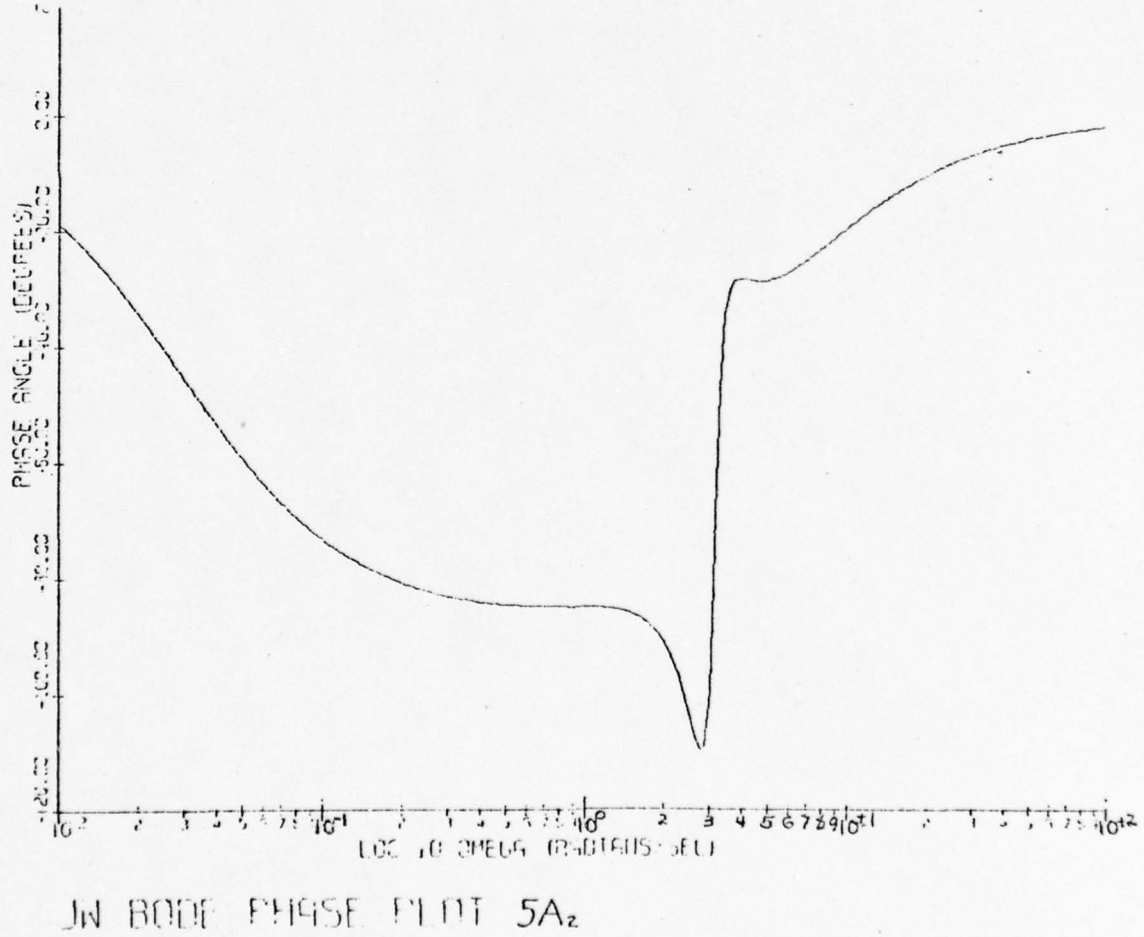

FIGURE C-4. FREQUENCY RESPONSE OF ALTITUDE LOOP (1st TRIAL)

Loop 2 also determines the open loop poles of loop 5, and the gain of loop 10. This is where the trade-off begins in this design. $2A_1$ was an attempt to close 2 at extremely low values of K_u on the order of .01. This attempt was abandoned rapidly however, in light of what it would do to the bandwidth of the speed response loop 10. Trial two was initiated at this point and $2A_2$ was an effort to drive complex poles into the zeros and the high frequency real pole out to remote frequencies.

It was found, however, in $5A_2$ that this approach, while it produced very nice gain and bandwidth, both for speed and for altitude control, was not an acceptable one since it left a rather high frequency lightly damped mode in the altitude response. This was deemed highly undesirable in this case, because of the high g loading that would result from gusts in that frequency regime. Fig. C-2A shows pictorially the steps in design trial two which lead to the above conclusion, and Fig. C-4 illustrates the frequency response characteristics of $5A_2$. Fig. C-8 is loop $10A_2$, which shows the benefits of K_u=1 on the speed response. This would certainly be a snappy system if the speed loop could have been closed at that gain. A new trial was initiated here and brought the process back to loop two again. $2A_3$ and Figs. C-3B, C-5, C-6, C-7, C-9 illustrate the third and last design trial. K_u=.0367 was selected as a compromize gain that would eliminate the undesirable mode present in $5A_2$ and maintain as much bandwidth as possible in $10A_3$, while still forcing the high frequency roots in loop 4 out to remote frequencies. Loops three and four are closed in each trial to obtain the open loop zeros for loop 5. To that extent these loops become design considerations in the closures of loops 1 and 2

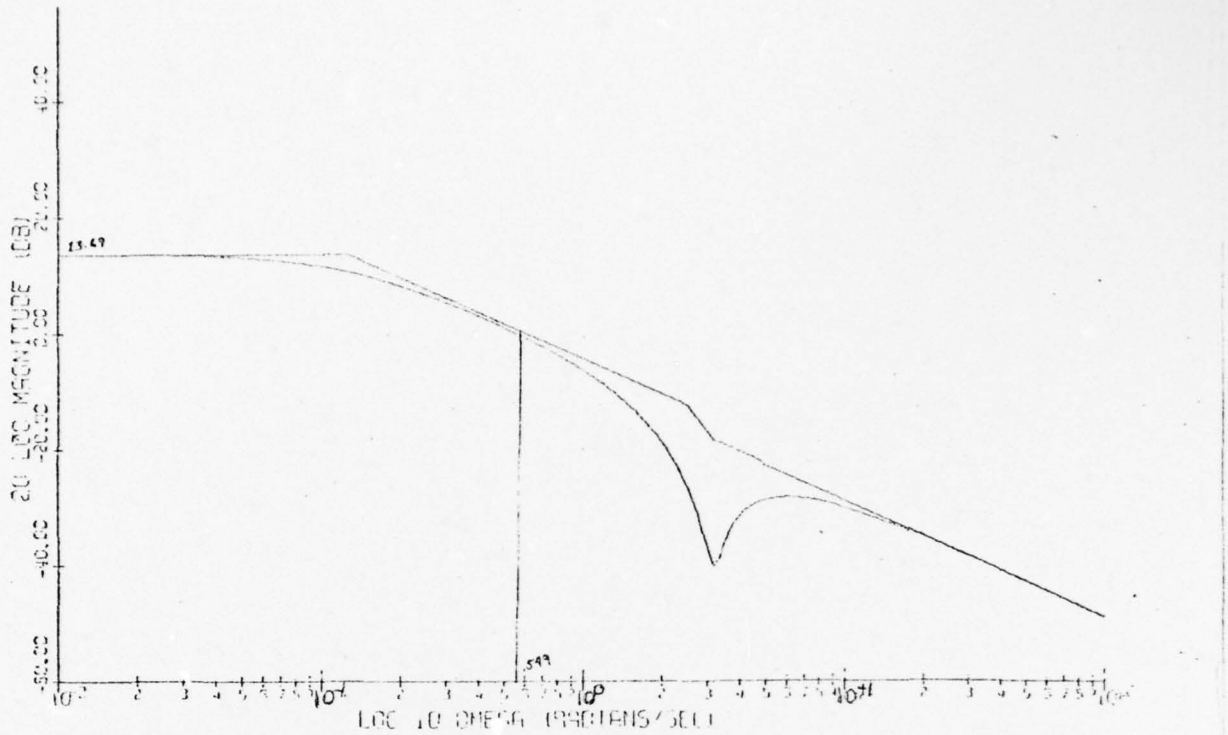

JW BODE MAGNITUDE PLOT $5A_3$

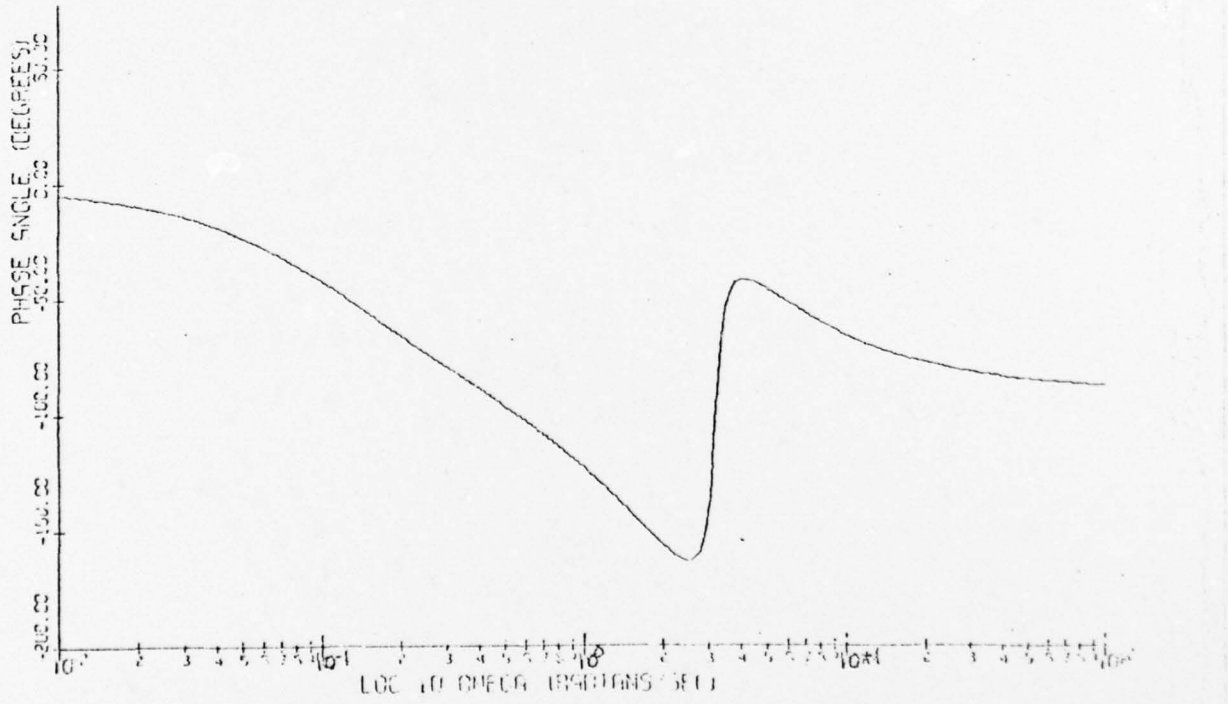

JW BODE PHASE PLOT $5A_3$

FIGURE C-5. FREQUENCY RESPONSE OF ALTITUDE LOOP (2nd TRIAL)

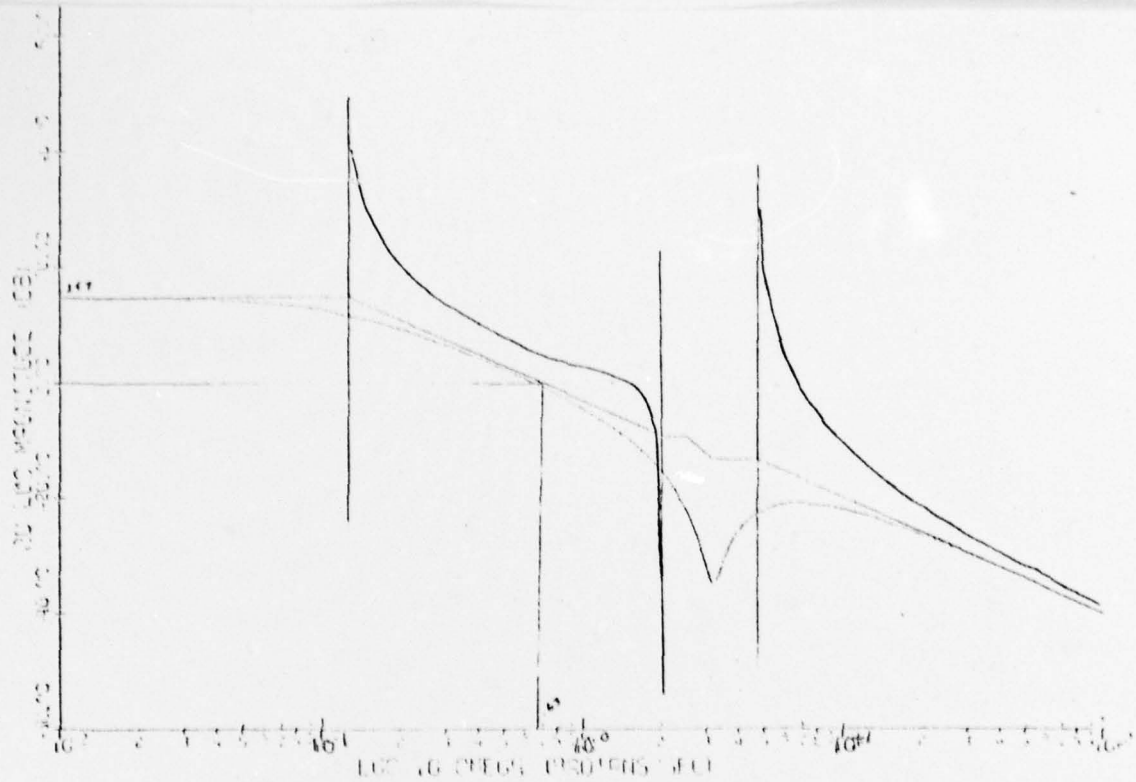

JN BODE MAGNITUDE PLOT $5B_3$

FIGURE C-6. FREQUENCY RESPONSE OF ALTITUDE LOOP (3rd TRIAL)

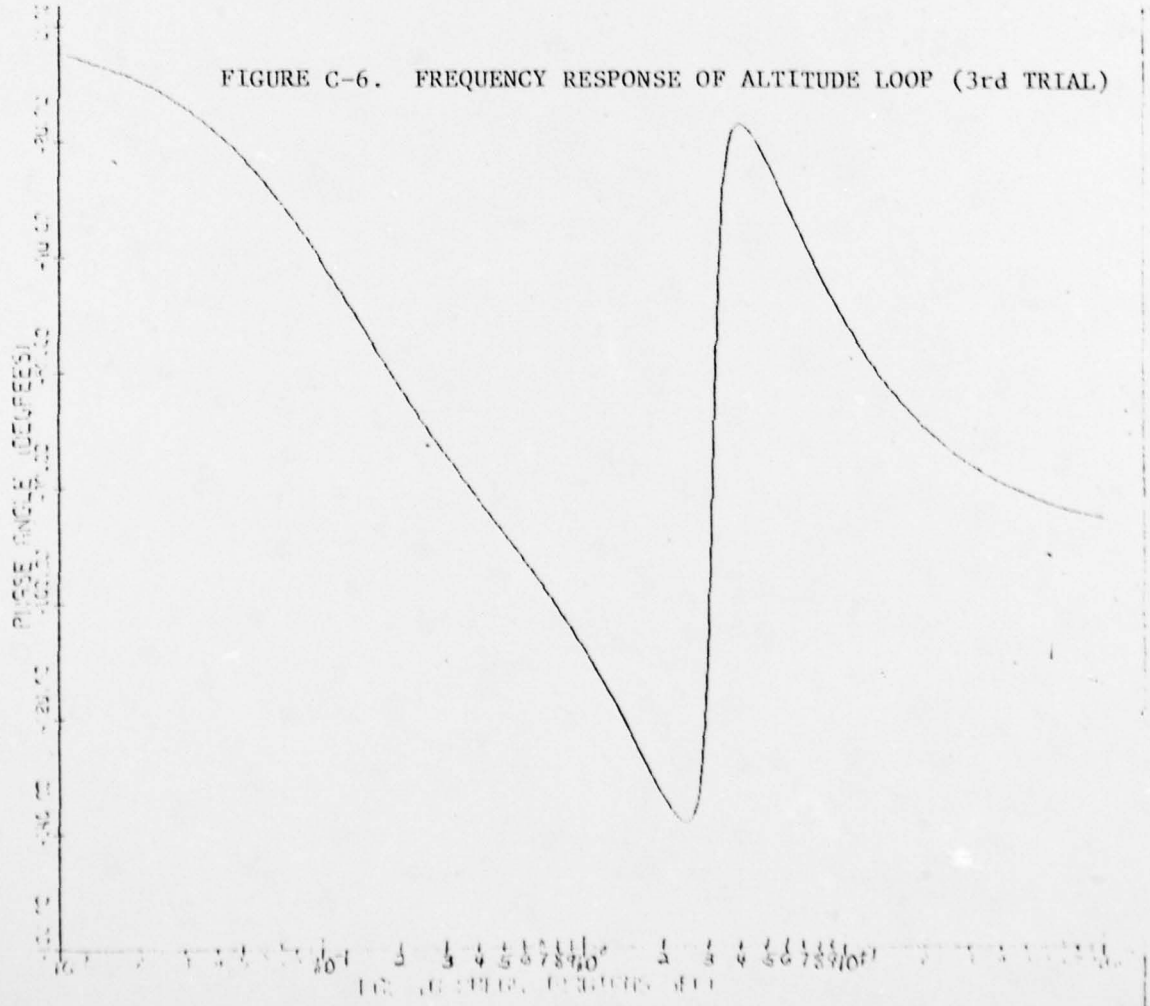

JN BODE PHASE PLOT $5B_3$

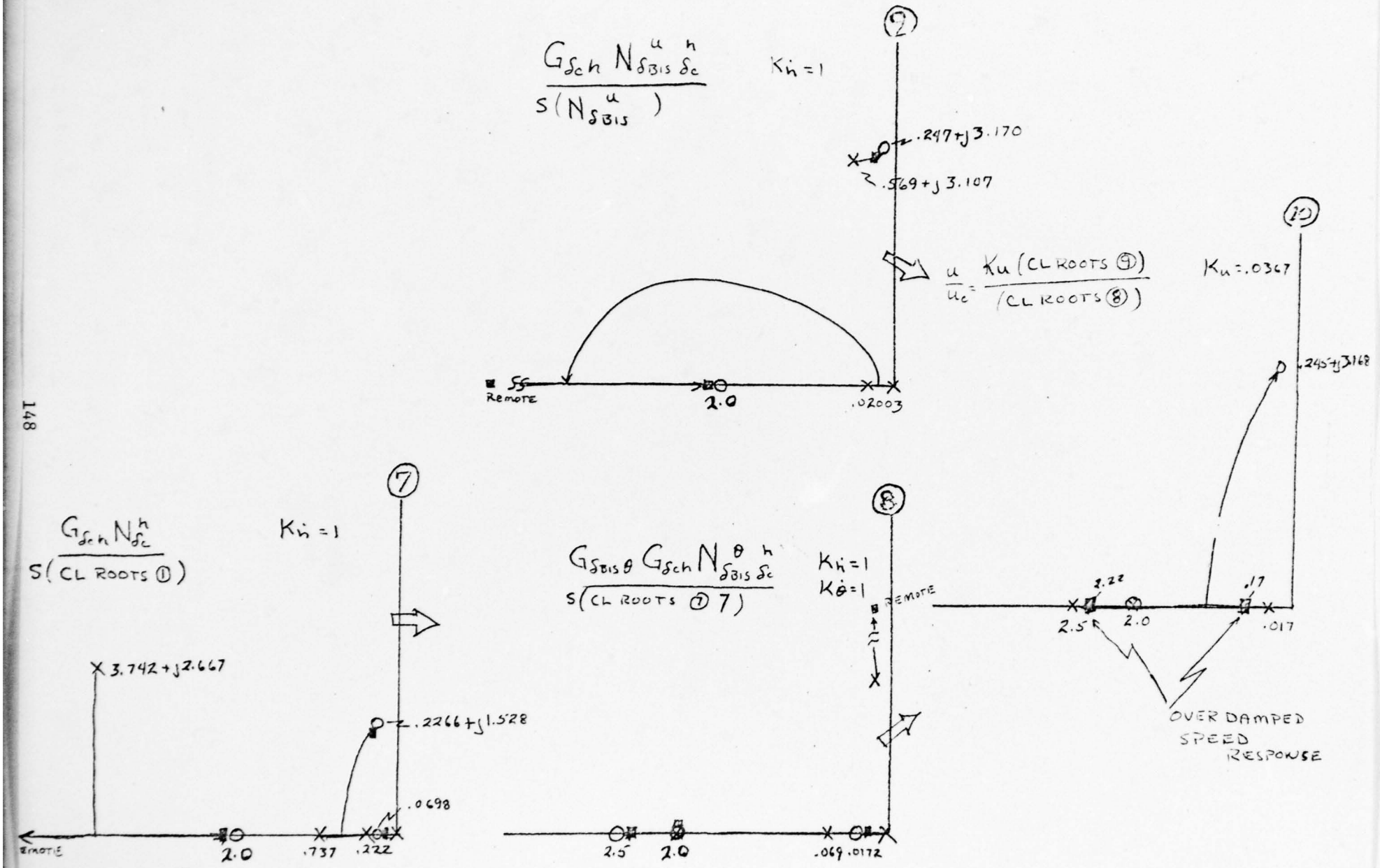

FIGURE C-7. ROOT LOCUS SKETCHES OF SPEED CONTROL LOOP CLOSURES

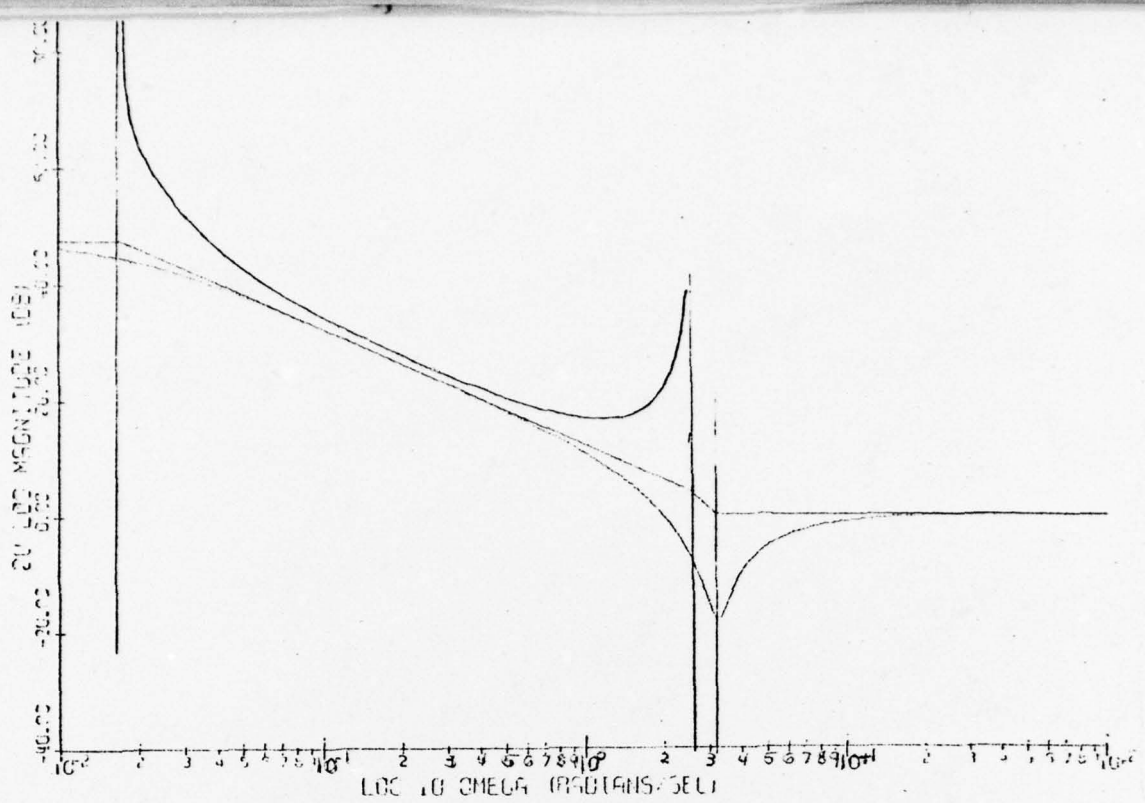

JW BODE MAGNITUDE PLOT $10A_2$

FIGURE C-8. FREQUENCY RESPONSE OF SPEED LOOP (1st TRIAL)

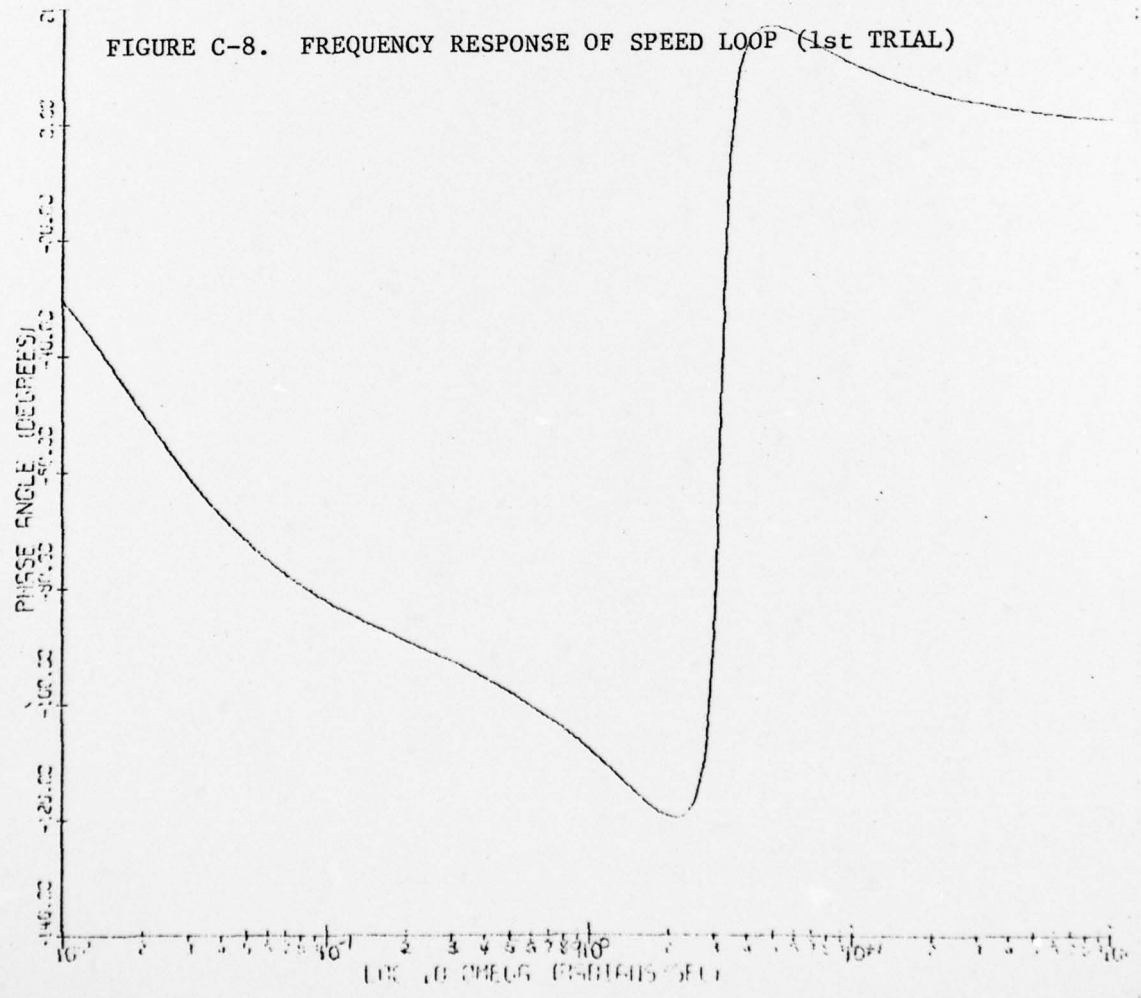

JW BODE PHASE PLOT $10A_2$

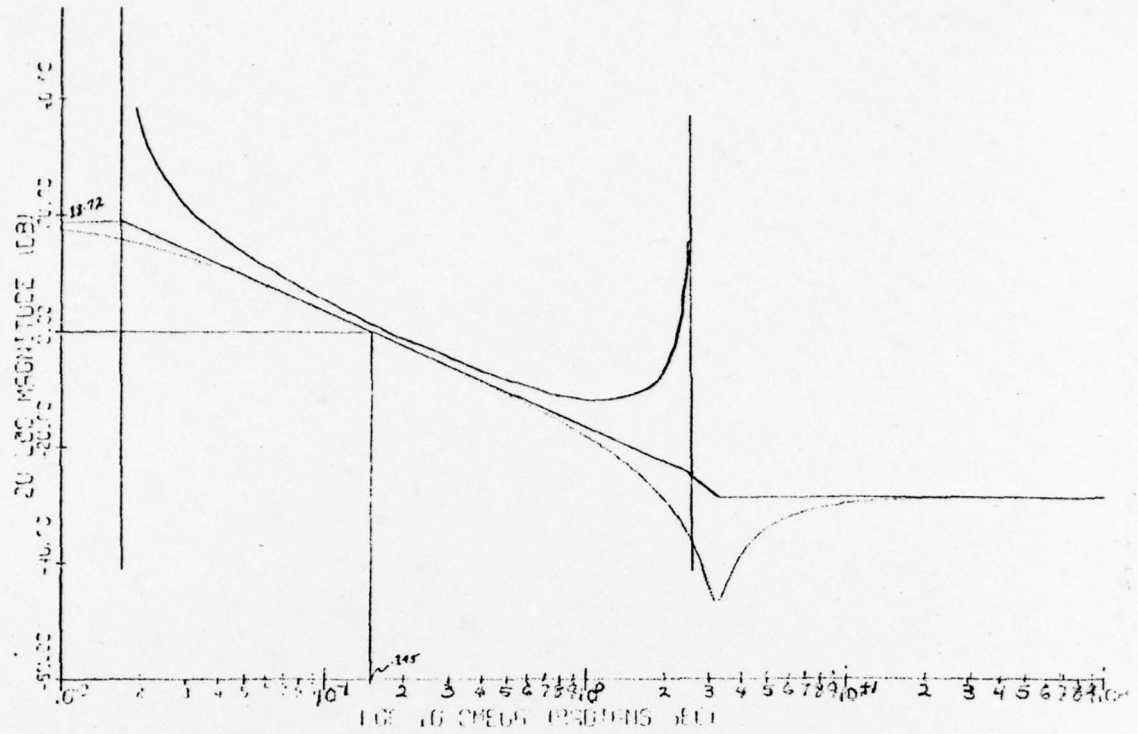

JW BODE MAGNITUDE PLOT $10A_3$

FIGURE C-9. FREQUENCY RESPONSE OF SPEED LOOP (2nd TRIAL)

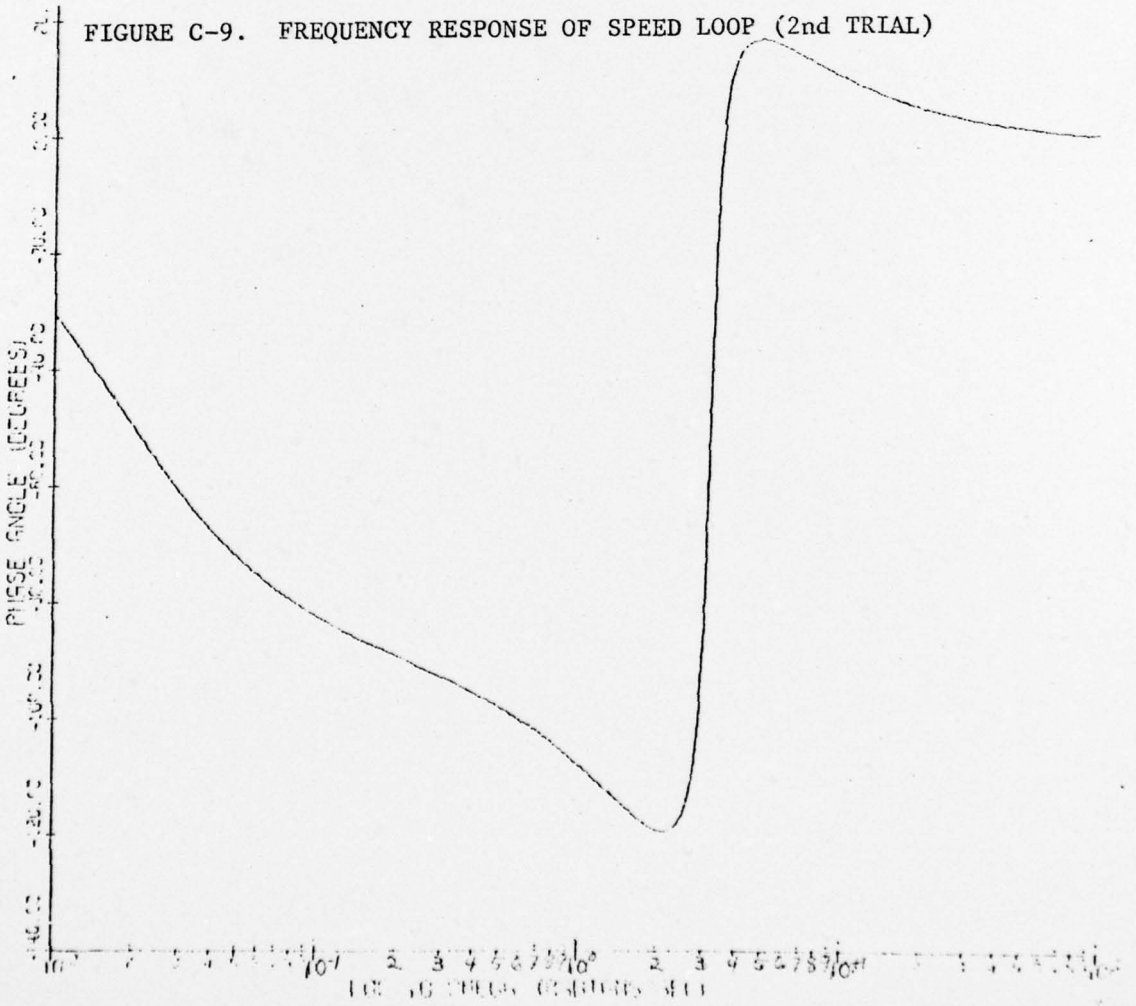

JW BODE PHASE PLOT $10A_3$

where their parameters are determined, but they are not design closures in and of themselves.

Loop 5, of course, is the pivot loop in the analysis. It displays the results of design efforts in the previous four and determines the parameters which dictate the behavior of 7 through 10. The altitude loop feedback gains were determined here through trial closures of 7, 8, and 9. It is obvious from the transfer functions of these loops (Fig. C-7) that almost any value of $K_{\dot{h}}$ will drive these loops at what amounts to infinite gain. Happily this allows the design of the compensator and feedback gain in 5 to be primarily a function of 5's closed loop characteristics with little compromise. $5B_3$ was an attempt to obtain a little more gain and bandwidth by moving the compensator to a higher time constant. The results are illustrated in a comparison of Figs. C-5 and C-6. While the damping ratio of .7-.8 was successfully maintained, the dc gain and bandwidth increase did not show significant improvement.

Loops 7 through 10 are closed for analysis, hence become consideration for design in loops 1-5. Fig. C-7 illustrates the closures and the results, of course, are depicted in $10A_3$ which shows the speed response as heavily damped and slow. It is not felt that this is an unreasonable result for speed response, in fact, it would be highly undesirable from a ride quality standpoint if it were very fast.

Lateral

The possibilities for a lateral controller are limited almost exclusively by the designers imagination. As in the case of the longitudinal controller however, history has shown a certain few feedbacks to be generally beneficial both from a stability standpoint and a handling/ride quality standpoint. These systems vary in complexity from wing levelers to analog/digital landing systems. For the purposes of this study, however, a basic attitude controller will be considered which is designed to maintain zero bank angle and yaw rate. This same system can be used to turn the aircraft by application of bank angle commands. The primary reasons for selecting this rather basic system are that the desired parameters are quickly and easily evaluated using approximate manual design techniques, and that the system is easily modified to provide heading hold and turn coordination capabilities. It should be noted here that although the following is a rather hasty treatment of the lateral case, it produces reasonable results on this basic system. The same detailed design techniques used in the longitudinal case could be applied here as well.

The block diagram of the lateral attitude controller shows the loops to be closed and the roll and yaw channel compensators to be determined.

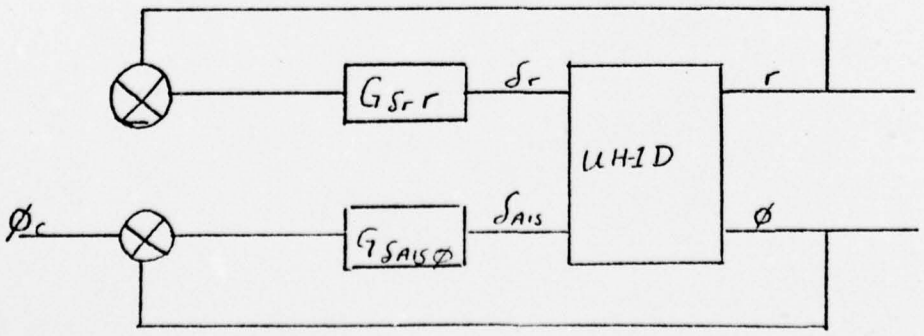

FIGURE C-10. BLOCK DIAGRAM OF LATERAL FEEDBACK SYSTEM

The equations of motion used to derive the lateral transfer functions are shown here in the matrix form for the unprimed derivatives

$$\begin{bmatrix} s-Y_v & -\frac{g}{U_o} & 1 \\ -L_\beta & (s-L_p)s & -(\frac{I_{xz}}{I_x}s + L_r) \\ -N_\beta & -(\frac{I_{xz}}{I_z}s + N_p)s & (s-N_r) \end{bmatrix} \begin{bmatrix} \beta \\ p \\ r \end{bmatrix} = \begin{bmatrix} Y_{Als} & Y_r & \delta_{Als} \\ L_{Als} & L_r & \\ N_{Als} & N_r & \delta_r \end{bmatrix}$$

The matrix multiplication of the above relationship invoking the stability derivatives previously given, results in the following set of numerator and denominator polynomials. The factors for the third and fourth degree polynominals were obtained using a Newton-Raphson digital subroutine.

$$\Delta_{Lat} = s^4 + 1.855s^3 + 6.501s^2 + 8.249s + 581 \qquad \{\zeta=.09,\ \omega=2.405\}$$
$$= (s+.075)(s+1.344)[s+.218\pm j2.395]$$

$$N^{\phi}_{\delta_{Als}} = 34(s^2 + .597s + 5.659)$$
$$= 34[s + .298\pm j2.360] \qquad \{\omega=2.379,\ \zeta=.126\}$$

$$N^{r}_{\delta_r} = -18.28[s^3 + 1.326s^2 + .121s + .288]$$
$$= -18.28\{(s + 1.388)[s -.031\pm j.454]\}$$

$$N^{\phi\ \ r}_{\delta_{Als}\ \delta_r} = -621.52(s-.154\ )$$

The transfer function for the multiloop analysis of bank angle

response to command is:

$$\frac{\phi}{\phi_c} = \frac{G_{\delta_{Als}\phi}\,(N_{\delta_{Als}}^{\phi} + G_{\delta_r r}\,N_{\delta_{Als}}^{\phi}\,\delta_r^r)}{\Delta_{lat} + G_{\delta_r r}\,N_{\delta_r} + G_{\delta_{Als}\phi}\,(N_{\delta_{Als}}^{\phi} + G_{\delta_r r}\,N_{\delta_{Als}}^{\phi}\,\delta_r^r)}$$

(12) — numerator

(11) — $G_{\delta_r r}\,N_{\delta_r}$ in the denominator

(13) — the entire denominator

and the loops to be closed are shown in the closure sequence selected.

A quick look at this system using root locus sketches, and assuming infinite gain on the inner yaw loop, disploses the fundamental stability problem. The yaw damper, while tending to stabilize the high frequency mode for lower gains, tends also to drive the lower frequency spiral-type mode toward instability. At high yaw rate feedback gains this can cause a real divergence in this mode. Although roll feedback will again tend to stabilize this condition, high gains in this channel will eventually result in the same spiral divergence. Figure C-11 shows the locus of roots for these closures and the approximate root locations for two levels of yaw rate feedback gain.

The dotted locus shown in Figure C-11c makes it clear that some sort of compensation is needed in order to produce a reasonable roll response with adequate damping. Computer analysis showed that the high frequency oscillatory roots in Figure C-11a and b move very close together over a range of gains from 1 to about 5. Since these roots are the poles and zeroes in loop 13, gains in this range will tend to negate the affects of this mode on the helicopter's rolling response.

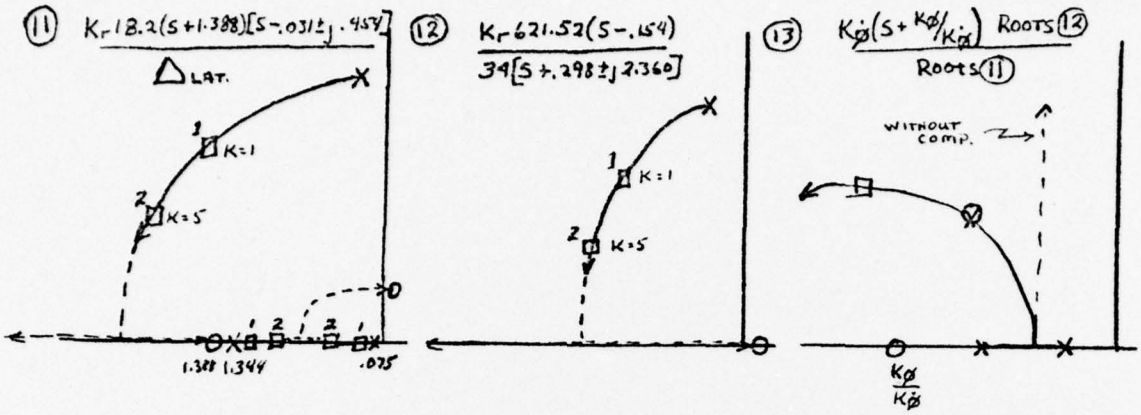

FIGURE C-11. ROOT LOCUS SKETCHES OF LATERAL LOOP CLOSURES

Because a heading hold system was to be used, it was desirable to keep the yaw damping as light as possible and a gain of 2.5 was selected. Also since a heading hold was to be used, consideration was given to a washout in this loop, since the yaw damper would tend to oppose the steady turn. The washout was not incorporated, however, because it was felt that the turns would be small and the additional pedal to trim would not be significant with the yaw damper gain. The poles and zeroes numbered with a 2 in Figure C-11c show the relative locations resulting from the yaw rate gain of 2.5. Since the selection of this gain resulted in the effective cancellation of the oscillatory mode, the rolling response can characterized by the two remaining real poles. Several loop closures confirmed this using a compensator consisting of roll rate and position feedback to achieve a well behaved response. The maximum bandwidth of the system, in this case, is largely a function of the ratio K_ϕ $K_{\dot{\phi}}$, when the feedback transfer function is:

$$G_{\delta_{Als}\phi} = K_{\dot{\phi}}(S+K_\phi/K_{\dot{\phi}})$$

The transfer function which characterizes the rolling response is:

$$\Delta\phi/\Delta\phi_c = \frac{K_{\dot{\phi}}(s+K_\phi/K_{\dot{\phi}})}{(s+1/T_{\phi 1})(s+1/T_{\phi 2})}$$

where $1/T_{\phi 1}$ and $1/T_{\phi 2}$ were at about -.2 and -1.3.

Values of $K_\phi/K_{\dot{\phi}}$ from 2.5 to 3.5 resulted in response times of .25 to .3 when $K_{\dot{\phi}}$ was in the neighborhood of 4 to 5.

At this point in the analysis, consideration was given to the comparison of pitching and rolling responses. Earlier the longitudinal design demonstrated the attempt to maximize bandwidth and resulted in pitching responses on the order of .2 seconds at a .8 damping ratio. Here again, in the roll channel,similar response times were obtained. While it would not be too difficult to produce a machine that would have a shorter response time, any effort in that direction would tend to jeopardize the system from a handling qualities standpoint. Since there is room here for fine tuning, however, the gains for the simulator were chosen to match the pitching and rolling responses as closely as possible. The following is a summary of the feedback transfer functions for the attitude system:

$$G_{\delta_{Bls}\theta} = K_{\dot{\theta}}(s+K_\theta/K_{\dot{\theta}}) \quad , \quad K_{\dot{\theta}} = .56 \quad K_\theta = 1.4$$

$$G_{\delta_{Als}\phi} = K_{\dot{\phi}}(s+K_\phi/K_{\dot{\phi}}) \quad , \quad K_{\dot{\phi}} = .184 \quad K_\phi = .45$$

$$G_{\delta_r r} = K_r = 2.5$$

REFERENCES

1. AGARD Conference Proceedings No. 148 on The Guidance and Control of V/STOL Aircraft and Helicopters at Night and in Poor Visibility, May 1974.

2. Aiken, E.W. and Schuler, J.M., "A Fixed-Base Ground Simulator Study of Control and Display Requirements for VTOL Instrument Landings With a Decelerating Approach to a Hover", Calspan Rept. No. AK-5113-F-2, Calspan Corp., Buffalo, N.Y., February 1974.

3. Born, G.J., Carico, D., Durbin, E.J., "A Dynamic Helicopter Performance and Control Model", U.S. Army Electronics Command, Technical Report No. ECOM-02421-11, August 1972.

4. Born, G.J., Dukes, T.A., Durbin, E.J., Sun, P.B., "Phase I and II, Final Report - Flight Path Control and Performance Analysis, Phase III, Final Report - Integrated Display", U.S. Army Electronics Command Technical Report No. ECOM-0161-72-F, July 1974.

5. Born, G.J., et.al., "Princeton Tasks, 3rd Annual Report", U.S. Army Electronics Command Technical Report No. ECOM-02412-5, October 1969.

6. Born, G.J., et.al., "Princeton Tasks, 4th Annual Report", U.S. Army Electronics Command Technical Report No. ECOM-02412-6, September 1970.

7. Coleman, R.P., Feingold, A.M., and Stempin, C.W., "Evaluation of the Induced-Velocity Field of an Idealized Helicopter Rotor", NACA Wartime Report No. L5E10, June 1945.

8. Curtiss, H.C., "Some Basic Considerations Regarding the Longitudinal Dynamics of Aircraft and Helicopters", Department of Aerospace and Mechanical Sciences Report No. 562, Princeton University, July 1961.

9. Department of the Army, Operators Manual Army Model UH-1D Helicopter, TM55-1520-210-10, Headquarters, Department of the Army, Washington, D.C., May 1969.

10. Dukes, T.A., "An Integrated Display Concept for Helicopters and VTOL Aircraft", American Helicopter Society Preprint No. 314, 25th Annual Forum Proceedings, Washington, D.C., May 1969.

11. Dukes, T.A., "Display for Approach and Hover With and Without Ground Reference", AGARD Reprint from Conference Proceedings No. 148 on "The Guidance and Control of V/STOL Aircraft and Helicopters at Night and In Poor Visibility", May 1974.

12. Dukes, T.A., Keane, W.P., and Tsoubanos, C.M., "Image and Superimposed Symbology - An Integrated Display for Helicopters", American Helicopter Society Preprint No. 724, 29th Annual Forum Proceedings, Washington, D.C., May 1973.

REFERENCES (continued)

13. Garren, J.F. Jr., Kelly, J.R., Sommer, R.W., and DeCarlo, D.J., "Flight Investigation of VTOL Control and Display Concept for Performing Decelerating Approaches to an Instrument Hover", NASA TND-6108, February 1971.

14. Gessow, A. and Myers, G.C. Jr., Aerodynamics of the Helicopter, Fredrick Unger Publishing Co., New York, 1967.

15. Harris, F.D., "Articulated Rotor Blade Flapping Motion at Low Advance Ratio", AHS Journal, Vol. 17, January 1972, pgs. 41-48, A72-20205.

16. Heyson, H.H., "A Momentum Analysis of Helicopters and Autogyros in Inclined Descent, With Comments on Operational Restrictions", NASA TND-7917, October 1975.

17. Kelly, J.R., Niessen, F.R., Thibodeaux, J.J., Yenni, K.R., Garren, J.F. Jr., "Flight Investigation of Manual and Automatic VTOL Decelerating Instrument Approaches and Landings", NASA TND-7524, July 1974.

18. Lebacqz, J.V. and Aiken, E.W., "A Flight Investigation of Control, Display, and Guidance Requirements for Decelerating Descending VTOL Instrument Transitions Using the X-22A Variable Stability Aircraft", Calspan Report No. AK-5336-F-1, Calspan Corp., Buffalo, N.Y., September 1972.

19. Lemons, J.L., "A Study of the Effect of Displayed Acceleration Information on VTOL Hover Performance", MSE Thesis, Princeton University, September 1974.

20. Loveday, Robert, Statistics, 2nd edition, Cambridge University Press, Great Britain, 1969.

21. McRuer, D.T., Ashkenas, I.L., Graham, D., Aircraft Dynamics and Automatic Control, Princeton University Press, Princeton, N.J., 1973.

22. Moen, G.C., DeCarlo, D.J., Yenni, K.R., "A Parametric Analysis of Visual Approaches for Helicopters", NASA TND-8275, December 1976.

23. Moen, G.C. and Yenni, K.R., "Simulation and Flight Studies of an Approach Profile Indicator for VTOL Aircraft", NASA TND-8051, November 1975.

24. Nicholson, R.M., Wolf, J.D., Clifford, R.R., et.al., Display Requirements Study for Helicopter IFR Formation Flight, JANAIR TR No. NR213-054, Honeywell, Inc., January 1968.

REFERENCES (continued)

25. Niessen, F.R., Kelley, J.R., Garren, J.F. Jr., Yenni, K.R., and Person, L.H., "The Effect of Variations in Controls and Displays on Helicopter Instrument Approach Capability", NASA TND-8385, February 1977.

26. Roberts, L.D., "An Analysis of Helicopter Control in Landing Approach", MSE Thesis, Princeton University, December 1967.

27. Savant, C.J. Jr., Control System Design, 2nd Edition, McGraw Hill Inc., New York, 1964.

28. Schmitz, F.H., "Take-Off Optimization for STOL Aircraft and Heavily Loaded Helicopters", Ph.D. Thesis, Princeton University, September 1969.

29. Seckel, E., Stability and Control of Airplanes and Helicopters, Academic Press Inc., New York, 1964.

30. Seckel, E. and Curtiss, H.C. Jr., "Aerodynamic Characteristics of Helicopter Rotors, Rotor Contributions to Helicopter Stability Parameters", Department of Aerospace and Mechanical Sciences Report No. 659, Princeton University, December 1963.

31. Sonneborn, W., Torres, I., UH-1C Data for Hybrid Computer Simulation, BHC Report 204-099-892, Fort Worth, Texas, February 1968.

32. Steinmetz, G.G., Morrello, S.A., Know, C.E., and Person, L.H. Jr., "A Piloted-Simulation Evaluation of Two Electronic Display Formats for Approach and Landing", NASA TND-8183, April 1976.

33. Tsoubanos, C.M., "An Investigation of a Helicopter Performance Meter (Steady State Flight Condition)", MSE Thesis, Princeton University, 1974.

34. Wolkovitch, J., Hoffman, J.A., "Stability and Control of Helicopters in Steep Approaches", Eustic Directorate, U.S. Army Air Mobility Research and Development Laboratory Technical Report No. 70-74A, May 1971.

35. Wolkovitch, J. and Johnston, D.E., "Automatic Control Considerations for Helicopters and VTOL Aircraft With and Without Sling Loads", STI Technical Report No. 138-1, November 1965.